KU LEUVEN

FACULTY OF
ENGINEERING SCIENCE

Thermal Response Tests for Geothermal Borefields – Reducing Test Duration through Transient Borehole Modeling and Comparing Constant Power and Constant Temperature Methods

Bart Vandenhout

Thesis submitted for the degree of
Master of Science in Mechanical
Engineering

Supervisor
Prof. dr. ir. L. Helsen

Assessors
Prof. dr. ir. M. Blommaert
Dr. ir. L. Hermans

Assistant-supervisors
Ir. L. Meertens
Ir. W. Peere

Academic year 2025 – 2026

© 2026 KU Leuven – Faculty of Engineering Science
Published by Bart Vandenhout,
Faculty of Engineering Science, Kasteelpark Arenberg 1 bus 2200, B-3001 Leuven

All rights reserved. No part of the publication may be reproduced in any form by print, photoprint, microfilm, electronic or any other means without written permission from the publisher. This publication contains the study work of a student in the context of the academic training and assessment. After this assessment no correction of the study work took place.

Preface

This thesis forms the culmination of my engineering degree, which gave me invaluable skills and made me look at the world differently. This research reflects my passion to tackle climate change and help lead the world toward a more sustainable place. I am grateful for all the opportunities I received, and I realize that being able to pursue this path is a privilege. With this research, I aimed to give something back to the environment that allowed me to become who I am today.

I enjoyed the versatility of this thesis, and I feel like it allowed me to make an actual contribution to both industry and the academic world. I loved getting my shoes dirty on the borefield in Lochristi, getting excited when the device worked, and being amazed by a simple crane moving it. On the other hand, I also enjoyed looking at Python code late at night to improve the underlying models. This research also brought me into contact with many people in industry, from suppliers to geothermal companies.

I want to thank my parents for providing me with everything I needed to succeed in my education. Throughout my life, they have constantly supported me, and during this thesis they allowed me to enthusiastically explain everything I was working on. After listening closely, they would ask critical questions, which led to insightful discussions. They inspire me to become a better engineer, but more importantly, a better person. I also want to thank my sister, because she allowed me to develop my social skills throughout my whole life and always makes me feel like we are a team. I also thank my girlfriend for being supportive throughout my studies, and for her sharp academic mindset, which makes her a great PhD researcher and increased the quality of my research.

I also want to thank everyone who made this research possible. A special thanks to Lone, whose guidance and support were invaluable throughout this project. I enjoyed working together, writing ideas on a whiteboard and brainstorming about results. Her sharp reasoning, professionalism, and enthusiastic can-do mindset contributed enormously to the quality of this research and made it a team effort. I also want to thank my promotor, Professor Lieve Helsen, for the support she gave me, not only during this research but also for my scholarship and further studies. Her positivity and enthusiasm, together with a critical academic mindset, are a source of inspiration.

Further, I want to thank Wouter for his contributions to the project. He watched over the project closely, guided me back on track when I made mistakes, and supported me positively. I also want to thank Kristof and Liesbeth of LOBO Geothermische Boringen, who deserve credit for the success of the TRT device and test results. I thank them for making time to assemble and operate the TRT device and to generate high-quality experiments. Their entrepreneurial mindset and willingness to fully commit to this investment are inspiring. I hope this thesis contributed to the success of their company and, more importantly, to ultimately reducing the cost of geothermal borefields in Belgium, which benefits society as a whole. Lastly, I also want to thank the jury for their critical assessment of this project.

I am proud of this research, but even more proud of how we are able, as a society, to make this all happen. It is inspiring to see people trying their best every day to make this world a better place. There is still room for improvement, but I believe it is up to the optimists to optimize it.

Bart Vandenhout

Contents

Preface i

Abstract vi

List of Figures and Tables vii

List of abbreviations and symbols ix

1 Introduction 1
- 1.1 Background and motivation . . . 1
- 1.2 Research Questions . . . 2
- 1.3 Thesis Outline . . . 4

I Literature Study 7

2 Geothermal Heat and Boreholes 9
- 2.1 Ground-source heat pumps . . . 9
- 2.2 Boreholes and Borefields . . . 10
- 2.3 Borefield Sizing . . . 11
- 2.4 Ground Design Parameters . . . 12
- 2.5 Conclusion . . . 14

3 Thermal Response Tests 15
- 3.1 Basic Principle of a TRT . . . 15
- 3.2 TRT Types . . . 16
- 3.3 Conclusion . . . 19

4 Analytical Borehole Modeling 21
- 4.1 General Heat Conduction Equation . . . 21
- 4.2 External Borehole Models for CP-TRT . . . 22
- 4.3 External Borehole Model for CIT-TRT . . . 24
- 4.4 G-functions . . . 25
- 4.5 Internal Borehole Model . . . 26
- 4.6 Conclusion . . . 27

5 TRT Parameter Estimation 29
- 5.1 Undisturbed Ground Temperature T_∞ . . . 29
- 5.2 Effective Thermal Conductivity k . . . 31
- 5.3 Effective Thermal Borehole Resistance R_b^* . . . 33

5.4 Conclusion 35

6 Transient Borehole Modeling **37**
6.1 Motivation for Transient Borehole Modeling 37
6.2 Limitations of Classical Models 38
6.3 Short Term Solution Model 38
6.4 Conclusion 40

II Setup **43**

7 TRT Device for Field Testing **45**
7.1 Design Requirements 45
7.2 System Layout 46
7.3 Components 47
7.4 Design Challenges 51
7.5 Conclusion 54

8 External Datasets **55**
8.1 Dataset Aydin 55
8.2 Dataset Terra Energy 56
8.3 Conclusion 57

III Methodology **59**

9 Transient Modeling Methodology **61**
9.1 STS Model Implementation 61
9.2 Verification of Parameter Estimation 62
9.3 Test Duration Reduction 62
9.4 Sensitivity Analysis 64
9.5 Conclusion 65

10 Methodology of Field Testing **67**
10.1 Test Setup 67
10.2 TRT Methodology 69
10.3 Comparison CP- and CIT-TRTs 71
10.4 Conclusion 72

IV Results and Discussion **73**

11 Transient Modeling Results **75**
11.1 STS Model Implementation 75
11.2 Verification of Parameter Estimation 76
11.3 Test Duration Reduction 79
11.4 Sensitivity Analysis 83
11.5 Conclusion 86

12 Field Test Results **89**
12.1 CP-TRTs 89
12.2 CIT-TRTs 95
12.3 Comparison of CP- and CIT-TRTs 99
12.4 Conclusion 100

V Conclusion and Suggestions for Further Research **103**

13 Conclusion **105**

14 Suggestions for Future Research **109**
14.1 TRT device 109
14.2 Transient modeling 111
14.3 CIT-TRTs 111

A Terra Energy TRTs **113**

Bibliography **119**

Code of Conduct **124**

Abstract

Ground-source heat pump (GSHP) systems can reduce heating and cooling emissions, but their wider implementation is limited by the high investment cost, mainly because of high drilling costs. Accurate borefield sizing therefore requires reliable on-site estimation of the effective ground thermal conductivity k, effective borehole thermal resistance R_b^*, and undisturbed ground temperature T_∞, typically obtained from thermal response tests (TRTs). This thesis investigates whether TRT duration can be reduced by incorporating transient borehole effects into the analysis and compares conventional constant power TRTs (CP-TRTs) with constant inlet temperature TRTs (CIT-TRTs). A Short Term Solution (STS) model, based on a hybrid g-function including short-term borehole effects, was implemented and evaluated on a dataset of 23 CP-TRTs. Compared with the conventional long-term Infinite Line Source (ILS) interpretation, the STS model produced consistent parameter estimates, with average deviations of 3.65% for k and 6.03% for R_b^*. More importantly, it reduced the average convergence time by 17.7 h, 9.8 h, and 5.5 h for accuracy bands of 10%, 5%, and 2.71%, corresponding to reductions of 24.2%, 13.4%, and 7.5% relative to the average test duration of approximately 73 h. In addition, a custom TRT device capable of performing both CP- and CIT-TRTs was designed, assembled, and tested on a borefield in Lochristi, Belgium. The CP-TRTs produced realistic and relatively consistent k-values, especially after improved insulation reduced ambient temperature effects, indicating that the device is ready for industry use in CP-TRT operating mode under sufficiently controlled conditions. The CIT-TRTs showed the expected thermal response, but were more sensitive to temperature-control instability and ambient conditions. In the conducted field tests, CIT-TRTs did not converge faster or produce more consistent parameter estimates than CP-TRTs. Overall, this thesis shows that a transient model such as STS significantly reduces CP-TRT duration, while the potential advantages of CIT-TRTs require further investigation with improved temperature-control stability.

List of Figures and Tables

List of Figures

1.1 Thesis structure overview 5

2.1 Residential GSHP system with vertical boreholes 10
2.2 Vertical borehole cross-section with single U-tube 11

3.1 Typical borehole TRT setup 15
3.2 CP-TRT measurement data 16
3.3 CIT-TRT measurement data 18

5.1 Fluid temperature logging during circulation 30
5.2 Mean fluid temperature versus logarithmic time for CP-TRT data . . . 32
5.3 Inverse thermal power versus logarithmic time for CIT-TRT data 33

6.1 Radial borehole discretization for short-term effects 40

7.1 TRT system design overview 46
7.2 TRT device inside insulated container 48
7.3 Grundfos MAGNA3 25-100 pump performance curve 50
7.4 Pipe insulation before and after improvement 53
7.5 Heater supply temperature sensor before and after insulation 54

8.1 Mean fluid temperature and injected thermal power for TRT7 57
8.2 Mean fluid temperature and injected thermal power for TRT3 57

9.1 Example convergence test for thermal conductivity 64

10.1 Test site ground plan 68

11.1 Mean fluid temperature versus hybrid G-function for TRT3 77
11.2 ILS and STS convergence test for TRT3 80
11.3 Influence of STS cutoff time on time reduction and k-difference 83
11.4 ILS sensitivity analysis for k and R_b^* 84
11.5 STS sensitivity analysis for k and R_b^* 85

12.1 Measured fluid temperatures for the CP-TRTs 90
12.2 Calculated thermal power for the CP-TRTs 91
12.3 Temperature response during initial circulation for CP-TRT1 92
12.4 Mean fluid temperature and ILS fit for the CP-TRTs 93
12.5 Convergence tests for the CP-TRTs 94
12.6 Measured fluid temperatures for the CIT-TRTs 96
12.7 Calculated thermal power for the CIT-TRTs 96
12.8 Inverse thermal power and linear fit for the CIT-TRTs 97
12.9 Convergence tests for the CIT-TRTs 99

A.1 Fluid temperature $\overline{T}_f$ and thermal power Q as a function of time for Terra Energy TRT1 and TRT2. 113
A.2 Fluid temperature $\overline{T}_f$ and thermal power Q as a function of time for Terra Energy TRT3–TRT8. 114
A.3 Fluid temperature $\overline{T}_f$ and thermal power Q as a function of time for Terra Energy TRT9–TRT14. 115
A.4 Fluid temperature $\overline{T}_f$ and thermal power Q as a function of time for Terra Energy TRT15–TRT20. 116
A.5 Fluid temperature $\overline{T}_f$ and thermal power Q as a function of time for Terra Energy TRT21–TRT25. 117

List of Tables

6.1 Input data for the STS borehole model 41

7.1 TRT device components and costs 52

10.1 Borefield geometry and material properties 68
10.2 Overview of CP- and CIT-TRT field tests 69

11.1 STS model input data for TRT3 76
11.2 ILS and STS parameter estimates for the Terra Energy dataset 78
11.3 ILS and STS convergence times for different accuracy bands 82

12.1 Overview of CP-TRT results 93
12.2 Overview of CIT-TRT results 98
12.3 Convergence times for the field tests 100

List of abbreviations and symbols

Abbreviations

GSHP	Ground-source heat pump
ASHP	Air-source heat pump
TRT	Thermal response test
CP-TRT	Constant power thermal response test
CIT-TRT	Constant inlet temperature thermal response test
CT-TRT	Constant temperature thermal response test
ILS	Infinite Line Source
FLS	Finite Line Source
ICS	Infinite Cylinder Source
STS	Short Term Solution
MAPE	Mean absolute percentage error

Symbols

k	Effective thermal conductivity [W/(mK)]
R_b^*	Effective borehole thermal resistance [mK/W]
R_b	Borehole thermal resistance [mK/W]
T_∞	Undisturbed ground temperature [°C]
T_f	Mean fluid temperature [°C]
T_b	Borehole wall temperature [°C]
T_1	Borehole inlet fluid temperature [°C]
T_2	Heater supply temperature [°C]
T_3	Borehole outlet fluid temperature [°C]
Q	Thermal power [W]
q	Thermal power per unit borehole length [W/m]
$\dot{V}$	Volumetric flow rate [m^3/h]
$\dot{m}$	Mass flow rate [kg/s]
ρ_f	Fluid mass density [kg/m^3]
$c_{p,f}$	Fluid specific heat capacity at constant pressure [J/(kgK)]
$(\rho c_p)_g$	Grout volumetric heat capacity [J/(m^3K)]
$(\rho c_p)_p$	Pipe volumetric heat capacity [J/(m^3K)]
α	Thermal diffusivity [m^2/s]
t_c	Convergence time [h]
t_{switch}	Switching time between short-term and long-term g-functions [s]
$g(t)$	G-function at time t [-]
$g_{ST}(t)$	Short-term G-function at time t [-]
$g_{LT}(t)$	Long-term G-function at time t [-]
$g_{ILS}(t)$	Infinite Line Source G-function at time t [-]
$g_{FLS}(t)$	Finite Line Source G-function at time t [-]
$g_{ICS}(t)$	Infinite Cylinder Source G-function at time t [-]
γ	Euler–Mascheroni constant [-]
Fo	Fourier number [-]
r_b	Borehole radius [m]
r_e	Equivalent radius [m]
r_{in}	Inner pipe radius [m]
r_{out}	Outer pipe radius [m]
H	Borehole length [m]
D	Borehole burial depth [m]
B	Borehole spacing [m]
D_s	Shank spacing [m]
n_p	Number of U-tubes [-]
k_p	Pipe thermal conductivity [W/(mK)]
k_g	Grout thermal conductivity [W/(mK)]
k_f	Fluid thermal conductivity [W/(mK)]
η	Dynamic viscosity [Pa s]
ϵ	Pipe roughness [m]

Chapter 1

Introduction

1.1 Background and motivation

Tackling climate change is one of humanity's greatest current challenges, requiring significant reductions in greenhouse gas emissions. In 2024, fossil-fuel-related CO_2 emissions represented 74.5% of global GHG emissions [1]. A major part of final energy consumption is associated with heating and cooling, which together represent approximately half of the European Union's final energy demand. More than 70% of this demand is still covered by fossil fuels [2]. In response, major economies have established ambitious decarbonization targets, including the European Union's objective of achieving climate neutrality by 2050 [3]. Within this transition, heat pumps are becoming increasingly important. When powered by low-carbon electricity, they can provide heating and cooling with substantially lower emissions compared to conventional fossil-fuel-based systems.

Ground-source heat pumps (GSHPs) are particularly attractive because they use the relatively stable temperature of the ground as a heat source or sink [4]. Compared to air-source heat pumps (ASHPs), this enables operation with a smaller and more stable temperature lift, resulting in higher efficiency and reduced sensitivity to outdoor temperature fluctuations. Despite these advantages, the widespread implementation of GSHP systems remains limited by their high initial investment costs. A major part of these costs is associated with borehole drilling [5]. Accurate borefield sizing is therefore essential as undersizing can lead to poor system performance and long-term ground temperature drift, whereas oversizing results in unnecessary drilling costs [6].

The accuracy of borefield sizing depends strongly on the estimation of key design parameters, mainly the effective ground thermal conductivity k [7], the effective borehole thermal resistance R_b^* [8], and the undisturbed ground temperature T_∞ [9]. These parameters depend on local geological conditions, borehole geometry, grout properties, pipe configuration, and installation quality. Using generic values therefore introduces uncertainty into the design process. Thermal response tests (TRTs)

are used to reduce this uncertainty by experimentally determining these parameters on-site.

Conventional TRT interpretation is mainly based on constant power thermal response tests (CP-TRTs), in which an approximately constant heat injection rate is imposed. These tests are well established in both research and industry [10]. However, they typically require long test durations before stable parameter estimates are obtained. This increases operational cost, delays project execution, and reduces on-site flexibility. In addition, the early-time data of a TRT are often excluded from conventional analysis because short-term transient effects inside the borehole are not sufficiently represented by standard borehole models [11]. As a result, potentially useful data are discarded, which partly explains the long duration required for conventional TRT interpretation [12].

To address this issue, this thesis investigates two possible routes for reducing the required duration of TRTs. First, it evaluates whether transient borehole effects can be incorporated into the TRT analysis procedure, allowing earlier measurement data to be used for parameter estimation. This was investigated using a short-term transient borehole model applied to external CP-TRT datasets. Second, it investigates constant inlet temperature thermal response tests (CIT-TRTs) as an alternative to the conventional CP-TRT method. CIT-TRTs impose a constant inlet fluid temperature instead of a constant heat injection rate and may therefore lead to different thermal behavior and convergence characteristics [13]. This comparison is not limited to test duration reduction, but also considers differences in parameter estimation and operational stability.

These two routes are investigated using a combination of external datasets and original field experiments. The external datasets consist of published academic data made available upon request and private TRT data provided by an industrial partner. In addition, original field experiments were conducted using a custom TRT device developed during this thesis. Accordingly, this thesis includes the design, assembly, and operation of a TRT device capable of performing both CP- and CIT-TRTs. The purpose of this device is to generate field data, evaluate practical implementation challenges, and compare both TRT methods under comparable field conditions.

1.2 Research Questions

The main objective of this thesis is formulated in the following main research question:

Main Research Question

To what extent can the required duration of TRTs be reduced by incorporating transient borehole effects into the TRT analysis, and how do CP- and CIT-TRTs compare in terms of parameter estimation and test duration?

This main research question is divided further into three research questions (RQs):

RQ1 **To what extent does incorporating transient borehole effects into TRT analysis improve parameter estimation and reduce the required test duration compared to conventional approaches?**

RQ2 **Can a TRT device capable of performing both CP- and CIT-TRTs be designed and developed to generate reliable experimental datasets, and what are the main challenges related to its design, implementation, and operation?**

RQ3 **How do CP- and CIT-TRTs compare in terms of thermal behavior, parameter estimation, operational stability, and required test duration?**

RQ1 investigates whether the required duration of CP-TRTs can be reduced by using a borehole model that includes short-term transient effects. This research question is addressed using the external Terra Energy dataset, which consists of multiple CP-TRTs performed for industry use. The conventional long-term approximation is compared with a transient model to evaluate both parameter agreement and convergence time reduction.

RQ2 focuses on the development and operation of the TRT device built for this research. The device must be capable of operating in both CP- and CIT-TRT modes and should generate experimental datasets suitable for parameter estimation and method comparison. This research question also includes the practical challenges encountered during device design and field operation, such as temperature stability, heat losses, measurement accuracy, and ambient temperature influence.

RQ3 compares CP- and CIT-TRTs based on the field tests performed with the developed device. Since both methods are tested on the same borefield, their thermal behavior, parameter estimation results, operational stability, and convergence characteristics can be compared directly. This allows evaluation of whether CIT-TRTs provide a practical advantage over conventional CP-TRTs in the developed setup.

1.3 Thesis Outline

This thesis is divided into five parts. Figure 1.1 provides a conceptual overview of the main elements of the research, linking the input datasets, TRT device, borehole models, and resulting parameter estimation.

Part I presents the literature study, which introduces the necessary theoretical background. Chapter 2 introduces geothermal heat, vertical boreholes, borefield sizing, and the relevant design parameters. Chapter 3 explains the principle of TRTs and introduces the CP-TRT and CIT-TRT methods. Chapter 4 discusses analytical borehole models, for which the Infinite Line Source (ILS) model is the most widely used, and the g-function framework used for TRT interpretation. Chapter 5 explains how TRT measurements are used to estimate T_∞, k, and R_b^*. Chapter 6 introduces transient borehole modeling and the Short Term Solution (STS) model used to address RQ1.

Part II describes the experimental and external data sources used in this thesis. Chapter 7 presents the design and development of the TRT device built for this research, thereby addressing the device-related part of RQ2. Chapter 8 introduces the external TRT datasets used for model implementation, verification, and comparison.

Part III presents the methodology. Chapter 9 describes the transient modeling methodology used to compare the STS model with the conventional ILS approach and to quantify potential test duration reduction, addressing RQ1. Chapter 10 describes the methodology used for the field tests, including the CP- and CIT-TRT procedures, parameter estimation methods, and comparison strategy, addressing RQ2 and RQ3.

Part IV presents and discusses the results. Chapter 11 evaluates the STS model on the Terra Energy dataset and quantifies the resulting convergence time reduction, addressing RQ1. Chapter 12 evaluates the developed TRT device and discusses the field test results for CP- and CIT-TRTs, addressing RQ2 and RQ3.

Finally, Part V provides the main conclusions and recommendations for future research. Chapter 13 formulates the answer to the research questions and the main research question. Chapter 14 presents suggestions for further development of the TRT device, transient modeling methodology, and CIT-TRT research.

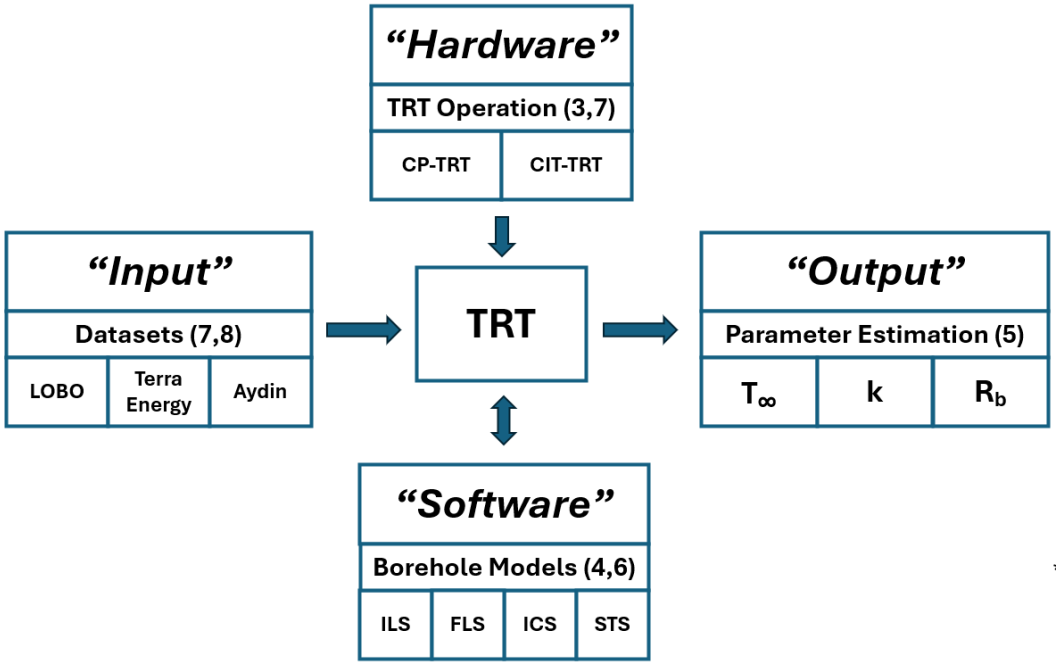


FIGURE 1.1: Conceptual overview of the relevant TRT concepts in this research, including the corresponding chapter numbers.

Part I

Literature Study

Chapter 2

Geothermal Heat and Boreholes

This chapter introduces the geothermal context needed to understand thermal response testing. First, ground-source heat pumps and vertical borehole heat exchangers are discussed. Then, the role of borefield sizing is introduced, followed by the three main design parameters that are commonly determined from a thermal response test: the effective ground thermal conductivity k, the effective borehole thermal resistance R_b^*, and the undisturbed ground temperature T_∞.

2.1 Ground-source heat pumps

Ground-source heat pumps (GSHPs) are systems that exchange heat with the ground through ground heat exchangers, most commonly vertical borehole heat exchangers. Since they are electrically driven, they enable fossil-free operation and generally achieve higher efficiencies than conventional combustion-based heating systems [4].

The main advantage of GSHPs lies in the relatively stable ground temperature, which results in a smaller and more consistent temperature lift across the heat pump. In contrast, air-source heat pumps (ASHPs) depend on fluctuating outdoor air temperatures, leading to less stable operating conditions and lower efficiency. As a result, GSHPs can achieve higher and more stable efficiencies while operating under more favorable conditions [5]. This improved performance reduces energy consumption, operational costs, and greenhouse gas emissions.

In addition, GSHP systems can provide passive cooling and are typically quiet because they do not require large outdoor fan units [4]. They can also enable seasonal thermal storage, which can improve long-term system efficiency [14]. Furthermore, they do not contribute to urban heat island effects, where cities experience higher temperatures due to accumulated heat from buildings and human activities [15].

Despite these advantages, widespread implementation of GSHP systems still faces challenges mainly due to their high initial investment cost compared to ASHP systems. This cost is mainly associated with drilling and installation [5]. Avoiding

unnecessary drilling through more accurate design reduces costs, and can therefore support wider adoption of GSHP systems.

2.2 Boreholes and Borefields

The heat exchange between a GSHP system and the ground takes place through ground heat exchangers. Vertical borehole heat exchangers are most commonly used. In these systems, one or more U-shaped pipes are installed inside drilled vertical boreholes, through which a heat carrier fluid circulates. Multiple boreholes can be connected to form a borefield, allowing the system to meet larger heating and cooling demands.

GSHP systems can generally be divided into closed-loop systems and open-loop systems. In closed-loop systems, a circulating heat carrier fluid exchanges heat with the ground through pipes without direct contact between the fluid and the surrounding ground. The heat carrier fluid is often a water-antifreeze mixture to prevent freezing under low-temperature operating conditions. However, pure water can also be used in some applications because of its favorable thermal properties and lower viscosity, which improve heat transfer and reduce pumping power [16]. In contrast, open-loop systems use groundwater or surface water directly as the heat exchange medium [17].

This research focuses on closed-loop systems with vertical borehole heat exchangers, shown schematically in Figure 2.1. Other configurations, such as horizontal ground heat exchangers, energy piles, and open-loop systems, are not considered further in this research.

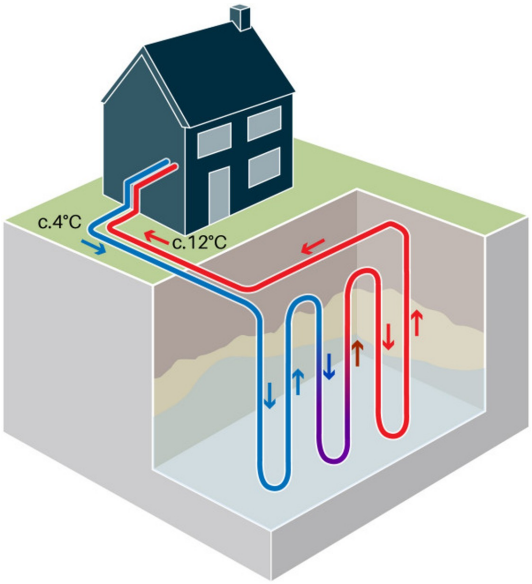


Figure 2.1: Schematic representation of a residential GSHP system with vertical boreholes (Reproduced from [18]).

Figure 2.2 shows the horizontal cross-section of a typical vertical borehole heat exchanger. The annular space between the pipes and the borehole wall is filled with grout, a thermally enhanced material that promotes efficient heat transfer from the pipes to the surrounding ground while also ensuring mechanical stability [19].

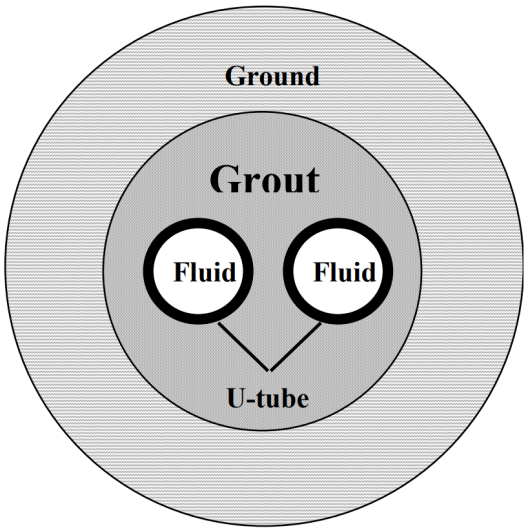


FIGURE 2.2: Horizontal cross-section of a typical vertical borehole with a single U-tube, showing the circulating fluid, pipe wall, grout, and surrounding ground (Reproduced from [20], originally from [19]).

2.3 Borefield Sizing

Borefield sizing involves determining the total borehole length and borefield configuration required to provide the heating and cooling demand while keeping the circulating fluid temperature within acceptable limits over the system lifetime. Correct borefield sizing is essential, as undersizing can lead to operational problems, such as the system reaching its temperature limits, long-term ground thermal depletion, or the inability to maintain thermal comfort in the building, while oversizing leads to unnecessary drilling costs [6].

Borefield sizing is based on modeling the heat transfer between the boreholes and the surrounding ground under variable thermal loads. These models link the fluid temperature evolution to the applied thermal loads, ground properties, borehole characteristics, and borefield configuration [6]. Borefield sizing itself is not the topic of this research, but its accuracy depends strongly on the reliability of the ground and borehole parameters used as model inputs. These parameters are discussed in detail in Section 2.4. They strongly influence the predicted fluid temperature evolution and therefore the required borehole length. Although generic values can be assumed based on geological data or typical average values, this often introduces

significant uncertainty into the design process and can result in over- or undersizing of the borefield [6].

To reduce this uncertainty, thermal response tests (TRTs) are commonly performed to experimentally determine the relevant parameters on site. These measured parameters can then be used as input for borefield sizing, reducing the risk of inaccurate sizing and its associated costs or operational problems. TRTs are the main subject of this research and are introduced in Chapter 3.

2.4 Ground Design Parameters

A TRT is mainly used to determine three design parameters: the thermal conductivity k, the thermal borehole resistance R_b^* and the undisturbed ground temperature T_∞. This section explains the meaning of these parameters and their importance for borefield sizing. The methodology for determining them from TRT data is discussed in Chapter 5.

2.4.1 Thermal Conductivity k

The thermal conductivity k of the ground is one of the most important parameters for borefield sizing [7]. It represents the ability of the surrounding ground to conduct heat. A higher value of k indicates better heat transfer, which reduces the required borehole length for a given thermal load. In practice, an effective value is used, representing an average value of k over the full borehole depth. In heterogeneous ground conditions, this effective value can differ significantly from local layer-specific values because of stratified soil layers or groundwater flow [21].

Heim et al. [22] estimated the thermal conductivity in the German state of Hamburg based on public geological data. They found average minimum, mean, and maximum values of 1.4, 1.9, and 2.8 $W/(mK)$, corresponding to an uncertainty range of approximately -26% to +47% around the mean value. Such uncertainty in a crucial sizing parameter can lead to suboptimal performance or even malfunctioning of GSHP systems. This demonstrates the need for a more accurate site-specific determination of k, which can be obtained through a TRT.

2.4.2 Borehole Resistance R_b^*

The borehole resistance R_b^* represents the total thermal resistance between the circulating fluid and the borehole wall. It is determined by the combined effect of convective heat transfer inside the pipes and conduction through the pipe walls and grout. Both material properties and geometric parameters of the borehole influence the R_b^* value.

Unlike k or T_∞, R_b^* is not a ground property but a borehole property. It depends on the specific borehole geometry, materials, and installation details, including pipe

configuration, borehole diameter, and grout properties. As a result, R_b^* can differ between boreholes within the same borefield. Similar to k, R_b^* is an effective value, representing the overall thermal resistance over the full borehole depth [8].

Accurate estimation of R_b^* is important because it directly affects the temperature difference between the fluid and the borehole wall. It therefore influences the fluid temperature evolution, the thermal performance of the borehole, and thus the required borefield size [8].

The uncertainty in R_b^* depends on the uncertainty in the material and geometric input parameters. For example, Lund et al. [17] calculated that R_b^* decreases by approximately 44% when grout conductivity is doubled. Remund [23] experimentally showed that R_b^* decreases by 15.3% to 19.5% for the same change in grout. This shows that uncertainty in borehole material properties can have a significant effect on the resulting R_b^* value. Therefore, estimating R_b^* from measurement data of the actual borehole is valuable, which is one of the purposes of a TRT.

2.4.3 Undisturbed Ground Temperature T_∞

The undisturbed ground temperature T_∞ represents the natural ground temperature in the absence of thermal disturbance caused by borehole operation. In theory, it corresponds to the ground temperature at an infinite distance from the borehole. In practice, it is defined at a distance where the thermal influence of the borehole has become negligible, which depends on the considered time scale and the thermal diffusivity of the ground [24]. Although T_∞ is represented as a single value in borehole models, the actual ground temperature is not strictly constant with depth. Near the surface, it is affected by seasonal temperature variations, while at greater depths these fluctuations are damped out. At sufficient depth, the temperature approaches a more stable value, although it may still vary gradually due to the geothermal gradient [25].

In borehole heat exchanger analysis, T_∞ serves as the reference temperature for heat transfer between the borehole and the surrounding ground. Gehlin et al. [25] stated that the error in the estimated k value from a TRT is proportional to the error in T_∞, except when line-source models are used, as explained in more detail in Chapter 4. The influence of T_∞ on borefield sizing can be significant. Ouzzane et al. [9] calculated that using an input value of 6 $^\circ C$ instead of 10 $^\circ C$ leads to oversizing the borefield length by 37.4%. Gehlin et al. [25] showed that, depending on the method used to determine T_∞ from measurement data, the error in T_∞ can reach up to 2 $^\circ C$. Considering its influence on borefield sizing, accurate determination of T_∞ is therefore important.

2.5 Conclusion

This chapter introduced the basic geothermal context of this research. GSHP systems require vertical borehole heat exchangers to exchange heat with the ground, and the correct sizing of these borefields depends strongly on reliable ground and borehole parameters. The effective ground thermal conductivity k, effective borehole thermal resistance R_b^*, and undisturbed ground temperature T_∞ directly influence the predicted fluid temperature evolution and therefore the required borehole length. Because generic parameter values can introduce significant uncertainty, TRTs are used to determine these parameters on site.

Chapter 3

Thermal Response Tests

Thermal response tests (TRTs) were invented to more accurately determine the design parameters k, R_b^*, and T_∞ for borefield sizing, as explained in Chapter 2. The first TRT prototype was built in 1995 [10]. Since then, several types of TRTs have been introduced. This chapter first explains the general concept and operation of a TRT. It then discusses the two main TRT types: constant power TRTs and constant temperature TRTs.

3.1 Basic Principle of a TRT

A TRT is a test that evaluates the thermal response of a borehole by circulating a heated fluid through the borehole while continuously measuring the flow rate and the inlet and outlet fluid temperatures. A TRT device consists of a heater, circulation pump, connecting pipes, and temperature and flow sensors [21]. A schematic of a typical TRT setup is shown in Figure 3.1.

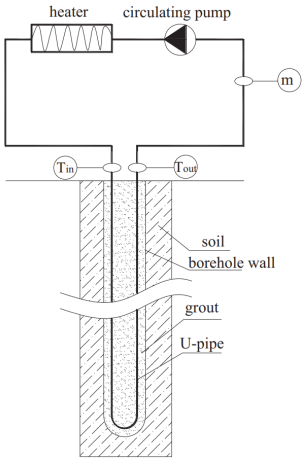


FIGURE 3.1: Schematic of a typical borehole TRT setup, showing the heater, circulation pump, flow sensor $\dot{m}$, and temperature sensors T_{in} and T_{out} connected to the borehole (Reproduced from [21]).

The measurements are used to determine the mean fluid temperature $\overline{T}_f(t)$, calculated in practice as the average of the measured inlet and outlet fluid temperatures, and the thermal power $Q(t)$ dissipated into the borehole. By fitting this data to a physical borehole model, the design parameters can be estimated [10]. The different borehole models used for this purpose are discussed in Chapter 4, while the methodology for estimating the design parameters from TRT data is explained in Chapter 5.

3.2 TRT Types

There are two main types of TRTs. Both determine the same design parameters, but are fundamentally different in their way of operating. The first and most widely used type is the constant power TRT, which keeps the thermal power injected into the borehole constant. The second and more recently developed type is the constant temperature TRT.

3.2.1 Constant Power TRT

A constant power TRT (CP-TRT) maintains a constant thermal power injected into the borehole. This is commonly achieved by keeping both the mass flow rate and the temperature difference between the inlet and outlet fluid temperatures constant. Figure 3.2 presents an example of experimental CP-TRT data from Aydin et al. [26], showing the imposed constant flow rate, temperature difference, and resulting thermal power. Although the thermal power is constant on average, the instantaneous variations can be significant, which is a well-known challenge in CP-TRTs [27].

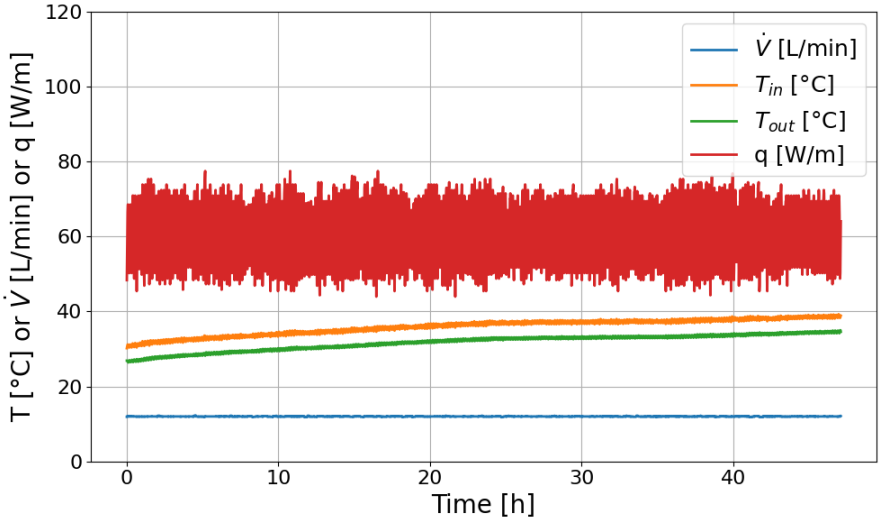


Figure 3.2: CP-TRT measurement data showing inlet temperature T_{in} [°C], outlet temperature T_{out} [°C], volumetric flow rate $\dot{V}$ [L/min], and thermal power per unit borehole length q [W/m] (Adapted from [26]).

The injected power is fixed to reach a constant heat flux at the borehole wall. This boundary condition enables the use of analytical borehole models for the interpretation of TRT results, thereby allowing the estimation of the design parameters. This is discussed in more detail in Chapter 4.

The CP-TRT is by far the most widely used type of TRT in research and industry, mainly because of several practical advantages. The test setup is relatively simple, cost-effective, and requires limited active control [13]. As the industry standard, it has been extensively studied and improved. Furthermore, it allows for straightforward mathematical analysis to determine the design parameters, as further explained in Chapter 4.

Nevertheless, CP-TRTs also have several disadvantages. The most important are the thermal power fluctuations, as shown in Figure 3.2, and the fact that a constant power input does not accurately represent actual GSHP operation. In addition, several studies indicate that CP-TRTs require more time to reach steady state, leading to longer test durations [28, 13, 29]. This directly relates to the main research question, which concerns reducing TRT duration.

3.2.2 Constant Temperature TRT

A constant temperature TRT maintains a constant fluid temperature during the test. More specifically, a constant inlet temperature TRT (CIT-TRT) imposes a constant inlet fluid temperature while maintaining a fixed mass flow rate. Figure 3.3 shows an example of CIT-TRT data from a real test, illustrating the imposed constant inlet temperature and flow rate, together with the resulting variation in outlet temperature and thermal power. By keeping the inlet temperature constant, the system evolves toward a steady-state condition characterized by a constant borehole wall temperature [30]. This boundary condition forms the basis for borehole model analysis, which is discussed in more detail in Chapter 4.

CIT-TRTs were first introduced by Wang et al. [13] in 2010. Since they are a relatively recent development, their practical adoption remains more limited than that of CP-TRTs. Nevertheless, they offer several potential advantages. Most importantly, and for this research in particular, several studies indicate that CIT-TRTs reach steady state faster [28, 13, 29], primarily because of the initially higher thermal power compared to CP-TRTs. This can be observed by comparing the CP-TRT in Figure 3.2 with the CIT-TRT in Figure 3.3, which were performed on the same borehole. The CIT-TRT measurements in Figure 3.3 show a short but much higher initial thermal power peak, which accelerates the thermal response compared to the slower response of the CP-TRT. Additional potential advantages include improved operational stability due to active control, a boundary condition that better resembles actual GSHP operation, and the potential for improved parameter estimation [29, 30].

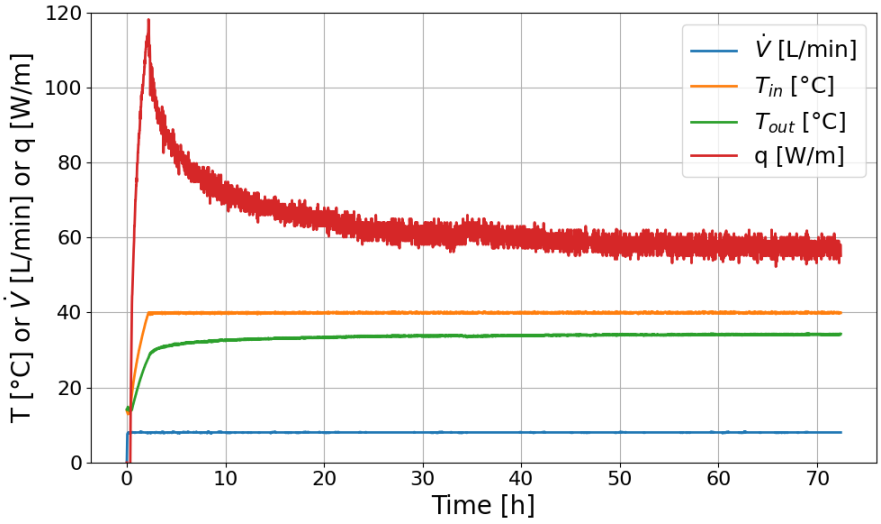


Figure 3.3: CIT-TRT measurement data showing constant inlet temperature T_{in} [°C], outlet temperature T_{out} [°C], volumetric flow rate $\dot{V}$ [L/min], and thermal power per unit borehole length q [W/m] (Adapted from [26]).

The main disadvantage of CIT-TRTs is the more complex and expensive setup, primarily due to the need for active control [13, 29]. In addition, several studies report a more complex data analysis for CIT-TRT [13, 31]. However, this limitation has been partly addressed by the methodology for estimating k proposed by Aydin et al. in 2019 [30]. Despite this progress, determining the effective borehole thermal resistance R_b^* remains significantly more challenging and less reliable for CIT-TRTs than for CP-TRTs, as discussed in more detail in Chapter 5.

It should also be noted that a flow-controlled constant temperature TRT (CT-TRT) exists, in which both inlet and outlet temperatures are maintained constant through active control of the mass flow rate. This method was introduced by Aydin et al. in 2024 [26]. Although the control becomes significantly more complex, this method shows potential because it may allow the borehole to reach steady state even faster. CIT-TRTs and CT-TRTs rely on the same underlying borehole model for parameter estimation. This research focuses only on CP- and CIT-TRTs, and not on CT-TRTs.

3.2.3 Other TRT Types

Several other TRT types have been proposed in literature. For example, Franco et al. [27] provided an overview of recent variations on classical TRT concepts. Many of these methods can be interpreted as extensions of the two main TRT types, for example by using temperature probes, performing cooling instead of heating tests, or conducting the test while drilling. Oscillating TRTs have also been proposed recently and show promising potential for reducing TRT duration [32]. These alternative TRT types are not considered further in this research.

3.3 Conclusion

This chapter introduced the general concept of thermal response testing and the two main TRT types considered in this thesis. CP-TRTs are widely used because of their simple setup, limited control requirements, and well-established analysis methods. However, they are affected by thermal power fluctuations and generally require relatively long test durations. CIT-TRTs offer several advantages, including faster thermal stabilization and boundary conditions that more closely resemble actual GSHP operation. However, these benefits come at the cost of increased control complexity and a more challenging estimation of R_b^*.

Chapter 4

Analytical Borehole Modeling

TRT measurements can only be used to estimate ground and borehole design parameters when they are interpreted with a borehole heat transfer model. These models describe the relation between the imposed thermal load, the thermal response of the borehole, and the surrounding ground properties. This chapter introduces the analytical borehole models used in TRT interpretation. First, the general heat conduction equation is presented. Then, the external borehole models for CP-TRTs and CIT-TRTs are discussed, followed by the g-function framework and the distinction between steady-state and transient internal borehole modeling.

4.1 General Heat Conduction Equation

All models discussed in this chapter are fundamentally derived from the general heat conduction equation. Equation 4.1 gives this equation for an axisymmetric case without internal heat generation [33].

$$\frac{1}{r}\frac{\partial}{\partial r}\left(r\,\frac{\partial T}{\partial r}\right)+\frac{\partial^2 T}{\partial z^2}=\frac{1}{\alpha}\,\frac{\partial T}{\partial t} \tag{4.1}$$

This transient two-dimensional heat conduction equation requires one initial condition and two boundary conditions. Initially, the borehole and the surrounding ground are assumed to be at the undisturbed ground temperature. In addition, the first boundary condition requires that the ground temperature remains equal to the undisturbed ground temperature at an infinite distance from the borehole. These conditions are expressed by Equations 4.2 and 4.3 respectively, and apply to all borehole models discussed in this chapter [33].

$$T(r, t=0)=T_\infty \tag{4.2}$$

$$\lim_{r\to\infty} T(r,t)=T_\infty \tag{4.3}$$

One additional boundary condition is required to solve the heat conduction equation. This boundary condition depends on the considered analytical model and on the type of TRT. The boundary condition for CP-TRTs is discussed in Section 4.2,

while the boundary condition for CIT-TRTs is discussed in Section 4.3.

Solving the general heat conduction equation gives an expression for the borehole wall temperature $T_b(t)$. However, TRT measurements provide the mean fluid temperature $T_f(t)$, not the borehole wall temperature $T_b(t)$. Therefore, a relation between $T_f(t)$ and $T_b(t)$ is required. This relation is commonly expressed using the effective borehole thermal resistance R_b^*, introduced in Section 2.4.2. Since R_b^* represents an effective value over the full borehole depth, the corresponding average fluid and borehole wall temperatures over the borehole depth are used, with the notation $\overline{T}_f(t)$ and $\overline{T}_b(t)$ to express the fact that they represent average values. The relation between both temperatures is shown in Equation 4.4 [34].

$$\overline{T}_f(t) = \overline{T}_b(t) + qR_b^* \tag{4.4}$$

4.2 External Borehole Models for CP-TRT

This section introduces the three basic external borehole models for the constant heat flux boundary condition, which is used for CP-TRTs. These models are called external because they describe heat transfer from the borehole wall into the surrounding ground, while neglecting the heat transfer processes within the borehole itself. The latter are captured by an internal borehole model, which relates the borehole wall temperature $\overline{T}_b(t)$ and the fluid temperature $\overline{T}_f(t)$. In its simplest form, this relationship is represented by the effective borehole resistance R_b^*. This is discussed further in Section 4.5.

The external models considered here are the Infinite Line Source (ILS), Finite Line Source (FLS), and Infinite Cylinder Source (ICS) models. For each model, the corresponding boundary condition and resulting temperature response are presented. When the expressions are written in terms of fluid temperature, the internal resistance term from Equation 4.4 is added separately [35].

4.2.1 Infinite Line Source Model

The ILS model represents the borehole as an infinitely long vertical line source. Because the borehole is assumed to be infinitely long, axial temperature variations are neglected and the problem becomes purely radial. The constant power boundary condition states that the heat flux at the borehole wall is constant. Since the borehole is represented as a line source, this boundary condition is applied at r approaching zero, as shown in Equation 4.5 [10].

$$-2\pi r k \left.\frac{\partial T}{\partial r}\right|_{r\to 0} = q \tag{4.5}$$

The exact solution for this partial differential equation is given in Equation 4.6 [33].

$$\overline{T}_f(t) = \frac{q}{4\pi k} E_1\left(\frac{r^2}{4\alpha t}\right) + qR_b^* + T_\infty \tag{4.6}$$

The exponential integral function E_1 has no elementary closed form, so for practical computation it is approximated by $E_1(x) \approx -\gamma - \ln(x)$, with γ the Euler-Mascheroni constant. This approximation is valid when the argument x is much smaller than 1, so when $t \gg \frac{r_b^2}{4\alpha}$. This leads to the long-term ILS approximation shown in Equation 4.7 [33].

$$\overline{T}_f(t) = \frac{q}{4\pi k}\left(\ln\left(\frac{4\alpha t}{r^2}\right) - \gamma\right) + q\,R_b^* + T_\infty \tag{4.7}$$

This expression is simple to evaluate and forms the basis of conventional TRT interpretation. Its mathematical simplicity explains why the ILS model remains widely used in both research and industry, as it provides reliable TRT results and can be implemented using straightforward spreadsheet calculations. However, because it is a long-term approximation, early-time TRT data has to be excluded from the analysis.

4.2.2 Finite Line Source Model

The FLS model differs from the ILS model because it represents the borehole as a line source with a finite length. As a result, axial heat transfer and boundary effects at the top and bottom of the borehole can be considered. Therefore, both radial (r) and axial (z) conduction terms in Equation 4.1 are relevant. The radial boundary condition remains the same as for the ILS model. The axial boundary conditions state that the temperature at the ground surface ($z = 0$) is the undisturbed ground temperature and the bottom of the borehole ($z = H$) is isolated, as expressed in Equations 4.8 and 4.9 [36].

$$T(r, z = 0, t) = T_\infty \tag{4.8}$$

$$\left.\frac{\partial T}{\partial z}\right|_{z=H} = 0 \tag{4.9}$$

The solution to this problem is more complex and is shown in Equation 4.10 [36].

$$\overline{T}_f(t) = T_\infty + \frac{q}{4\pi k}\int_{1/\sqrt{4\alpha t}}^{\infty} \exp(-r^2 s^2)\frac{Y(Hs, Ds)}{Hs^2}\,ds + qR_b^* \tag{4.10}$$

$$\text{with} \quad Y(h,d) = 2\,\text{ierf}(h) + 2\,\text{ierf}(h+2d) - \text{ierf}(2h+2d) - \text{ierf}(2d),$$

$$\text{and} \quad \text{ierf}(x) = x\,\text{erf}(x) - \frac{1}{\sqrt{\pi}}\left(1 - e^{-x^2}\right)$$

The FLS model is preferred over the ILS model when axial heat transfer or boundary effects at the top and bottom of the borehole become relevant. This can be important for shallow boreholes or for cases exhibiting strong axial temperature gradients [37]. The considered timescale is also important. For typical boreholes, top and bottom boundary effects are generally limited during the short timescales of TRTs, which usually last from several hours to a few days. These effects become more relevant for long-term borefield simulations over months or years [38].

4.2.3 Infinite Cylinder Source Model

The ICS model also assumes an infinitely long borehole, but represents it as a cylinder with a finite radius instead of a line source. The constant heat flux boundary condition is therefore applied at the borehole radius r_b, as shown in Equation 4.11. This leads to the analytical expression shown in Equation 4.12, which is typically evaluated numerically [35].

$$-2\pi r k \left.\frac{\partial T}{\partial r}\right|_{r=r_b} = q \tag{4.11}$$

$$\overline{T}_f(t) = T_\infty + \frac{q}{\pi^2 k}\int_0^\infty \frac{e^{-u^2 \mathrm{Fo}} - 1}{u^2\left[J_1^2(u) + Y_1^2(u)\right]}\left[J_0(\rho u)Y_1(u) - J_1(u)Y_0(\rho u)\right]\, du + qR_b^* \tag{4.12}$$

The advantage of the ICS model is that it represents the borehole geometry more realistically, since an actual borehole has a finite cylindrical radius rather than the zero radius assumed in a line-source model. This introduces a larger modeled heat transfer area, which can improve accuracy when the ICS model is coupled to a short-term model, as discussed in Chapter 6. However, without such a short-term correction, the model can overestimate the heat transfer. At sufficiently long times, when the thermal response inside the cylinder approaches steady state, the ILS and ICS models show similar behavior. During transient conditions, however, the finite borehole radius can lead to significant differences between both models [11].

4.3 External Borehole Model for CIT-TRT

This section introduces the external borehole model used for CIT-TRTs. This framework is based on the solution proposed by Aydin et al. [30]. This approach is based on a constant temperature boundary condition and leads to an ILS-like formulation for interpreting CIT-TRT data. The constant temperature boundary condition states that the borehole wall temperature is kept constant at the borehole radius r_b, as shown in Equation 4.13.

$$T(r = r_b, t) = \overline{T}_b = \text{constant} \tag{4.13}$$

Solving the heat conduction equation with this boundary condition gives the analytical constant temperature solution shown in Equation 4.14. In this expression, $q(t)$ is the time-dependent thermal power per unit borehole length, k is the effective ground thermal conductivity, α is the ground thermal diffusivity, and γ is the Euler–Mascheroni constant.

$$\frac{1}{q(t)} = \frac{1}{4\pi k\left(\overline{T}_f - T_\infty\right)}\left[\ln(t) + \ln\left(\frac{4\alpha}{e^\gamma (r_b)^2}\right)\right] \tag{4.14}$$

This formulation is analogous to the long-term ILS solution used for CP-TRTs, but the dependent variable changes. In a CP-TRT, the fluid temperature increases approximately linearly with $\ln(t)$ under constant heat injection. In a CIT-TRT,

the inverse thermal power $1/q(t)$ increases approximately linearly with $\ln(t)$ under constant temperature conditions. Consequently, a linear regression of $1/q(t)$ versus $\ln(t)$ can be used to estimate the ground thermal conductivity k, as discussed in Chapter 5 [30].

4.4 G-functions

The g-function was introduced by Eskilson and Claesson [39] as a generalized, dimensionless representation of external borehole heat transfer. It describes the transient response of the borehole wall temperature $\overline{T}_b(t)$ to a thermal power per unit borehole length q, relative to the undisturbed ground temperature T_∞. In essence, the g-function is a normalized solution of the ground heat conduction equation, separated from the ground thermal conductivity. It is defined in Equation 4.15 [39].

$$\overline{T}_b(t) - T_\infty = \frac{q}{2\pi k}\, g(t) \tag{4.15}$$

The main advantage of the g-function formulation is that it provides a unified framework for describing different external borehole models. Instead of solving the heat conduction equation separately for each case, the thermal response can be represented by a response function $g(t)$, which depends on borehole geometry, boundary conditions, and timescale [35]. This makes it possible to compare different analytical borehole models within the same mathematical framework.

The g-function framework does not introduce a fundamentally new external borehole model. Rather, it reformulates the previously discussed analytical solutions into a dimensionless response-function form. This allows the ILS, FLS, and ICS solutions to be evaluated consistently, with the model differences contained in the corresponding g-functions. Parameter estimation and model comparison can therefore be performed using the same general equation while changing only the selected response function.

For the ILS, FLS, and ICS models, the corresponding g-functions are given by Equations 4.16, 4.17, and 4.18 [35].

$$g_{\mathrm{ILS}}(r,t) = \frac{1}{2}\, E_1\!\left(\frac{r^2}{4\alpha t}\right) \tag{4.16}$$

$$g_{\mathrm{FLS}}(r,t;H,D) = \frac{1}{2}\int_{1/\sqrt{4\alpha t}}^{\infty} \exp\!\left(-r^2 s^2\right) \frac{Y(Hs,Ds)}{H\, s^2}\, \mathrm{d}s \tag{4.17}$$

$$g_{\mathrm{ICS}}(r,t) = \frac{2}{\pi}\int_0^{\infty} \frac{e^{-s^2 \mathrm{Fo}} - 1}{s^2\left[J_1^2(s) + Y_1^2(s)\right]} \left[J_0(\mu s)\, Y_1(s) - J_1(s)\, Y_0(\mu s)\right] \mathrm{d}s \tag{4.18}$$

However, the g-function framework only describes external ground heat conduction and thus provides the borehole wall temperature response, whereas TRT measurements do not directly measure the borehole wall temperature but rather the fluid

temperature inside the borehole pipes. Therefore, an internal borehole model is required to relate the borehole wall temperature to the measured fluid temperature. This is discussed further in Section 4.5.

4.5 Internal Borehole Model

The external borehole models discussed previously describe heat conduction in the ground surrounding the borehole, whereas internal borehole models describe the heat transfer between the circulating fluid and the borehole wall. Inside the borehole, heat is transferred through the fluid, pipe walls, and grout before reaching the surrounding ground. Depending on the required level of detail, this internal heat transfer can be represented either by a simplified steady-state thermal resistance model or by a more detailed transient model that also accounts for heat storage inside the borehole components. This section only covers the internal borehole models for CP-TRTs, as literature on CIT-TRTs does not cover this.

4.5.1 Steady-State Internal Borehole Model

Under steady-state conditions, the thermal interaction between the circulating fluid and the borehole wall is commonly represented by the effective borehole thermal resistance R_b^*, previously introduced in Equation 4.4. This parameter combines the thermal resistances associated with fluid convection, pipe conduction, and grout conduction into one effective resistance term [8].

By combining the steady-state internal resistance model in Equation 4.4 with the external g-function framework in Equation 4.15, the commonly used TRT formulation shown in Equation 4.19 is obtained [35].

$$\overline{T}_f = T_\infty + \frac{q}{2\pi k} g(t) + q R_b^* \tag{4.19}$$

This formulation assumes that the internal borehole heat transfer can be represented by a steady-state effective thermal resistance. Once the g-function is known, both k and R_b^* can be determined through linear regression, as discussed in Chapter 5.

The steady-state resistance approach is most commonly used in conventional TRT analysis because parameter estimation usually focuses on long-term data, where short-term transient effects inside the borehole have largely decayed. Consequently, short-term TRT data is often excluded when using the conventional long-term approximation ILS model.

4.5.2 Transient Internal Borehole Model

During short-term operation, transient thermal capacitances inside the borehole can become important. In that case, the assumption of an instantaneous steady-state thermal resistance becomes less accurate, since heat is temporarily stored in the

fluid, pipes, and grout. Transient internal borehole models include thermal capacitances to capture the time-dependent thermal behavior inside the borehole. These models are particularly relevant when analyzing short-term TRT data or when attempting to reduce the required TRT duration [20].

Since this research focuses on reducing TRT duration by using short-term measurement data, transient internal borehole modeling plays a central role. The transient model used in this research is discussed in Chapter 6.

4.6 Conclusion

This chapter introduced the analytical borehole models used to interpret TRT measurements. For CP-TRTs, the ILS, FLS, and ICS models describe the external ground response under a constant heat flux boundary condition. For CIT-TRTs, a constant-temperature formulation is used. The g-function framework provides a consistent way to compare these external models, but an internal borehole model is still required to relate borehole wall temperature to measured fluid temperature. This distinction between external ground response and internal borehole behavior is essential for understanding the transient model introduced in Chapter 6.

Chapter 5

TRT Parameter Estimation

This chapter presents the methodologies used to estimate the key parameters k, R_b^*, and T_∞ from TRT measurement data for both CP- and CIT-TRTs. For CP-TRTs, the methodology is well established and extensively documented in literature. In contrast, literature on CIT-TRTs is less extensive and mainly focuses on k, while a clear methodology for R_b^* is absent.

Section 5.1 first discusses the determination of the undisturbed ground temperature T_∞, which is independent of the TRT type and therefore identical for CP- and CIT-TRTs. Section 5.2 then explains the estimation of the effective thermal conductivity k using the analytical models introduced in Chapter 4. Finally, Section 5.3 addresses the determination of the effective borehole thermal resistance R_b^*.

5.1 Undisturbed Ground Temperature T_∞

As introduced in Chapter 2, the undisturbed ground temperature T_∞ represents the natural ground temperature unaffected by heat transfer from the borehole. Although T_∞ is commonly described as one of the three main parameters obtained from TRT analysis, it is usually determined prior to the actual TRT itself. Consequently, the methodology for estimating T_∞ is independent of the TRT type and is therefore the same for CP- and CIT-TRTs. For accurate determination of T_∞, the fluid inside the borehole pipes should initially be in thermal equilibrium with the surrounding ground. Ideally, the borehole should remain filled with water for sufficient time before the TRT starts [25].

Gehlin and Nordell [25] reported two main methods for determining T_∞. The first method involves direct temperature profiling by lowering a temperature probe into the borehole and is called direct temperature profiling. The second method consists of circulating fluid through the borehole without activating the heating system and is therefore called fluid circulation profiling.

The first method, using a temperature probe, is the fastest and most accurate approach. In addition, it allows the vertical temperature profile to be determined when measurements are taken consistently along the full borehole depth [25]. The second method consists of circulating fluid through the borehole using the TRT setup itself, without activating the heater. This approach is operationally simpler and cheaper, since no additional equipment beyond the TRT device is required. Initially, temperature fluctuations occur because the fluid circulation disturbs the thermal equilibrium within the borehole, where temperature varies with depth. As circulation continues, the inlet and outlet fluid temperatures gradually converge to a stable value representative of the undisturbed ground temperature [25].

Figure 5.1 shows this second method from the work of Gehlin and Nordell [25] for a 30 m borehole. Initially, temperature fluctuations occur because circulation mixes thermally stratified water layers inside the borehole, where the ground temperature varies with depth. As circulation continues, the mixing gradually reduces these fluctuations and the inlet and outlet temperatures converge to a stable mean value representative of the undisturbed ground temperature. A stable temperature of 11.8 $°C$ was reached after 20 minutes, corresponding to the value measured with the probe. Continued circulation increased the measured temperature to 12.2 $°C$ after 30 minutes and 13.8 $°C$ after 60 minutes due to heat gain from the circulation pump. These differences are significant, especially considering the importance of T_∞ for borefield sizing, as discussed in Section 2.4.3. Gehlin and Nordell [25] therefore concluded that approximately 20 minutes of circulation provided the most satisfactory result for their setup. They also stated that the influence of pump heating and ambient conditions becomes less significant for deeper boreholes and lower mass flows.

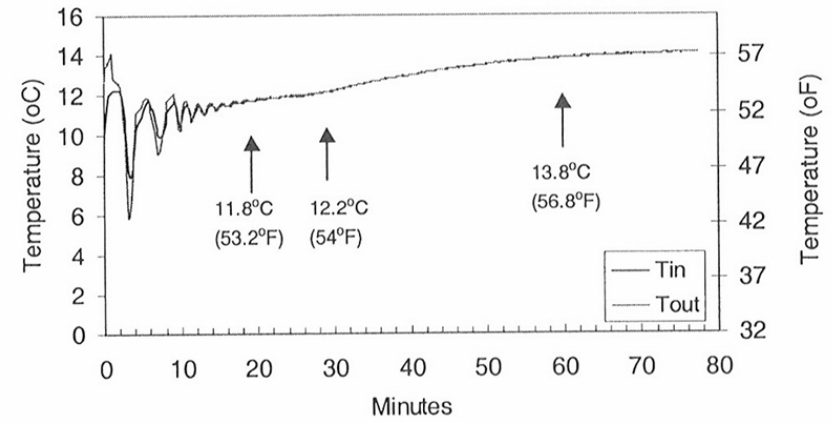


Figure 5.1: Temperature logging of the fluid inlet and outlet temperatures at 10-second intervals (Reproduced from [25]).

In summary, T_∞ can be determined either by direct temperature profiling or by fluid circulation without thermal injection. Temperature profiling is generally faster

and more accurate, but requires additional equipment. Fluid circulation is simpler and cheaper, as it uses the TRT setup itself, but is generally less accurate and more sensitive to disturbances, while also providing an average value and not an actual temperature profile.

5.2 Effective Thermal Conductivity k

The methodology for determining the effective thermal conductivity k is similar for both CP- and CIT-TRTs. The fundamental difference lies in the analytical solution used as the basis for parameter estimation, as discussed in Section 4.2.1. In practice, both methods typically rely on a long-term approximation for easier computation. Section 5.2.1 discusses the determination of k for CP-TRTs, while Section 5.2.2 addresses the methodology for CIT-TRTs.

5.2.1 Effective Thermal Conductivity k for CP-TRTs

For CP-TRTs, the long-term ILS approximation results in a linear relation between the mean fluid temperature $\overline{T}_f(t)$ and $\ln(t)$, which forms the basis for estimating k and R_b^*. The long-term ILS approximation introduced in Chapter 4 as Equation 4.7 is repeated here as Equation 5.1. The other models introduced in Chapter 4, such as the FLS and ICS models, could also be used, but they introduce greater mathematical complexity. For this reason, the long-term approximation of the ILS model is the most widely used in industry and thus the most relevant reference for comparison.

$$\overline{T}_f(t) = \frac{q}{4\pi k}\left(\ln\left(\frac{4\alpha t}{r_b^2}\right) - \gamma\right) + q\,R_b^* + T_\infty \tag{5.1}$$

During the TRT, the inlet and outlet fluid temperatures, as well as the flow rate, are continuously measured. The mean fluid temperature $\overline{T}_f(t)$ is calculated as the average of the borehole inlet and outlet fluid temperatures. Strictly speaking, $\overline{T}_f(t)$ is therefore not the actual mean fluid temperature over the full borehole length. From this point onward, it is referred to as the mean fluid temperature for simplicity. The thermal power per unit borehole length q is calculated as the product of the mass flow rate, fluid heat capacity, and fluid temperature difference over the borehole, divided by the borehole length. In a CP-TRT, this thermal power should remain constant [10].

To estimate k, a linear regression is performed between the measured mean fluid temperature $\overline{T}_f(t)$ and $\ln(t)$. This gives a slope a and intercept b, such that $\overline{T}_f(t)$ equals $a \cdot \ln(t) + b$. Combined with Equation 5.1, k is then given by Equation 5.2.

$$k = \frac{q}{4\pi a} \tag{5.2}$$

Thus, the thermal conductivity k is obtained from the TRT measurement data $\overline{T}_f(t)$, $\ln(t)$, and q. Figure 5.2 shows an example of this linear fitting procedure for CP-TRT data from Aydin et al. [26]. Only the later-time region of the TRT data should

be used for the linear regression. The horizontal axis is logarithmic, representing $\ln(t)$. At early times, short-term transient effects inside the borehole still significantly influence the thermal response, causing deviations from the linear behavior predicted by the long-term ILS approximation. In conventional TRT analysis, a cutoff time of approximately 10 hours is often assumed sufficient for these transient effects to have largely decayed. This is visible in Figure 5.2, where the data begins to follow an approximately straight line after the early-time region. Once these transient effects have sufficiently decayed, the relation between $\overline{T}_f(t)$ and $\ln(t)$ becomes approximately linear, allowing k to be estimated from the fitted slope [26].

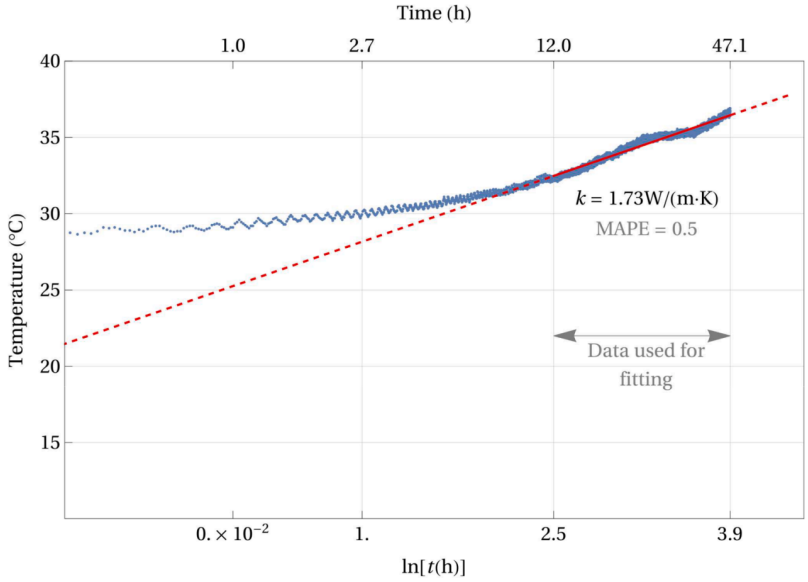


Figure 5.2: Mean fluid temperature $\overline{T}_f(t)$ [°C] as a function of $\ln(t)$, with t in hours, for CP-TRT data, including the linear fit with slope $\frac{q}{4\pi k}$ (Reproduced from [26]).

5.2.2 Effective Thermal Conductivity k for CIT-TRTs

For CIT-TRTs, the same general regression principle is applied, but starting from the constant temperature solution instead of the constant power solution. The constant temperature solution introduced in Chapter 4 as Equation 4.14 is repeated here as Equation 5.3.

$$\frac{1}{q(t)} = \frac{1}{4\pi k \left(\overline{T}_f - T_\infty\right)} \left[\ln(t) + \ln\left(\frac{4\alpha}{e^\gamma (r_b)^2}\right)\right] \tag{5.3}$$

The measured quantities are obtained similarly to CP-TRTs, but the key difference is that the thermal power per unit borehole length $q(t)$ is now variable over time, while the mean fluid temperature $\overline{T}_f$ is assumed to be constant. For a CIT-TRT, only the inlet temperature is actively controlled to remain constant, while the outlet temperature evolves over time. However, because the outlet temperature typically

stabilizes relatively quickly, treating the mean fluid temperature as approximately constant is considered a reasonable approximation [26].

To estimate k, a linear fit is performed between $\frac{1}{q(t)}$ and $\ln(t)$. This results in a slope a and intercept b, such that $\frac{1}{q(t)}$ equals $a \cdot \ln(t) + b$. Combined with Equation 5.3, k is then given by Equation 5.4.

$$k = \frac{1}{4\pi a(\overline{T}_f - T_\infty)} \tag{5.4}$$

Figure 5.3 illustrates this procedure for CIT-TRT data from Aydin et al. [26] and shows that the inverse thermal power $\frac{1}{q(t)}$ increases approximately linearly with $\ln(t)$. Similar to the CP-TRT case, only the later-time region is used for fitting to reduce the influence of short-term transient effects. Compared to Figure 5.2, the data appears to approach the linear region slightly earlier, which suggests that CIT-TRTs may reach steady state faster and could therefore allow shorter test durations compared to CP-TRTs. However, the deviations from the fitted linear trend also appear slightly larger, indicating a somewhat less stable linear behavior.

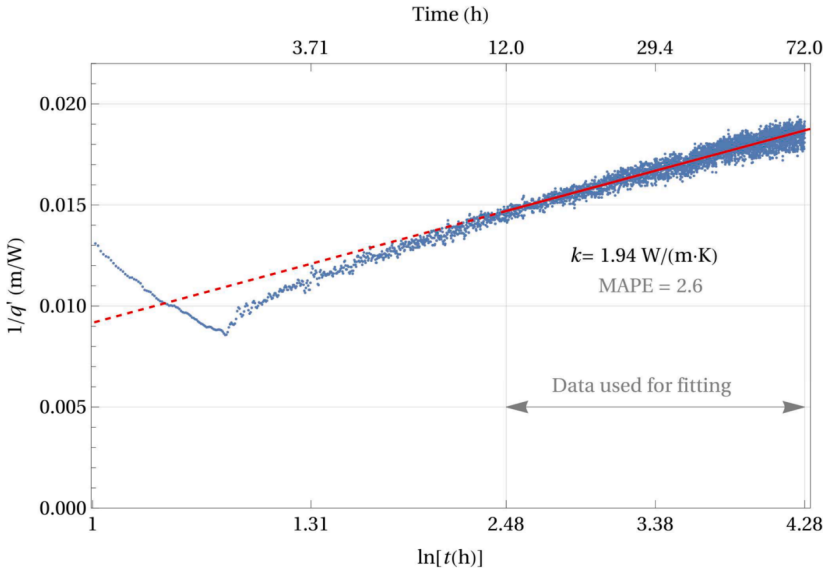


FIGURE 5.3: Inverse thermal power per unit borehole length $\frac{1}{q(t)}$ [m/W] as a function of $\ln(t)$, with t in hours, for CIT-TRT data, including the linear fit with slope $\frac{1}{4\pi k(\overline{T}_f - T_\infty)}$ (Reproduced from [26]).

5.3 Effective Thermal Borehole Resistance R_b^*

While the thermal conductivity k can be obtained directly from the slope of the linear fit, determining the effective borehole thermal resistance R_b^* is more complex.

Multiple estimation approaches exist, with important differences between CP- and CIT-TRTs. Two commonly used methods are discussed here. Section 5.3.1 introduces the intercept method, which is based on TRT measurement data but is only applicable to CP-TRTs. Section 5.3.2 then discusses the multipole method, an a priori approach that is independent of TRT type and can therefore be applied to both CP- and CIT-TRTs.

5.3.1 Intercept Method

The intercept method determines R_b^* from the same linear regression used to estimate k. Instead of using the slope a, it uses the intercept b. This method is only possible for CP-TRTs because R_b^* explicitly appears in the heat transfer solution shown in Equation 5.1. So, for CP-TRTs, R_b^* is calculated as shown in Equation 5.5.

$$R_b^* = \frac{(b - T_\infty)}{q} - \frac{1}{4\pi k}\left[\ln\left(\frac{4\alpha}{r_b^2}\right) - \gamma\right] \tag{5.5}$$

This method is straightforward and remains the standard approach for estimating R_b^* from CP-TRT data. However, it cannot be applied to CIT-TRT data, as the constant temperature solution shown in Equation 5.3 does not contain an explicit R_b^* term. As a result, no equivalent intercept-based formulation exists for CIT-TRT data.

5.3.2 Multipole Method

The multipole method is fundamentally different from the intercept method because it does not derive R_b^* from TRT measurement data. Instead, it is an a priori method used to estimate borehole thermal resistance based solely on borehole geometry and material properties. It is commonly applied during borehole design and modeling, before drilling. It is therefore more theoretical than the intercept method, but becomes relevant for CIT-TRTs, for which the intercept method is not applicable [8].

The multipole method consists of constructing a thermal resistance network of the borehole components, including pipe wall resistance, fluid-to-pipe convection resistance, and grout resistance. The combined resistance between the circulating fluid and the borehole wall over the entire borehole depth is then defined as the effective borehole thermal resistance R_b^* [8].

Because the multipole method does not depend on TRT operating conditions or measurement data, it is independent of TRT type. In theory, if all borehole parameters and ground properties are perfectly known, the R_b^* value from the multipole method should align with that of the intercept method. In practice, discrepancies arise due to uncertainties in construction details, material properties, installation quality, and measurement errors.

5.4 Conclusion

This chapter described how the main TRT parameters are estimated from measurement data. The undisturbed ground temperature T_∞ is determined before the actual TRT, either by temperature profiling or by circulation without heat injection. The effective thermal conductivity k can be estimated from both CP- and CIT-TRT data using linear regression based on the corresponding analytical solution. In contrast, the effective borehole thermal resistance R_b^* is straightforward to obtain from CP-TRTs using the intercept method, while for CIT-TRTs no equivalent measurement-based intercept formulation is available, making the multipole method the most practical alternative.

Chapter 6

Transient Borehole Modeling

This chapter introduces the transient borehole model used in this research. First, the need for transient borehole modeling is explained by discussing the limitations of conventional TRT interpretation during the early-time period. Then, the Short Term Solution model is introduced, including the hybrid g-function formulation, the construction of the long-term and short-term response functions, and the practical input requirements of the model.

6.1 Motivation for Transient Borehole Modeling

The borehole models discussed in Chapter 4 are commonly used for TRT interpretation, but they do not capture the short-term transient behavior inside the borehole. In conventional analysis, the internal borehole heat transfer is represented by a steady-state borehole resistance, while the external ground response is described using simplified analytical boundary conditions. For CP-TRTs this corresponds to a constant heat flux at the borehole wall, and for CIT-TRTs to a constant borehole wall temperature.

In practice, these idealized boundary conditions are not established immediately at the start of a TRT. During the initial phase, heat is partly stored in the fluid, pipe, and grout before propagating fully into the surrounding ground. The measured fluid temperature is therefore influenced by transient heat storage and heat transfer inside the borehole. This is referred to as the transient borehole response. For this reason, conventional TRT analysis applies a cutoff time to exclude early-time data affected by transient behavior. This cutoff time is typically around 10 hours. As a result, a significant part of the measured TRT data is discarded [10].

If these transient effects can be modeled reliably, early-time data can be included in the parameter estimation. This may reduce the total required TRT duration and thereby decrease the operational cost of performing TRTs, which is one of the main objectives of this research.

6.2 Limitations of Classical Models

6.2.1 Long-term ILS approximation

As discussed in Chapter 4, the long-term ILS approximation is widely used in industry for TRT parameter estimation due to its mathematical simplicity. However, this formulation is a long-term asymptotic approximation and is therefore not suitable for describing short-term transient effects. Consequently, reliable application requires a sufficiently large cutoff time, leaving a substantial part of the TRT data unused.

6.2.2 Exact ILS, FLS, and ICS models

Chapter 4 also introduced the exact (without long-term approximation) ILS, FLS, and ICS models. Although these models remove the mathematical restriction of the long-term ILS approximation, they still have an important physical limitation: they do not account for transient heat storage and heat transfer inside the borehole. At the start of a TRT, thermal energy is first stored in and transferred through the fluid, pipe, and grout before affecting the surrounding ground.

The previously introduced ILS, FLS, and ICS models do not include these internal transient effects, which makes them insufficient for reliably describing the earliest TRT period. If short-term borehole effects can be modeled reliably, the early-time data that is normally excluded can be used for parameter estimation. This may significantly reduce the required test duration. The model used in this research to incorporate these effects is the Short Term Solution model, introduced in Section 6.3.

6.3 Short Term Solution Model

The transient model used in this research is based on the model of Meertens et al. [20, 40] and is implemented in GHEtool, in the Issue26-branch [41]. This model extends the classical g-function framework by constructing a hybrid g-function that combines long-term and short-term borehole effects.

6.3.1 Hybrid g-function

This model still uses the same equation as in Chapter 4, specifically Equation 4.19, repeated here as Equation 6.1. The fitting procedure to determine k and R_b^* explained in Chapter 5 remains exactly the same. The difference lies in the calculation of the g-function.

$$\overline{T}_f(t) = T_\infty + \frac{q}{2\pi k} g(t) + q R_b^* \tag{6.1}$$

The hybrid g-function combines a long-term and short-term g-function, as shown in Equation 6.2.

$$g(t) = \begin{cases} g_{ST}(t), & t \leq t_{\text{switch}} \\ g_{LT}(t), & t > t_{\text{switch}} \end{cases} \tag{6.2}$$

In this way, the model combines the physically more detailed short-term response with the more computationally efficient long-term analytical formulation. The switching time t_{switch} is defined as the point in time where $g_{ST}(t)$ and $g_{LT}(t)$ first meet, ensuring continuity between both parts of the hybrid g-function. Section 6.3.2 explains how $g_{LT}(t)$ is constructed, while Section 6.3.3 discusses $g_{ST}(t)$.

6.3.2 Long-term g-function g_{LT}

The long-term g-function $g_{LT}(t)$ is based on an analytical formulation derived from the ILS, FLS, and ICS models. It combines these models as shown in Equation 6.3.

$$g_{LT}(t) = g_{FLS}(t) + (g_{ICS}(t) - g_{ILS}(t)) \tag{6.3}$$

This formulation, originally proposed by Li et al. [42], consists of the FLS g-function $g_{FLS}(t)$ corrected by the term $(g_{\text{ICS}}(t) - g_{\text{ILS}}(t))$. This correction replaces the inaccurate short-time line-source behavior of the ILS model with the finite-radius behavior of the ICS model, while preserving the long-term behavior of the FLS formulation. Li et al. [42] showed that this model performs better over a broad time range, including both short- and long-term behavior. Since TRTs typically last only a few days, they mainly fall within the short-term regime. Therefore, FLS and ILS are expected to give similar results for typical TRT timescales, so this formula will typically give a value close to $g_{ICS}(t)$ for TRT application.

6.3.3 Short-term g-function g_{ST}

The short-term g-function $g_{ST}(t)$ is based on a numerical finite volume model that represents the borehole by a one-dimensional radial discretization. The model assumes radial heat transfer only and neglects axial heat transfer. In this specific model [20], the discretization consists of three fluid cells, one convection layer cell, four pipe cells, 27 grout cells, and 300 soil cells. Figure 6.1 schematically shows the fluid, pipe, grout, and soil regions next to each other.

Transient energy conservation is applied to each cell individually, allowing the model to resolve time-dependent heat storage and heat transfer throughout the radial borehole structure. This results in a transient fluid temperature response $\overline{T}_f(t)$, which is used to compute the short-term g-function $g_{ST}(t)$ using Equation 6.4.

$$g_{ST}(t) = 2\pi k \left(\frac{\overline{T}_f(t) - T_\infty}{q} - R_b^* \right) \tag{6.4}$$

Equation 6.4 is obtained by rearranging the governing TRT temperature equation shown in Equation 6.1. In this formulation, the term qR_b^* already accounts separately for the steady-state thermal resistance between the fluid and the borehole wall. Therefore, R_b^* is subtracted again in Equation 6.4 to avoid including this resistance contribution twice in the short-term g-function $g_{ST}(t)$.

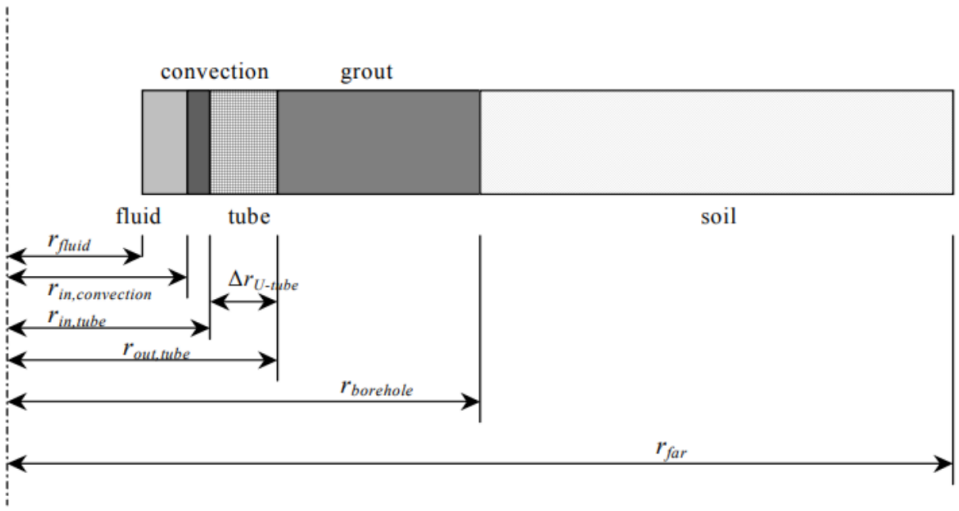


Figure 6.1: Schematic overview of the radial borehole discretization used for modeling short-term effects, showing the fluid, pipe, grout, and soil regions (Reproduced from [20], originally from [19]).

6.3.4 Practical Implications

Compared to classical analytical borehole models, the short-term model requires substantially more input parameters. In addition to the borehole geometry, accurate characterization of the fluid, pipe, grout, and ground properties is required. The ground thermal conductivity is initially unknown, since determining this parameter is one of the main purposes of conducting TRTs, and therefore it needs to be estimated iteratively. Table 6.1 summarizes the required input data for the STS model.

This increased parameter dependence introduces additional uncertainty and computational complexity. However, it also enables a more physically detailed representation of the transient TRT period. If the additional input parameters are sufficiently well characterized, the model can potentially support reliable parameter estimation at earlier time points and thereby reduce the required TRT duration.

6.4 Conclusion

This chapter introduced the added value of transient borehole modeling and described the STS model used in this thesis. Classical analytical models are insufficient for the earliest TRT period because they do not represent transient heat storage inside the borehole. The hybrid g-function approach combines a short-term finite volume model with a long-term analytical response, allowing early-time data to be included in the parameter estimation. This improved physical representation comes at the cost of additional input parameters and increased model uncertainty.

Table 6.1: Required input data for the STS borehole model.

Category	Symbol	Description
Ground	T_∞	Undisturbed ground temperature
	α	Ground thermal diffusivity
	k	Ground thermal conductivity
Fluid	$\dot{m}$	Mass flow rate per borehole
	k_f	Fluid thermal conductivity
	ρ_f	Fluid density
	$c_{p,f}$	Fluid specific heat capacity
	η	Fluid dynamic viscosity
Borehole	H	Borehole length
	D	Borehole burial depth
	r_b	Borehole radius
	k_g	Grout thermal conductivity
	$(\rho c_p)_g$	Grout volumetric heat capacity
	r_{in}	Pipe inner radius
	r_{out}	Pipe outer radius
	k_p	Pipe thermal conductivity
	$(\rho c_p)_p$	Pipe volumetric heat capacity
	D_s	Shank spacing
	n_p	Number of U-tubes
	ϵ	Pipe roughness

Part II

Setup

Chapter 7

TRT Device for Field Testing

For this research, a TRT device was designed and developed to generate original field data and enable direct comparison between CP-TRTs and CIT-TRTs on the same borefield. This included the design and selection of the main components, supervision of the device assembly, execution of the field tests, and subsequent analysis of the experimental results. The device was funded and is owned by LOBO Geothermische Boringen [43], a Belgian drilling company that also carried out the assembly.

This chapter discusses the design requirements that formed the basis of the device development in Section 7.1, the overall system layout in Section 7.2, the main components in Section 7.3, and the most important practical design challenges encountered during field operation in Section 7.4.

7.1 Design Requirements

The general TRT concept was introduced in Chapter 3 and formed the basis for the design of the TRT device. The essential components are a heater, circulation pump, connecting pipes, and measurement sensors. A buffer tank was included to damp short-term temperature fluctuations generated by the heater, thereby improving the stability of the temperature measurements. In addition, all pipes were insulated to reduce heat losses to the environment and limit the influence of ambient temperature, as explained in more detail in Section 7.4.

A primary design requirement was that the device had to operate in both constant power and constant temperature modes. This dual functionality was necessary to allow direct experimental comparison between CP-TRTs and CIT-TRTs using the same TRT setup. The design was inspired by the multifunctional TRT device proposed by Aydin et al. [26], which also enabled multiple TRT operating modes within one device.

The fundamental difference between CP-TRTs and CIT-TRTs is the control strategy. The selected heater was therefore required to maintain either a constant thermal power setpoint or a constant temperature setpoint. A possible future extension of the TRT system is the implementation of active flow rate control. This would make it possible to control not only the borehole inlet fluid temperature, but also the outlet temperature, by varying the pump flow rate. This type of flow-controlled constant temperature TRT is the main subject of the research of Aydin et al. [26], but was considered beyond the scope of this research.

7.2 System Layout

Figure 7.1 presents a conceptual schematic of the TRT system design, including the electric heater, buffer tank, circulation pump, borehole, flow meter, and temperature sensors. The system layout was designed to provide stable thermal operation while measuring the key variables required for TRT analysis.

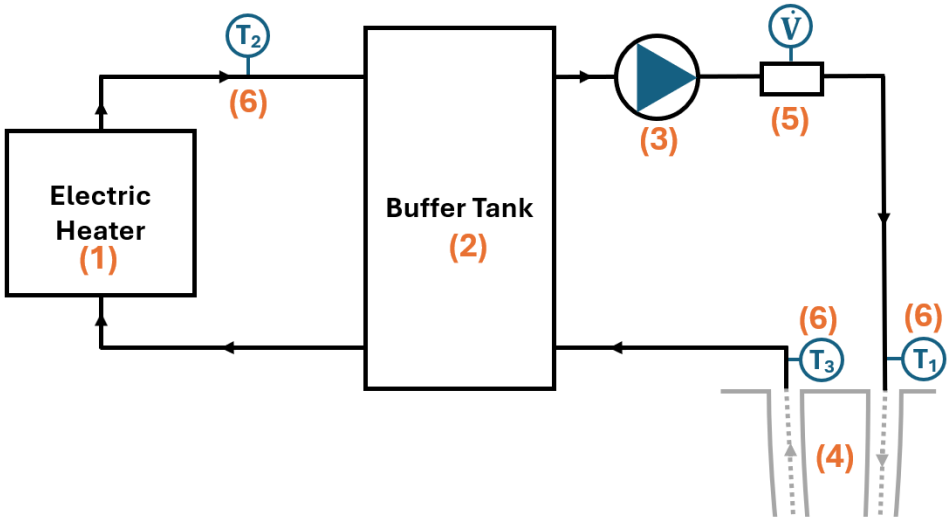


Figure 7.1: Schematic overview of the TRT system design used for this research, showing the electric heater (1), buffer tank (2), circulation pump (3), borehole (4), flow meter (5), and temperature sensors (6).

The placement of the temperature sensors and flow meter was carefully considered. The borehole inlet and outlet fluid temperatures are measured by T_1 and T_3, respectively. The volumetric flow rate $\dot{V}$ is measured using a flow meter installed in series with the circulation pump. These measurements allow the injected thermal power to be calculated from the fluid temperature difference over the borehole, the volumetric flow rate, the fluid density, and the specific heat capacity.

In addition to T_1 and T_3, the heater outlet fluid temperature T_2 was also measured. This temperature, also referred to as the heater supply temperature, is the control

variable actively maintained by the heater during constant temperature operation and is therefore particularly important for CIT-TRTs.

7.3 Components

Figure 7.2 shows the TRT device. It is installed inside a mobile container for practical transportation and on-site deployment. This setup contains all previously discussed components: the electric heater, the buffer tank, the circulation pump, the flow meter, the temperature sensors, as well as a control system and data acquisition system.

This section discusses the component selection for the TRT device, which was based on functional requirements, control flexibility, measurement reliability, and cost. Since the reliability of TRT results strongly depends on stable and accurate measurements, careful component selection was a critical part of the overall system design. The following subsections discuss the most important components in more detail, together with the reasoning behind their selection and integration.

7.3.1 Electric Heater

For the electric heater, the Vaillant eloBLOCK VE 9 electric wall heater [44] was selected, with a maximum thermal power output of 9 kW. This heater was chosen primarily because it can operate with both constant power and constant temperature setpoints, which are required for CP-TRTs and CIT-TRTs, respectively. The maximum power of 9 kW was considered sufficient for this application.

An important advantage is its ability to modulate thermal power in 1 kW increments. During CP-TRTs, this allows controlled heat injection, while during CIT-TRTs it allows the heater to maintain a fixed supply temperature T_2. This dual functionality made it suitable for performing both TRT methods using the same device. An electric heater was also preferred for practical reasons, since it only requires an electrical power supply.

7.3.2 Buffer Tank

A relatively large buffer tank was intentionally included in the device design, although such tanks are often absent or considerably smaller in many CP-TRT systems. The selected unit was the Vaillant allSTOR plus VPS 300/3 [45], with a total volume of 303 L. This volume is substantial compared to the approximate fluid volume within the borehole pipes, which is around 100 L.

The main purpose of the buffer tank was to damp short-term temperature fluctuations, particularly those caused by the heater. This temperature stability, resulting from thermal inertia, is particularly relevant for CIT-TRT operation, where the objective is to maintain a constant fluid temperature. Since this is less critical for

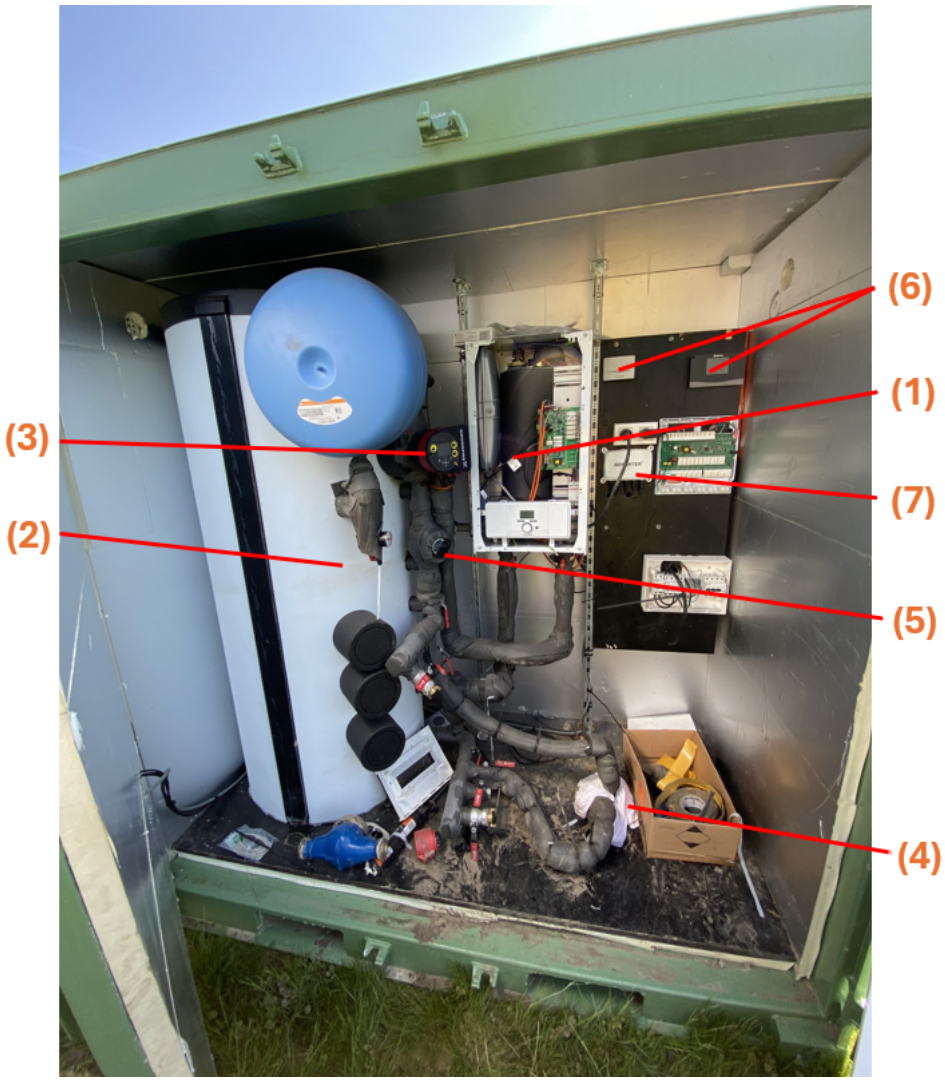


Figure 7.2: Image of the TRT device installed inside the insulated container, showing the electric heater (1), buffer tank (2), circulation pump (3), borehole entrance (4), flow meter (5), control system (6), and data acquisition system (7).

CP-TRTs, which are the most common TRT type, buffer tanks are often absent in typical TRT devices. In addition, the larger thermal mass reduces the relative influence of pump heating on the circulating fluid, which is especially useful when determining the undisturbed ground temperature T_∞.

However, the large buffer tank also introduces several disadvantages. First, determining T_∞ through fluid circulation becomes more challenging, since the measured fluid temperature is influenced not only by the water in the borehole, but also by the larger volume of water inside the buffer tank. This effect is especially relevant when the ambient temperature differs significantly from the ground temperature. For this

reason, adding a bypass around the buffer tank would be useful in future versions of the setup, as it would allow T_∞ to be measured more reliably. Furthermore, the large buffer tank increases the investment cost of the device, as well as transport costs due to its size and weight, and operational costs due to the increased amount of water that must be heated. Overall, the buffer tank represents a clear trade-off between improved thermal stability, mainly important for CIT-TRT operation, and increased system complexity and cost.

7.3.3 Circulation Pump

The circulation pump is a crucial component of the TRT device, as it ensures continuous fluid circulation through the hydraulic circuit and borehole. For this setup, the Grundfos MAGNA3 25-100 [46] was selected. The most important design criteria for pump selection were the required pump head and the operational flow rate range.

The pump head refers to the hydraulic pressure required to overcome frictional losses in the piping system, borehole circuit, and system components such as the heater, flow meter, and valves. Based on engineering estimates of roughness and pressure drops, and including a safety margin, a pump with a maximum head of approximately 10 m was considered appropriate. The selected MAGNA3 25-100 satisfies this requirement, where 25 mm refers to the connection diameter and 100 dm refers to the maximum pump head.

For both CP-TRT and CIT-TRT operation, a constant flow rate is required. In this research, the flow rate was set at 2.4 m^3/h, which was considered a practical compromise between sufficient heat transfer and measurement stability, while limiting excessive investment and operational costs. Once this target flow rate and estimated pump head were defined, the pump suitability was verified using the manufacturer's pump performance curve, shown in Figure 7.3. This curve shows the pump head H as a function of volumetric flow rate Q. Additional practical requirements included an appropriate operating temperature range and suitable connection dimensions.

7.3.4 Control System

The control system regulates the heater to maintain the required operating conditions for both CP- and CIT-TRTs. The circulation pump does not require active control in this setup, since both TRT types are performed at a constant flow rate.

In CP-TRT mode, the electric heater provides a constant thermal power. In CIT-TRT mode, the heater instead maintains a constant heater supply temperature T_2 by continuously adjusting its thermal power output in discrete 1 kW increments. When T_2 drops below the setpoint, the thermal power is increased, and vice versa.

This dual control functionality was enabled through the Vaillant sensoCOMFORT VRC 720 controller [47] in combination with the VR 71 module [48], which provided

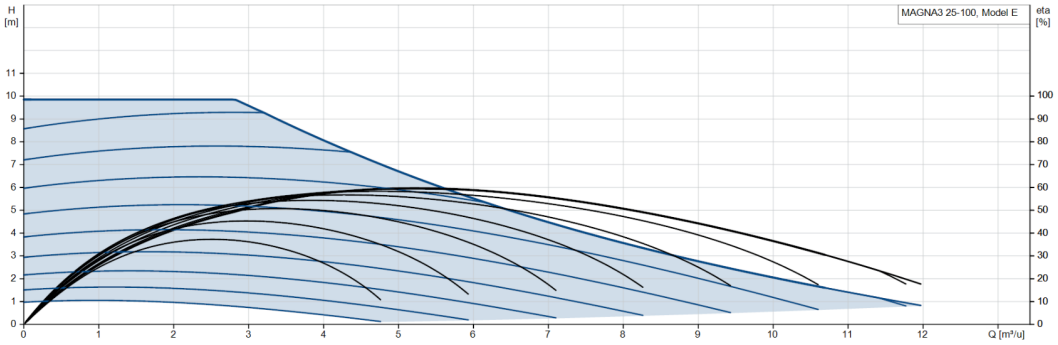


Figure 7.3: Pump head H [m] and efficiency η [%] as a function of volumetric flow rate Q [m^3/h] for the Grundfos MAGNA3 25-100 pump, showing the available pump head, operational window, and efficiency characteristics for water at 20 °C (Reproduced from [46]).

the required interface for configuring both CP- and CIT-TRT operating modes. This also explains the choice of the type of heater, since compatibility with this controller enabled a user-friendly control system.

7.3.5 Sensors and Data Acquisition System

Accurate and reliable measurement of fluid temperatures and flow rate is essential for TRT performance, since these variables directly determine the calculated thermal power and subsequent parameter estimation. For this reason, the sensors and data acquisition system were selected mainly based on compatibility and accuracy. Crodeon [49] was chosen as the primary supplier because it provided a complete data acquisition system with compatible sensors.

As discussed in Section 7.2, the TRT device uses three fluid temperature sensors and one flow meter. The selected Crodeon temperature sensors [49] provide a measurement accuracy of $\pm$ 0.5 $°C$ over an operating range of -10 to 80 $°C$, with a resolution of 0.1 $°C$. They are also suitable for water contact and outdoor conditions. These specifications were considered acceptable for this application. To enable direct contact with the fluid inside the pipes, the sensors were installed in stainless steel 316 screw-in fittings mounted directly into the pipe.

For flow measurement, the Maddalena R160 H DN40 1:1 flow meter [50] was selected based on its suitable flow range, pulse output frequency, and practical compatibility with the data acquisition system. This mechanical flow meter generates one pulse per liter of water passing through it. At the selected operating flow rate of 2.4 m^3/h, this corresponds to approximately 40 pulses per minute, which is sufficient for monitoring near-constant flow conditions.

The measurements are logged every 30 seconds, resulting in a volumetric flow resolution of 0.12 m^3/h. A longer measurement interval would improve the flow rate resolution, but the short measurement interval is better for capturing the temperature changes. This results in a trade-off between flow rate resolution and temperature tracking. Since the flow rate is expected to remain nearly constant, its resolution was considered less critical than the temperature measurements.

Data acquisition was performed using the Crodeon Reporter [49], which was selected because of its compatibility with the installed sensors and its ability to provide remote online access to live measurements. The system has a capacity of four sensors, which matches this application.

7.3.6 Additional Components

To complete the TRT device, several additional components were required for practical operation. The full TRT device was installed inside a mobile steel container of 1.2 x 2.20 x 2.26 m, insulated with 6 cm polyurethane (PUR) to reduce the influence of ambient temperature on system operation and measurements. An opening in the container floor provided access for the borehole pipes, while additional ventilation openings were included for heat dissipation and possible future implementation of active ambient temperature control.

Standard hydraulic pipes, fittings, and valves were used to connect the heater, buffer tank, and borehole. All above-ground pipes were insulated to reduce thermal losses and ambient temperature influence, which proved particularly important in practice and is discussed further in Section 7.4. Standard electrical components were installed to provide power supply for the heater, pump, controller, and data acquisition system. Table 7.1 gives an overview of all components of the TRT device, their specifications, and costs, resulting in a total cost of € 11 717.

7.4 Design Challenges

During field operation, the most significant challenge was the unintended influence of ambient temperature on the TRT measurements. This effect became visible through temperature fluctuations in the measurement data, particularly afternoon temperature peaks, which indicated that the system was not sufficiently insulated. Since TRT analysis depends strongly on stable and reliable temperature measurements, reducing this external influence was crucial.

7.4.1 Insulation of Pipes

To reduce the effect of ambient temperature and heat losses to the environment, additional insulation material was applied to all accessible above-ground pipes between the electric heater, buffer tank, and borehole. This modification aimed to minimize external heat gains and losses and thereby improve thermal stability of

Table 7.1: Main components, specifications, and costs of the developed TRT device, including 21% VAT.

Component	**Specification**	**Cost [€]**
Electric heater	Vaillant eloBLOCK VE 9 electric wall boiler, 9 kW [44]	€ 2 945
Buffer tank	Vaillant allSTOR plus VPS 300/3 [45]	€ 1 734
Circulation pump	Grundfos MAGNA3 25-100 180 [46]	€ 1 811
Controller	Vaillant VR 71 module [48] + sensoCOMFORT VRC 720 [47]	€ 842
Temperature sensors	3 Crodeon temperature sensors [49] + stainless steel 316 screw-in pieces	€ 525
Flow meter + pulse emitter	Maddalena R160 H DN40 1:1 + Maddalena Reed pulse emitter [50]	€ 199
Data acquisition reporter	Crodeon Reporter + subscription [49]	€ 822
Adapters	Crodeon Power Adapter 220V + Digital/Analog Input Adapter [49]	€ 167
Pump set + valves	EURO INDEX Pump Set 5 [51]	€ 74
Container	Steel, 1.20 x 2.20 x 2.26 m	€ 2 057
Additional components	Pipes, insulation, electrical components	€ 400
Additional costs	Shipping and packaging	€ 141
Total cost		**€ 11 717**

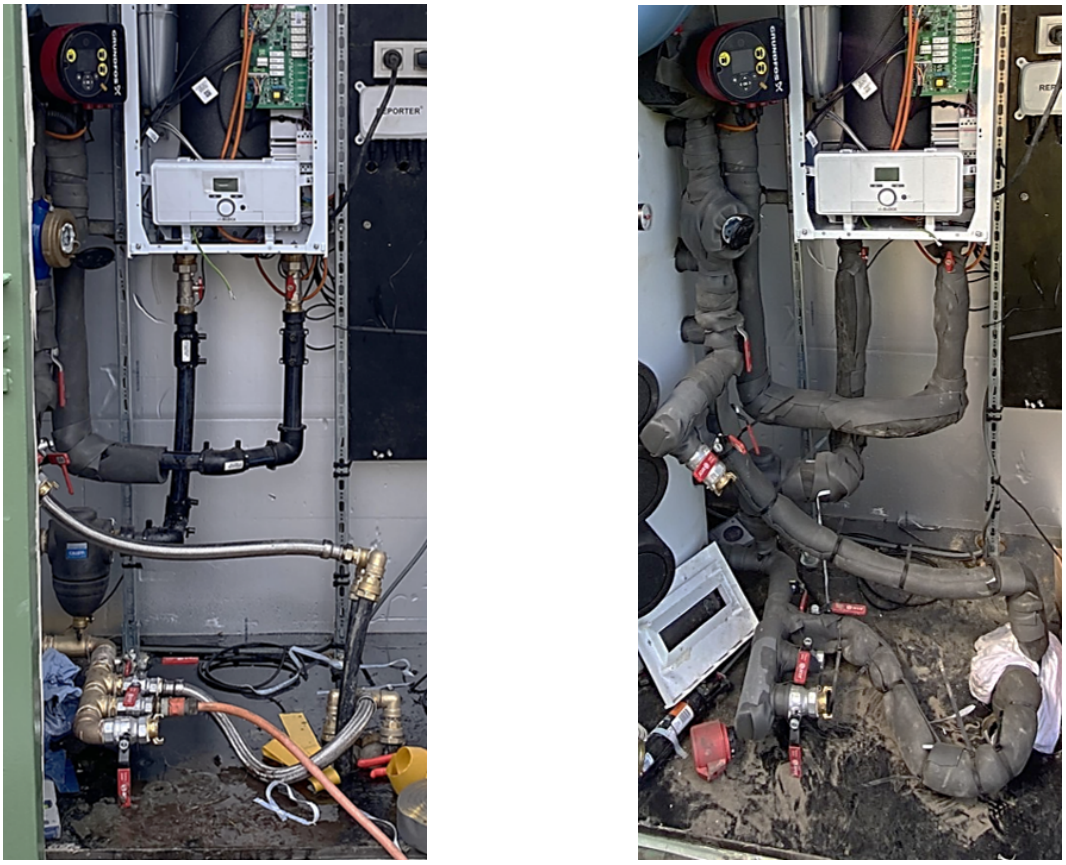
the circulating fluid. Figure 7.4 shows the system before and after applying this additional pipe insulation.

7.4.2 Insulation of Temperature Sensor

A second important issue was identified at the heater supply temperature sensor T_2, which is the control variable used by the electric heater during CIT-TRT operation. Because CIT-TRT performance depends directly on maintaining a stable supply temperature, any ambient influence on this sensor can disturb heater control and reduce temperature stability.

The T_2 sensor was initially mounted on a pipe section with insufficient insulation, making it more susceptible to ambient temperature effects. This contributed significantly to the observed temperature instability, particularly during CIT-TRTs. To reduce this influence, additional insulation material was applied around both the sensor and the surrounding pipe section. Figure 7.5 shows the situation before and

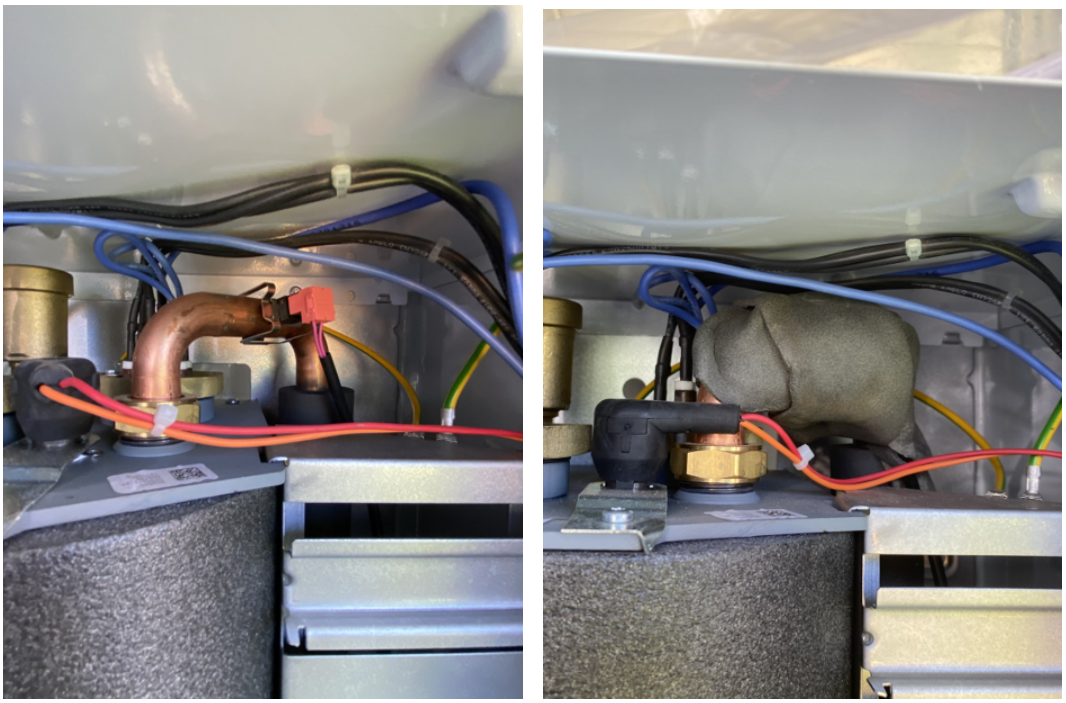
after this extra insulation.



(a) Before applying additional pipe insulation

(b) After applying additional pipe insulation

FIGURE 7.4: Close-up of the pipe insulation between the electric heater, buffer tank, and borehole before (a) and after (b) applying additional insulation.



(a) Before applying insulation around the heater supply temperature sensor

(b) After applying insulation around the heater supply temperature sensor

Figure 7.5: Close-up of the heater supply temperature sensor before (a) and after (b) applying additional insulation.

7.5 Conclusion

This chapter described the design and development of the TRT device used for the field tests in this research. The device was designed to perform both CP- and CIT-TRTs using the same setup, with the electric heater, buffer tank, circulation pump, sensors, and control system selected accordingly. The main practical challenge during operation was the influence of ambient temperature on the measurements and heater control, which required additional insulation of both the above-ground pipes and the heater supply temperature sensor. These practical issues are important for interpreting the field test results discussed later in this thesis.

Chapter 8

External Datasets

In addition to the field data generated within this research, external experimental TRT datasets were used for two main reasons. First, they allowed the applied methodologies to be developed and tested before original field data was available. Second, they enabled broader evaluation of the developed methods across multiple datasets, which is particularly relevant for investigating short-term transient effects.

Through collaboration with external partners, two relevant datasets were obtained. Section 8.1 discusses a dataset from the research of Professor M. Aydin [26], containing one CP-TRT, one CIT-TRT, and three CT-TRTs (flow-controlled constant temperature TRTs), performed on the same borehole. Section 8.2 then discusses a dataset provided by the Belgian company Terra Energy [52], consisting of 25 CP-TRTs, which are primarily used to evaluate the influence of short-term effects on TRT duration.

8.1 Dataset Aydin

Aydin et al. [26] published a study in 2024 comparing CP- and CIT-TRTs on the same borehole. In addition to CP- and CIT-TRTs, they introduced the flow-controlled CT-TRT, which keeps both inlet and outlet fluid temperatures constant by varying the flow rate. This differs from a CIT-TRT, which only maintains a constant inlet temperature while keeping the flow rate constant.

To the author's knowledge, Aydin et al. [26] are the only researchers who have compared a CP-TRT and a CIT-TRT on the same borehole. This makes their dataset particularly relevant for this research.

Their measurement data was shared for this research upon request and was primarily used to implement and test different borehole models for both the standard CP-TRT and the less extensively documented CIT-TRT methodology. In addition, this dataset provided an initial basis for comparing CP- and CIT-TRT performance in terms of parameter estimation and required test duration.

Their methodology, results, and conclusions are extensively documented in their published work [26]. Figures 3.2 and 3.3 in Chapter 3 present the measurement data of their CP- and CIT-TRT, respectively.

8.2 Dataset Terra Energy

Terra Energy [52] is a Belgian company specialized in geothermal systems and one of the major companies in Belgium that performs TRTs as part of its services. The company provided measurement data for this research from 25 CP-TRTs conducted on different boreholes across Belgium.

This dataset is particularly valuable because it allows different borehole models to be evaluated over 25 separate real-world cases. This strengthens the ability to identify and quantify general trends, particularly for CP-TRT methodologies. To ensure confidentiality, the individual test locations and projects were anonymized and are referred to throughout this thesis as TRT1 to TRT25.

Within this research, the Terra Energy dataset is used to compare the standard long-term approximation ILS model with the STS model, which incorporates short-term transient thermal effects. Two out of the 25 TRTs, namely TRT17 and TRT20, resulted in highly unrealistic thermal conductivity estimates, while all others were close to independent reference values, as is explained in more detail in Chapter 11. These results likely indicate an issue in the measurement data or test conditions. Therefore, TRT17 and TRT20 are excluded from the final analysis, leaving 23 TRTs for the final comparison.

Figure 8.1 shows an example of TRT7, one of the 23 retained TRTs. This test shows CP-TRT measurement data with a relatively stable injected thermal power and the corresponding increase in $\overline{T}_f(t)$ over time. Figure 8.2 shows TRT3, which also aims to maintain constant thermal power but shows significantly larger power fluctuations. These fluctuations clearly affect the resulting temperature response.

Across the full dataset, the tests show varying degrees of power stability, likely due to practical factors such as voltage fluctuations, heater-related operational issues, or control limitations. The measurements may also be influenced by ambient conditions, such as ambient temperature fluctuations or rainfall, depending on the enclosure and insulation of the TRT device. Terra Energy applies a practical minimum test duration of 60 hours, and across the provided tests, the average total test duration is 73 hours. Appendix A provides the test data for all 25 Terra Energy TRTs.

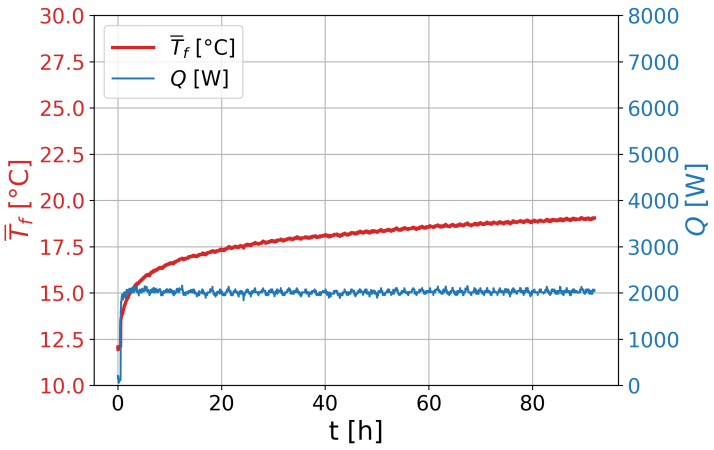


FIGURE 8.1: Mean fluid temperature $\overline{T}_f(t)$ [°C] and injected thermal power Q [W] as a function of time t [h] for TRT7.

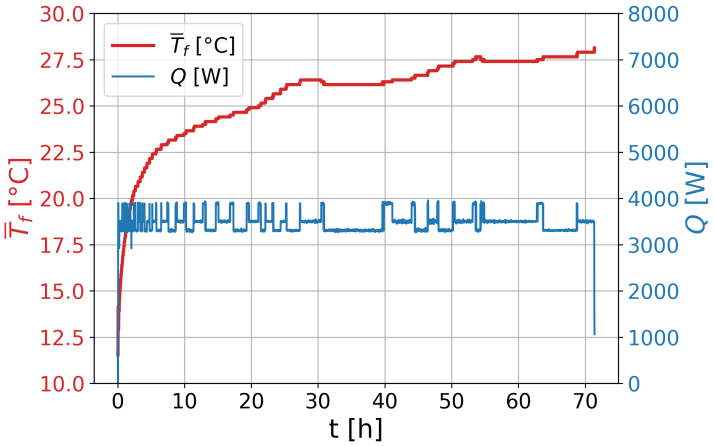


FIGURE 8.2: Mean fluid temperature $\overline{T}_f(t)$ [°C] and injected thermal power Q [W] as a function of time t [h] for TRT3.

8.3 Conclusion

This chapter introduced the external datasets used in this research. The Aydin dataset provides a direct comparison between CP-, CIT-, and CT-TRTs on the same borehole and is mainly used to support the implementation of the CP- and CIT-TRT methodologies. The Terra Energy dataset provides a set of 23 practical CP-TRTs and is therefore used to evaluate the effect of short-term transient modeling on parameter estimation and test duration reduction. Together, these datasets provide the basis for the methodology and results presented in the following chapters.

Part III

Methodology

Chapter 9

Transient Modeling Methodology

One of the main goals of this research is to reduce the operational cost of TRTs by decreasing the required test duration. This may be achieved by incorporating short-term transient effects into borehole modeling. By using a transient borehole model such as the STS model introduced in Section 6.3, measurement data from the first hours of the TRT can be used instead of being discarded, as is done when using the ILS model. If these early-time measurements can be used reliably, the total required TRT duration can potentially be reduced.

This chapter discusses the methodology used for transient borehole modeling on the Terra Energy dataset introduced in Section 8.2. The dataset originally consists of 25 CP-TRTs, named TRT1 to TRT25, of which TRT17 and TRT20 are excluded from the final analysis due to apparent measurement errors. The remaining 23 TRTs provide a basis for comparing the transient STS model with the conventional ILS model and for quantifying the potential test duration reduction.

9.1 STS Model Implementation

The implementation of the STS model in this research is based on the methodology introduced in Section 6.3. The thermal conductivity k and the borehole thermal resistance R_b^* are determined by performing a linear fit between the hybrid g-function $g(t)$ and the mean fluid temperature $\overline{T}_f(t)$.

The construction of the hybrid g-function is based on the methodology provided by Meertens et al. [20, 40], and implemented in GHEtool in the Issue26-branch [41], as discussed in Section 6.3. An important advantage of the STS model is that it represents the borehole physics much more realistically by incorporating short-term transient effects. However, this also requires a larger set of input parameters compared to conventional TRT interpretation methods. The required input parameters were listed before in Table 6.1.

Two particularly important input parameters are the ground thermal conductivity k and the ground thermal diffusivity α. Since determining the thermal conductivity of the ground is one of the primary objectives of a TRT, the STS methodology requires an iterative procedure. An initial estimate for k is used as input for the model, after which the resulting calculated k-value is used as a new input estimate. This procedure is repeated until the relative difference between successive iterations falls below 0.1%. For the thermal diffusivity α, no direct measurement is available, so an estimated value must be assumed. It is therefore important to assess how sensitive the STS results are to α and other model parameters. This is discussed further in Section 9.4.

9.2 Verification of Parameter Estimation

To evaluate the implementation and consistency of the transient STS model discussed in Chapter 6, its results are compared with those obtained using the conventional ILS model. For the 23 CP-TRTs of the Terra Energy dataset, the values of k and R_b^* are determined using both methods. The ILS model is applied with a conventional cutoff time of 10 hours, while the transient STS approach is applied with a practical cutoff time of 1 hour. This first hour is excluded to remove start-up effects, such as delayed heater activation. The resulting comparison is discussed in Section 11.3.

Since the actual values of k and R_b^* are unknown, no absolute verification is possible. However, if the STS model is implemented correctly and produces physically consistent results, both models should produce comparable parameter estimates for the same TRT data. Similar output values for the ILS and STS approaches therefore indicate consistency between both methods, but should not be interpreted as proof that either value is the true parameter value.

In addition, the obtained k-values of both models are compared with estimates from Smart Geotherm [53], an online tool that estimates the effective ground thermal conductivity based on geological data. By providing the borehole location and depth, the tool returns an estimated effective ground thermal conductivity. These values are used as an additional cross-check for the obtained results, although they remain approximate estimates. As a reference for R_b^*, the values obtained with the ILS and STS models were compared with those calculated with the multipole method, which was explained in Chapter 5. As an additional comparison, the k and R_b^* values are also compared with the ones calculated by Terra Energy themselves using the ILS model.

9.3 Test Duration Reduction

Once the STS model has been compared with the conventional ILS approach, the next objective is to evaluate whether it can reduce the required TRT duration. To

quantify the potential reduction in test duration, several concepts are introduced, including a convergence test, the end value, the convergence time t_c, and an accuracy band.

First, a convergence test evaluates the evolution of a TRT output parameter (k or R_b^*) over time. For example, k is calculated repeatedly using progressively larger time windows of the TRT data. Starting from a fixed cutoff time, the parameter is first calculated from 10 h to 11 h, then from 10 h to 12 h, and so on until the end of the test. As more measurement data are included, the calculated k-value is expected to converge toward a stable value. Second, the end value is defined as the parameter value obtained when the full TRT dataset is used. This corresponds to the final value of the convergence test. Third, the convergence time t_c is then defined as the earliest point in time after which the calculated parameter remains permanently within a specified deviation from this end value. Lastly, the accuracy band represents this deviation and is expressed as a percentage.

Figure 9.1 illustrates an example of a convergence test, indicating the end value, the convergence time t_c, and the corresponding accuracy band. As an example, consider a TRT with a converged end value of $k = 2.0\ W/(mK)$. For an accuracy band of 5%, the convergence time t_c is defined as the earliest point after which all subsequent calculated k-values remain between 1.9 and 2.1 $W/(mK)$. In other words, the point in time right before t_c is the last value outside the selected accuracy band. The accuracy band is therefore a convergence band relative to the final value, not an absolute accuracy interval relative to the unknown true value. Although the same methodology can also be applied to R_b^*, the convergence analysis in this research is primarily conducted using k, since it is generally considered the most important TRT output parameter.

After defining the relevant concepts for quantifying TRT time reduction, the next step is to select suitable accuracy bands. Several possible approaches exist. First, one can consider the typical uncertainty range on TRT-derived k-values reported in literature. Second, the convergence behavior of the 23 Terra Energy TRTs interpreted with the conventional ILS model can be analyzed by evaluating the average deviation between the end value and the parameter value obtained after 70%, 80%, or 90% of the total test duration. Finally, the average difference between the parameter estimates obtained with the ILS and STS approaches can also be considered.

Based on these considerations, three representative accuracy bands are selected in Section 11.3 and applied to all 23 Terra Energy TRTs. For each selected accuracy band, the convergence time t_c is determined for both the conventional ILS model and the STS model. The difference in convergence time between both approaches is then calculated to evaluate whether the STS model provides a reduction in required TRT duration. To the author's knowledge, no peer-reviewed academic study has explicitly investigated TRT duration reduction using transient borehole modeling. However, Liu et al. [12] presented a technical report in which an R-C model was

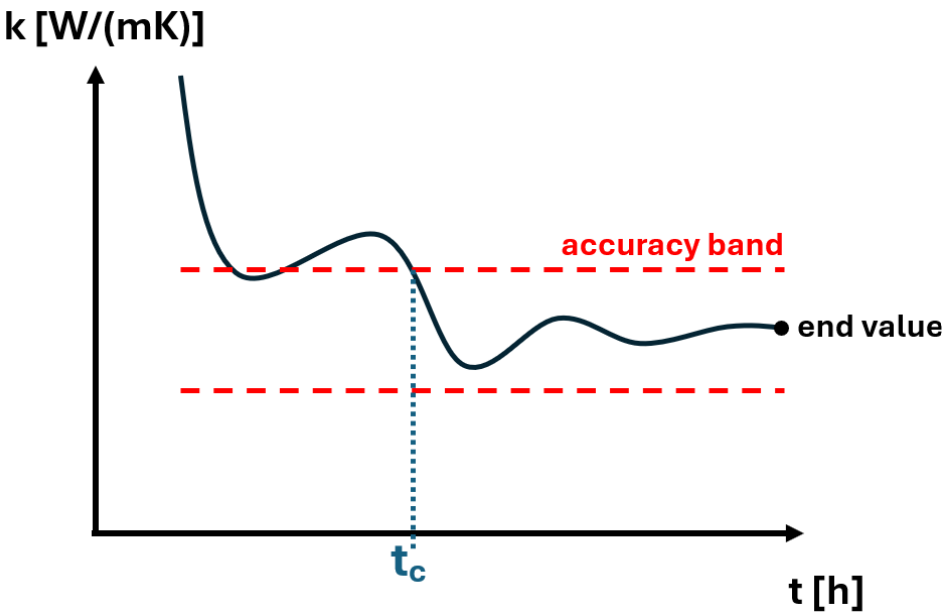


Figure 9.1: Example convergence test for thermal conductivity k [W/(mK)] as a function of time t [h], showing the end value, accuracy band, and convergence time t_c.

used to reduce the required TRT duration and to develop stopping-criterion algorithms for determining when sufficient TRT data had been collected. Although this report does not constitute peer-reviewed academic literature, it is methodologically relevant to the STS approach used in this research. Therefore, its reported time reductions are used in Chapter 11 as a reference for comparison with the TRT duration reductions obtained in this thesis.

Finally, the influence of the cutoff time on this comparison is also investigated. As discussed previously, the STS model can potentially reduce TRT duration by using early-time measurement data that is excluded in the conventional ILS methodology due to the standard 10 h cutoff time. Therefore, the STS model is additionally evaluated for cutoff times between 1 and 10 hours, and the influence on both the time reduction and the difference in final k-value between ILS and STS is analyzed.

9.4 Sensitivity Analysis

The STS model has two important disadvantages compared to the ILS model: more complex computation and a larger number of required input parameters. The first issue may limit practical adoption. However, in terms of computation time, the STS model requires calculations on the order of minutes, compared to seconds for the conventional ILS model. Relative to the total duration of a TRT, which typically spans several days, this additional computation time is insignificant.

This section therefore mainly focuses on the second issue: the larger number of required input parameters. Besides the practical challenge of gathering all relevant input data, several of these parameters are either unknown or only known within a relatively large uncertainty range. It is therefore necessary to evaluate the influence of these uncertainties on the resulting TRT output parameters k and R_b^* for both the ILS and STS methodologies by conducting a sensitivity analysis.

For both the ILS model and the STS model, and for each of the 23 TRTs, the values of k and R_b^* are recalculated while applying deviations of -50%, -25%, -10%, 0% (base value), +10%, +25%, and +50% to each individual input parameter. During this procedure, only one parameter is varied at a time while all other parameters are kept constant.

The resulting deviations in the calculated output parameters k and R_b^* are then averaged over all 23 TRTs, providing an indication of the sensitivity of each model to the different input parameters. This allows the overall uncertainty associated with both the ILS and STS methodologies to be assessed. Since the STS model requires substantially more input parameters than the conventional ILS model, the overall uncertainty of the STS approach is expected to be larger.

For the ILS model, the analyzed input parameters are the borehole depth H, the borehole radius r_b, the thermal diffusivity α, and the undisturbed ground temperature T_∞. For the STS model, the previously mentioned parameters are included together with the mass flow rate $\dot{m}$, the burial depth D, the grout thermal conductivity k_g, the volumetric heat capacity of the grout $(\rho c_p)_g$, the pipe thermal conductivity k_p, the volumetric heat capacity of the pipes $(\rho c_p)_p$, the initial thermal conductivity estimate k, the fluid thermal conductivity k_f, the fluid density ρ_f, the fluid heat capacity $c_{p,f}$, the dynamic viscosity η, the inner and outer pipe radii r_{in} and r_{out}, the shank spacing D_s, and the pipe roughness ϵ. Section 11.4 discusses the results of this sensitivity analysis.

9.5 Conclusion

This chapter described the methodology used to evaluate the STS model on the Terra Energy dataset. The STS model is compared with the conventional ILS model to assess parameter consistency, after which convergence tests are used to quantify potential TRT duration reduction. The methodology defines the end value, convergence time, and accuracy bands used in the analysis, while also clarifying that these bands describe convergence relative to the final value rather than absolute accuracy. Finally, a sensitivity analysis is introduced to evaluate the influence of uncertain input parameters on both the ILS and STS results. The results are discussed in a similar structure in Chapter 11.

Chapter 10

Methodology of Field Testing

Chapter 7 described the design and development of the TRT device used in this research. This chapter describes the methodology used for the field tests conducted with this device. The objective of these tests is twofold. First, the tests are used to evaluate whether the developed TRT device can generate usable CP- and CIT-TRT measurement data under practical field conditions. Second, the results are used to compare CP- and CIT-TRTs in terms of operating behavior, parameter estimation, and convergence time.

The comparison between CP- and CIT-TRTs is particularly relevant because literature suggests that CIT-TRTs may reach stable thermal conditions faster than CP-TRTs. However, this still needs to be evaluated experimentally for this setup, since the practical performance depends strongly on the stability of the test setup, the control system, and the measurement conditions.

Section 10.1 discusses the test setup, including the test site, borefield configuration, borehole specifications, and test procedure. Section 10.2 then describes the methodology used to process the measurement data, estimate the design parameters, and evaluate convergence. Finally, Section 10.3 explains how the CP- and CIT-TRT results are compared.

10.1 Test Setup

10.1.1 Test Site

The field tests for this research were performed in Lochristi, Belgium, on a borefield consisting of four boreholes arranged in an L-shape. The layout is shown in Figure 10.1, with the four boreholes indicated as B1, B2, B3, and B4.

The borefield specifications are summarized in Table 10.1. The table includes the relevant borehole geometry and thermal conductivities of the pipes and the grout. Different grout materials were used for the four boreholes. Borehole B1 was grouted with MÖRTEL-ENERGIE-OPTIMUM grout from RKV [54], while B2 was grouted

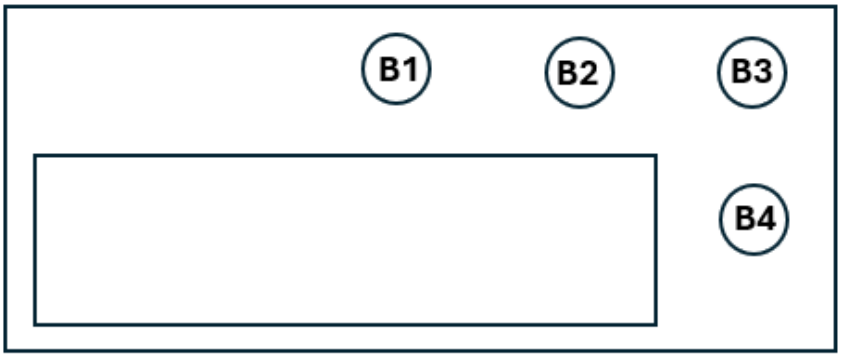


Figure 10.1: Ground plan of the test site, showing a residential building (rectangle) and the four boreholes arranged in an L-shape: B1, B2, B3, and B4.

with the same grout mixed with water. Borehole B3 was grouted with GEOTHERM-X PRO grout from Euroquartz [55], while B4 was grouted with the same grout mixed with water. The corresponding thermal conductivities are shown in Table 10.1.

Table 10.1: Borefield geometry and material properties used for the field tests.

Symbol	Value	Explanation
Borehole		
r_b	70 mm	Borehole radius
H	99 m	Borehole length
B	10 m	Spacing between boreholes
Pipe		
r_{in}	13 mm	Pipe inner radius
r_{out}	16 mm	Pipe outer radius
k_p	0.4 $W/(mK)$	Pipe thermal conductivity
Grout		
$k_{g,B1}$	1.8 $W/(mK)$	Grout thermal conductivity for B1
$k_{g,B2}$	1.6 $W/(mK)$	Grout thermal conductivity for B2
$k_{g,B3}$	1.8 $W/(mK)$	Grout thermal conductivity for B3
$k_{g,B4}$	1.7 $W/(mK)$	Grout thermal conductivity for B4

10.1.2 Test Procedure

A total of five field tests were conducted: three CP-TRTs and two CIT-TRTs. The CP-TRTs were performed at different heater power setpoints, while the CIT-TRTs were performed at different heater supply temperature setpoints. Only two CIT-TRTs were performed due to the time limitations of the research. The tests were not all performed on separate boreholes. CP-TRT1 and CP-TRT3 were both performed on borehole B2, CP-TRT2 was performed on borehole B3, CIT-TRT1 was performed on borehole B2, and CIT-TRT2 was performed on borehole B4.

Each test started with one hour of free water circulation without activating the heater. This was used to determine the undisturbed ground temperature T_∞. After one hour, the heater was activated with the desired power or temperature setpoint. All tests were performed with a constant flow rate of 2.4 m^3/h as discussed in Chapter 7. The test duration was 96 hours, which is sufficient for a typical TRT. Table 10.2 provides an overview of the performed tests and their corresponding operating conditions. Borehole B1 was only used for short test runs.

TABLE 10.2: Overview of the CP- and CIT-TRT field tests.

Test	Borehole	Setpoint	Flow rate	Duration
CP-TRT1	B2	2 kW	2.4 m^3/h	96 h
CP-TRT2	B3	4 kW	2.4 m^3/h	96 h
CP-TRT3	B2	6 kW	2.4 m^3/h	96 h
CIT-TRT1	B2	20°C	2.4 m^3/h	96 h
CIT-TRT2	B4	30°C	2.4 m^3/h	96 h

10.2 TRT Methodology

This section describes the methodology used to analyze the CP-TRT and CIT-TRT measurement data. Section 10.2.1 explains how the measured data is processed and how the injected thermal power is calculated. Section 10.2.2 describes how the parameters T_∞, k, and R_b^* are estimated from the measurement data. Section 10.2.3 then discusses the convergence analysis used to evaluate the stability of the parameter estimation.

10.2.1 Test Output

As explained in Chapter 7, the measurement system records data every 30 seconds using four sensors: three temperature sensors and one flow sensor. The relevant measured temperatures are the borehole inlet temperature T_1, the heater supply temperature T_2, and the borehole outlet temperature T_3, as shown previously in Figure 7.1.

The injected thermal power is calculated using Equation 10.1, based on the volumetric flow rate $\dot{V}$ measured by the flow meter, the density ρ and specific heat capacity c_p of the water, and the temperature difference between T_1 and T_3. For CP-TRTs, the thermal power should remain approximately constant throughout the test. For CIT-TRTs, the thermal power varies over time because the heater attempts to maintain a constant inlet temperature while the outlet temperature evolves.

$$\dot{Q} = \rho \, c_p \, \dot{V} \, (T_1 - T_3) \tag{10.1}$$

The measured temperature and thermal power profiles are used to evaluate the practical operation of the TRT device. For CP-TRTs, the main criterion is the stability of the injected thermal power. For CIT-TRTs, the main criterion is the stability of the controlled heater supply temperature T_2 and the resulting evolution of thermal power.

10.2.2 Parameter Estimation

The goal of a TRT is to estimate the main design parameters T_∞, k, and R_b^* from the measured data, as discussed in Chapter 5.

The undisturbed ground temperature T_∞ is determined from the initial circulation period before heater activation. During this period, water is circulated through the borehole, and the inlet and outlet temperatures are analyzed. Following the discussion in Chapter 5, the most representative value is expected to occur after 20 minutes of circulation time according to Gehlin and Nordell [25], before pump heating and the temperature of the buffer tank disturb the measurement. Because this TRT setup has a higher flow rate than the setup used by Gehlin and Nordell [25], a circulation time of less than 20 minutes may yield better results.

For this TRT setup, the determination of T_∞ is influenced by the relatively large buffer tank. The buffer tank has a volume of 303 L, which is substantially larger than the water volume of approximately 100 L inside the borehole pipes. As a result, the measured fluid temperature during the circulation period is influenced not only by the water initially present in the borehole, but also by the water in the buffer tank. This effect is especially important when the initial buffer tank temperature differs from the actual ground temperature. Therefore, the selected T_∞ value is based on the early part of the circulation period, where the influence of the borehole water is expected to be most representative.

The methodology for estimating k and R_b^* depends on the TRT type. For CP-TRTs, the mean fluid temperature is fitted as a function of $\ln(t)$ using the long-term ILS approximation, shown in Equation 5.1. The slope of this fit is used to determine k, while the intercept is used to estimate R_b^*.

For CIT-TRTs, the parameter estimation is based on the constant-temperature analytical solution, shown in Equation 5.3. In this case, the inverse thermal power per unit borehole length is fitted as a function of $\ln(t)$, and the slope of this fit is used to determine k. The estimation of R_b^* for CIT-TRTs is more challenging based on measurement data, because no equivalent intercept-based formulation is available. Therefore, the CIT-TRT analysis focuses mainly on k, while R_b^* is treated separately using the multipole method as discussed in Chapter 5.

To assess the quality and reliability of the linear fit, the mean absolute percentage error (MAPE) was calculated as a percentage-based measure of the relative devia-

tion between the experimental and fitted values. For the CIT-TRTs, the MAPE was calculated following the formulation used by Aydin et al. [26], by comparing the experimental and fitted inverse heat transfer rate $1/q$. This is equivalent to evaluating the relative deviation between the modeled and experimental heat transfer rate q. For the CP-TRTs, the MAPE was calculated by comparing the measured and fitted mean fluid temperature response, based on the temperature rise $\overline{T}_f$ - T_∞. In both cases, the MAPE provides an indication of how well the linear model represents the experimental data.

10.2.3 Convergence

To evaluate the reliability of the parameter estimation, the convergence behavior of the calculated k-values is analyzed. This is done by calculating the parameter value repeatedly over progressively longer time windows, as introduced in Chapter 9. The purpose is to assess whether the estimated parameter approaches a stable end value as more measurement data are included.

For the CP-TRTs, convergence is evaluated by comparing the k-values obtained for different cutoff times, including 10 h, 20 h, and 30 h. If these curves approach similar end values, the test is considered to show stable convergence behavior. Large differences between the curves indicate that the estimated parameter remains sensitive to the selected fitting window, which reduces confidence in the result.

The same convergence approach is applied to the CIT-TRTs. However, for CIT-TRTs, convergence is expected to be more sensitive to fluctuations in the controlled inlet temperature. Therefore, the stability of the heater supply temperature T_2 is an important factor in interpreting the CIT-TRT convergence behavior.

In addition to visually comparing convergence curves, convergence times are determined for selected accuracy bands around the final k-value. The same accuracy bands as those defined in Chapter 9 are used. This allows the CP- and CIT-TRTs to be compared quantitatively in terms of how quickly their estimated k-values stabilize. The convergence times are later used in Chapter 12 to evaluate whether CIT-TRTs show faster parameter stabilization compared to CP-TRTs in the conducted field tests.

10.3 Comparison CP- and CIT-TRTs

The CP- and CIT-TRTs are compared using three main criteria: operational stability, estimated parameter values, and convergence time.

First, the operational behavior of both test types is evaluated using the measured temperature and thermal power profiles. For CP-TRTs, the key requirement is a stable injected thermal power. For CIT-TRTs, the key requirement is a stable heater supply temperature, since this temperature defines the constant inlet temperature

boundary condition. Any instability in this controlled temperature directly affects the thermal power profile and therefore the parameter estimation.

Second, the estimated k-values are compared between the different tests. Since the tests were not all performed on the same borehole, and because different grout materials were used, the comparison cannot be interpreted as a perfect one-to-one comparison between CP- and CIT-TRTs. However, the values should still be within a realistic range for the same site. Large deviations may indicate measurement instability or operational problems.

Third, the convergence behavior is compared. The convergence time is used as an indicator of how quickly a test provides a stable k-value. Literature suggests that CIT-TRTs may reach stable conditions faster than CP-TRTs. Therefore, the field results are used to assess whether this theoretical advantage is observed in practice with the developed TRT device.

10.4 Conclusion

This chapter described the methodology used for the field tests conducted with the developed TRT device. Five tests were performed: three CP-TRTs and two CIT-TRTs. The methodology includes processing the measured temperatures and flow rate, calculating the injected thermal power, estimating T_∞, k, and R_b^*, and evaluating the convergence behavior of the resulting parameter estimates. The comparison between CP- and CIT-TRTs is based on operational stability, parameter estimation, and convergence time. This methodology provides the basis for interpreting the field test results presented in Chapter 12.

Part IV

Results and Discussion

Chapter 11

Transient Modeling Results

This chapter discusses the results obtained using the methodology described in Chapter 9 for the Terra Energy dataset. Section 11.1 presents the STS model implementation for one example test. Section 11.2 then applies the same methodology to all 23 TRTs and compares the obtained k- and R_b^*-values with the ILS results and reference estimates. This comparison is used to evaluate the consistency of the STS approach. Section 11.3 quantifies the potential test duration reduction obtained with the STS model. Finally, Section 11.4 presents the sensitivity analysis, investigating the influence of variations in the different input parameters on the resulting output parameters for both the ILS and STS models.

11.1 STS Model Implementation

In this section, the methodology described in Section 9.1 is demonstrated for one example TRT, namely TRT3. All other TRTs were analyzed using the same procedure. As a reference, the conventional ILS model is first applied following the methodology described in Chapter 5. This results in a thermal conductivity k of 2.31 $W/(mK)$ and a borehole thermal resistance R_b^* of 0.087 mK/W.

For the STS model, all relevant borehole, ground, and fluid input parameters are first collected for TRT3, as listed in Table 11.1. Using these input parameters, a borehole model is assembled in GHEtool using the corresponding ground, fluid, and pipe data. The hybrid g-function is then calculated using the implementation developed by Meertens et al. [20] in GHEtool [41]. Subsequently, a linear fit is performed between the mean fluid temperature $\overline{T}_f(t)$ and the hybrid g-function $g(t)$ following Equation 6.1. The k-value is determined from the slope of this fit, while R_b^* is obtained from the intercept. Figure 11.1 shows the mean fluid temperature data together with the resulting linear fit for TRT3. This initial STS calculation results in a thermal conductivity k of 2.271 $W/(mK)$ and a borehole thermal resistance R_b^* of 0.088 mK/W.

Table 11.1: Input data used for the STS model implementation for TRT3, based on information provided by Terra Energy.

Category	Symbol	Value
Ground	T_∞	12.1 $°C$
	α	10^{-6} m^2/s
	k_{ILS}	2.31 $W/(mK)$
Fluid	$\dot{m}$	0.140 kg/s
	k_f	0.6 $W/(mK)$
	ρ_f	995 kg/m^3
	$c_{p,f}$	4180 $J/(kgK)$
	η	$0.8{\cdot}10^{-3}$ Pas
Borehole	H	100 m
	D	1 m
	r_b	0.080 m
	k_g	1.2 $W/(mK)$
	$(\rho c_p)_g$	$1.8{\cdot}10^6$ $J/(m^3K)$
	r_{in}	0.013 m
	r_{out}	0.016 m
	k_p	0.38 $W/(mK)$
	$(\rho c_p)_p$	$1.9{\cdot}10^6$ $J/(m^3K)$
	D_s	0.054 m
	n_p	2
	ϵ	10^{-6}

As discussed previously in Section 9.1, the STS model requires an initial estimate of the ground thermal conductivity k as an input parameter. The value obtained with the ILS model provides a suitable initial estimate. To improve the consistency of the STS result, the calculation is repeated iteratively using the newly calculated STS value of k as the updated input parameter. This iterative procedure is repeated until the relative difference between two consecutive calculated k-values becomes smaller than 0.1%. For TRT3, convergence is reached after three iterations, resulting in a final k-value of 2.273 $W/(mK)$ and R_b^*-value of 0.089 mK/W.

11.2 Verification of Parameter Estimation

The output parameters k and R_b^* are determined for all 23 Terra Energy TRTs using the same methodology described previously for TRT3 in Section 11.1. To further evaluate the consistency of the obtained k-values, the results are additionally compared with thermal conductivity estimates obtained from Smart Geotherm, an online tool that estimates effective ground thermal conductivity for boreholes in Belgium based on geological data, location, and borehole depth.

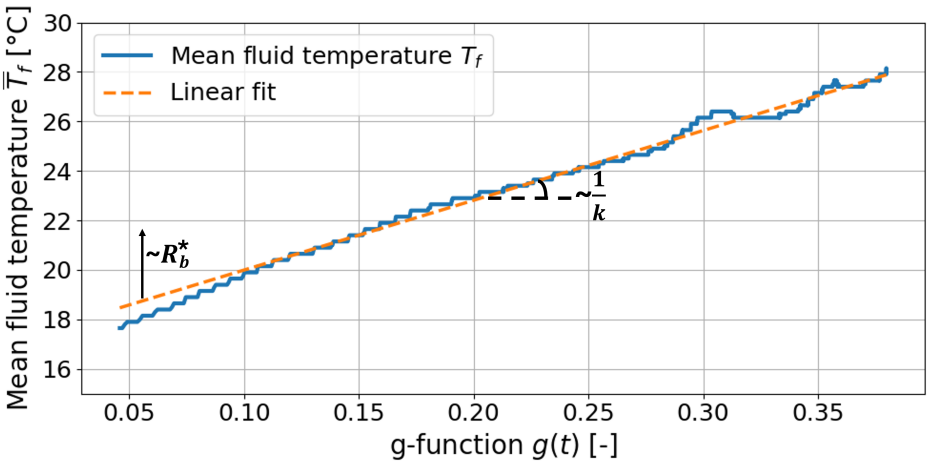


FIGURE 11.1: Mean fluid temperature $\overline{T}_f(t)$ as a function of the hybrid g-function $g(t)$ for TRT3, including the corresponding linear fit.

The results are summarized in Table 11.2. For each TRT, the table shows the thermal conductivity values obtained from Smart Geotherm, the ILS model, and the STS model, together with the relative difference between the ILS and STS results. The same comparison is shown for the borehole thermal resistance R_b^*. As an independent reference for R_b^*, the multipole method is used and also shown in Table 11.2. In addition, both the average relative difference and the average deviation over the full dataset are included. These values provide an indication of both the systematic deviation and the average absolute deviation between the ILS and STS methodologies. As an additional check, the k and R_b^* values were very close to those calculated by Terra Energy based on the ILS model.

Both methods show matching results. For the thermal conductivity k, the average relative difference between ILS and STS equals -0.84%, while the average deviation equals 3.65%. For the borehole thermal resistance R_b^*, the average relative difference equals -4.29%, with an average deviation of 6.03%. This is expected, since R_b^* is generally associated with larger uncertainty than k. The average differences are small. For k, no significant systematic under- or overestimation is observed, while for R_b^*, the STS model shows a slight systematic underestimation compared to ILS.

To evaluate the similarity between both methods on an individual TRT basis, the relative differences are categorized into three ranges: highly similar below 2.71% (green), reasonably similar between 2.71% and 5% (yellow), and deviating above 5% (red). For R_b^*, which generally has a larger uncertainty, the corresponding categories are: under 5% (green), between 5% and 10% (yellow) and above 10% (red). For the thermal conductivity k, eleven TRTs fall within the green category, six within the yellow category, and six within the red category. For R_b^*, nine TRTs are green, eleven are yellow, and three are red. The largest difference in k-values occurs

Table 11.2: Differences (Diff) between the ILS and STS model obtained k and R_b^* values for the 23 Terra Energy TRTs. Smart Geotherm (SG) conductivity estimates are included as geological reference values for k, while multipole (MP) estimates are included as reference values for R_b^*.

TRT	k **[W/(mK)]**				R_b^* **[mK/W]**			
	SG	**ILS**	**STS**	**Diff [%]**	**MP**	**ILS**	**STS**	**Diff [%]**
TRT1	1.7	1.81	1.86	+2.8%	0.097	0.103	0.102	-1.5%
TRT2	1.8	1.75	1.69	-3.4%	0.104	0.164	0.150	-9.0%
TRT3	2.0	2.31	2.27	-1.7%	0.088	0.087	0.089	+2.0%
TRT4	1.8	2.16	2.20	+1.9%	0.099	0.052	0.055	+5.4%
TRT5	1.8	2.46	2.24	-8.9%	0.099	0.110	0.103	-7.2%
TRT6	1.7	1.99	1.86	-6.5%	0.097	0.129	0.116	-10.8%
TRT7	1.6	1.44	1.51	+4.9%	0.135	0.101	0.092	-9.7%
TRT8	1.7	1.62	1.64	+1.2%	0.096	0.109	0.100	-8.6%
TRT9	1.8	2.04	1.87	-8.3%	0.095	0.131	0.116	-13.2%
TRT10	1.8	1.69	1.85	+9.5%	0.102	0.068	0.075	+9.4%
TRT11	2.0	2.22	2.18	-1.8%	0.098	0.079	0.077	-1.7%
TRT12	2.0	1.92	1.89	-1.6%	0.097	0.089	0.081	-9.7%
TRT13	1.7	1.67	1.59	-4.8%	0.095	0.184	0.164	-12.0%
TRT14	1.8	1.94	2.01	+3.6%	0.094	0.081	0.084	+3.3%
TRT15	1.9	2.49	2.30	-7.6%	0.100	0.087	0.081	-7.1%
TRT16	1.8	2.64	2.49	-5.7%	0.097	0.079	0.078	-1.6%
TRT18	1.9	1.84	1.90	+3.3%	0.095	0.109	0.108	-1.3%
TRT19	1.8	2.09	2.06	-1.4%	0.090	0.092	0.090	-2.2%
TRT21	1.7	1.57	1.60	+1.9%	0.134	0.173	0.163	-5.9%
TRT22	1.9	1.94	1.95	+0.5%	0.099	0.103	0.097	-6.8%
TRT23	1.9	2.08	2.08	+0.0%	0.099	0.092	0.091	-1.8%
TRT24	1.7	1.57	1.59	+1.3%	0.097	0.096	0.088	-8.5%
TRT25	2.0	2.12	2.15	+1.4%	0.090	0.045	0.045	-0.1%
			Average	**-0.84%**			**Average**	**-4.29%**
			Average deviation	**3.65%**			**Average deviation**	**6.03%**

for TRT10, with a difference of +9.5%. For R_b^*, it occurs for TRT9, with a difference of -13.2%.

Comparing the ILS results with the Smart Geotherm estimates based on geological data gives an average deviation of 12.48%, while the STS results show an average deviation of 10.41%. For both methodologies, these deviations remain within a realistic and acceptable range. The STS model shows slightly better agreement with the Smart Geotherm estimates, although the difference compared to ILS remains limited. The overall deviation for both models is in the expected range as local variations can differ from large-scale geological data.

As an additional comparison, the R_b^*-values obtained with the ILS and STS models were compared with the multipole estimates. Using the multipole values as reference, the average deviation equals 23.54% for ILS and 20.33% for STS. The STS model again shows slightly better agreement, but overall the values show a significant deviation. This shows that the multipole method is an approximate method to calculate R_b^*. This is because it is an a priori method and is based on a physical model of the borehole, which can differ from the actual setup. There can be differences between theory and practice, for example the actual borehole depth, spacing between the pipes, and grout moisture content.

These results indicate that the STS model provides a consistent alternative to the conventional ILS model. The next important question is whether the STS model also results in lower convergence times t_c compared to the ILS model, thereby enabling a reduction in required TRT duration, which is the main objective of this research. Section 11.3 presents and discusses these results.

11.3 Test Duration Reduction

After evaluating the consistency of the STS model, the next step is to assess the potential reduction in TRT duration, or equivalently, the difference in convergence time t_c between the ILS and STS approaches. This concept was introduced in Section 9.3.

To determine the convergence time t_c, an appropriate accuracy band first needs to be selected. There are three possible approaches here. The first is the average deviation of the thermal conductivity k from its converged value when using only a part of the TRT duration. For the 23 Terra Energy TRTs interpreted with the ILS model, the average deviation at 90%, 80%, and 70% of the total test duration equals 2.71%, 3.92%, and 5.07%, respectively. The second reference is the average deviation between the k-values obtained with the ILS and STS models, which equals 3.65%. Finally, the uncertainty associated with TRT measurements themselves can also be considered. Although this uncertainty is not available for the Terra Energy dataset, Aydin et al. [26] reported a typical uncertainty of approximately 5% for

TRT-derived thermal conductivity values. Based on these considerations, three representative accuracy bands are selected for the convergence analysis: a strict band of 2.71%, a realistic band of 5%, and a loose band of 10%.

The convergence time t_c is then determined as the earliest point after which the calculated k-values remain permanently within the selected accuracy band around the final converged value. Figure 11.2 illustrates this procedure for TRT3, showing the convergence behavior of both the ILS and STS model for an accuracy band of 5%. It shows a convergence time of 39 h for ILS and 35 h for STS, corresponding to a reduction of 4 hours in required TRT duration for this specific test.

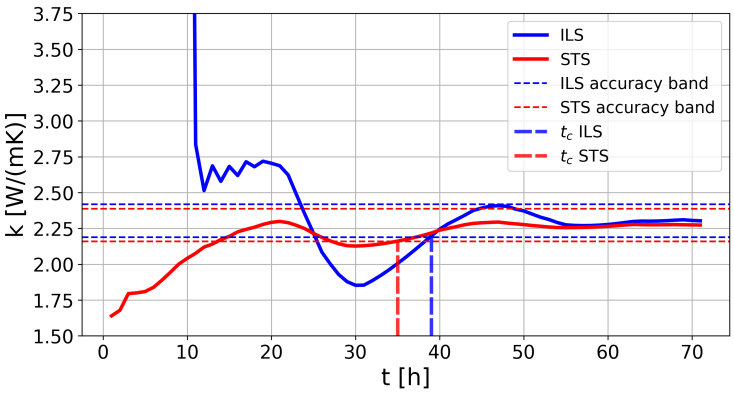


Figure 11.2: Convergence test comparing the ILS and STS model for TRT3, showing the calculated k-values, 5% accuracy band, and corresponding convergence time t_c for both methods.

Table 11.3 summarizes the convergence analysis for all 23 TRTs and for the three selected accuracy bands. Strikingly, the obtained reductions are significant. The STS model reduces the convergence time on average by 17.7 h for the 10% accuracy band, by 9.8 h for the 5% accuracy band, and by 5.5 h for the strict 2.71% accuracy band. Considering the average TRT duration of approximately 73 h, these reductions correspond to relative decreases in required test duration of respectively 24.2%, 13.4%, and 7.5%. These reductions are substantial, especially considering that both methodologies are applied to the same underlying measurement data.

Liu et al. [12] reported TRT time reductions between 21 and 46% for eight out of the nine TRTs in their dataset using an R-C model, with reductions defined relative to the total TRT duration and using a 5% accuracy band. For a consistent comparison, the STS results on the Terra Energy TRTs were also evaluated using this definition. This gives an average time reduction of 48.7% for the 23 Terra Energy TRTs, with 13 TRTs exceeding the maximum reduction reported by Liu et al. [12]. These results indicate that the STS approach achieves substantially larger duration reductions than the previously reported R-C model results.

In Table 11.3, negative differences indicate faster convergence of the STS model relative to ILS, while positive differences indicate slower convergence. For the 10% accuracy band, 18 TRTs show a reduction in convergence time and five show an increase. For the 5% accuracy band, 20 TRTs show a reduction and three show an increase. For the strict 2.71% accuracy band, 18 TRTs show a reduction and five show an increase. This shows that the STS model generally reduces convergence time, but not for every individual test. For the tests that showed an increase, no clear pattern could be identified. The reliability and quality of the linear fits did not appear to explain this behavior. The observed increase may be related to specific operational conditions, such as rainfall or ambient temperature fluctuations, but this remains speculative. The test data of all Terra Energy TRTs is shown in Appendix A.

The main reason for the reduced convergence time of the STS model compared to ILS is most likely the ability of the STS model to use the early-time TRT data that is discarded by the ILS methodology due to the standard 10 h cutoff time. This is confirmed by the results for the realistic 5% accuracy band, where the average reduction in convergence time equals 9.8 h, which is very close to the 10 h cutoff.

To test the hypothesis that the time reduction achieved by the STS model is mainly caused by the use of early-time data that is discarded in conventional ILS analysis, the influence of the cutoff time should be further investigated. Figure 11.3 shows the average convergence time reduction for the three selected accuracy bands as a function of the STS cutoff time, varied between 1 h and 10 h. The figure additionally shows the average deviation in calculated k-values between the STS and ILS methodologies as a function of this cutoff time.

The results confirm the expected behavior. As the STS cutoff time increases, the difference in convergence time between STS and ILS gradually decreases and even becomes slightly positive for the larger accuracy bands when the cutoff exceeds approximately 8 h. At the same time, the relative difference between the calculated k-values of both models decreases from approximately 4.5% for a 1 h cutoff to below 2% for a 10 h cutoff. This is expected because the measurement data used by both models become increasingly similar as the STS cutoff approaches the 10 h cutoff used for ILS. An additional observation is that the convergence time reduction decreases more rapidly for the larger accuracy bands. As a result, only the strictest accuracy band of 2.71% still shows a reduction in time over the full investigated cutoff range. Interestingly, the 17.7 h time reduction corresponding to the 10% accuracy band is significantly larger than the 10 h of previously discarded data. This is because the early-time data dampens further measurement instabilities in the convergence test and shows much more stable k-values. The effects of including the early-time data are much stronger than originally expected.

Table 11.3: Difference (Diff) in convergence times t_c [h] for the ILS and STS model using accuracy bands of 10%, 5%, and 2.71% for the 23 Terra Energy TRTs. Negative differences indicate faster convergence of STS relative to ILS, while positive differences indicate slower convergence. The bottom row shows the average time reduction.

TRT	t_c **10%** [h]			t_c **5%** [h]			t_c **2.71%** [h]		
	ILS	**STS**	**Diff**	**ILS**	**STS**	**Diff**	**ILS**	**STS**	**Diff**
TRT1	40	9	-31	44	11	-33	64	41	-23
TRT2	28	15	-13	32	23	-9	34	42	+8
TRT3	37	11	-26	39	35	-4	51	39	-12
TRT4	45	10	-35	64	41	-23	70	63	-7
TRT5	18	33	+15	36	43	+7	38	57	+19
TRT6	18	9	-9	47	41	-6	50	47	-3
TRT7	12	2	-10	12	3	-9	22	4	-18
TRT8	23	14	-9	57	30	-27	62	60	-2
TRT9	33	18	-15	35	23	-12	36	26	-10
TRT10	50	1	-49	53	41	-12	55	52	-3
TRT11	25	9	-16	28	19	-9	49	37	-12
TRT12	59	11	-48	64	59	-5	66	63	-3
TRT13	12	21	+9	22	37	+15	35	46	+11
TRT14	31	8	-23	61	27	-34	66	31	-35
TRT15	15	17	+2	52	48	-4	60	63	+3
TRT16	44	15	-29	56	47	-9	66	62	-4
TRT18	62	9	-53	66	59	-7	68	64	-4
TRT19	50	9	-41	58	48	-10	63	56	-7
TRT21	11	1	-10	43	34	-9	56	53	-3
TRT22	51	50	-1	64	62	-2	68	66	-2
TRT23	25	30	+5	41	52	+11	60	67	+7
TRT24	42	22	-20	59	25	-34	63	37	-26
TRT25	10	11	+1	57	56	-1	64	64	0
Average	32.2	14.5	**-17.7**	47.4	37.6	**-9.8**	55.0	49.6	**-5.5**

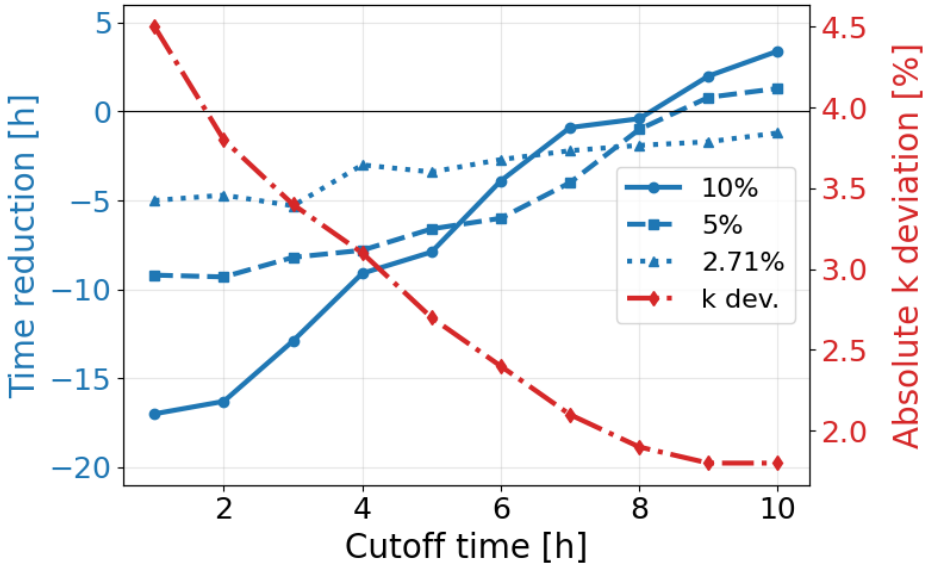


FIGURE 11.3: Average convergence time reduction of STS compared to ILS for accuracy bands of 10%, 5%, and 2.71%, together with the average relative difference in k between STS and ILS as a function of STS cutoff time, averaged over the 23 Terra Energy TRTs.

11.4 Sensitivity Analysis

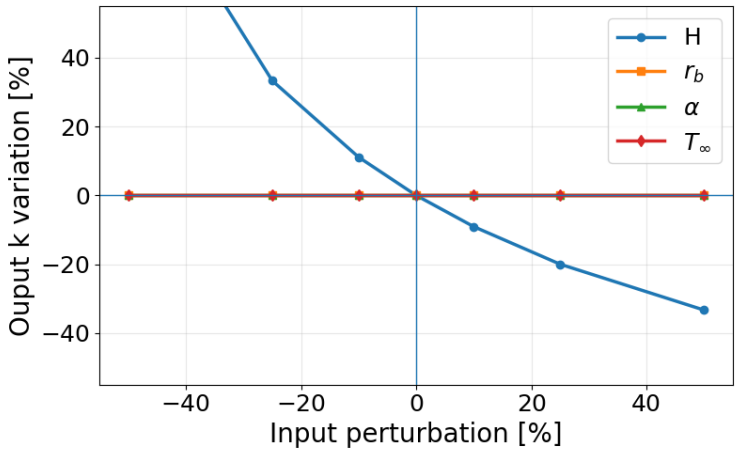
As shown in Section 11.3, the STS model provides significant reductions in required TRT duration. However, the model relies on a large number of input parameters, many of which are associated with some level of uncertainty. It is therefore important to evaluate the sensitivity of the STS methodology to these input parameters.

First, the sensitivity of the ILS model is analyzed. The relevant ILS input parameters are the borehole depth H, the borehole radius r_b, the thermal diffusivity α, and the undisturbed ground temperature T_∞. Each of these parameters was varied by $\pm 10\%$, $\pm 25\%$, and $\pm 50\%$ relative to its base value, after which the resulting k- and R_b^*-values were recalculated. The relative deviation of the calculated output parameters as a function of the applied input variation is shown in Figure 11.4(a) for k and Figure 11.4(b) for R_b^*.

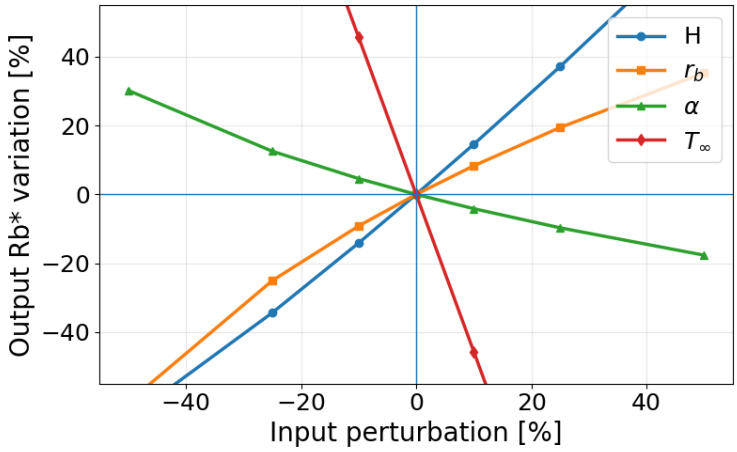
The borehole depth H has a strong influence on k and propagates almost linearly into the calculated result. The parameters r_b, α, and T_∞ show zero influence on the calculated k-value, which is expected since they are not directly involved in the ILS calculation of k.

For R_b^*, all four parameters have a significant influence. The undisturbed ground temperature T_∞ has by far the largest effect, where a perturbation in T_∞ results

in an approximately four times larger relative perturbation in R_b^*. The borehole depth H shows a similar influence as for k, while r_b and α also have significant, although smaller, effects on the calculated R_b^*-values.



(a) Sensitivity analysis k ILS

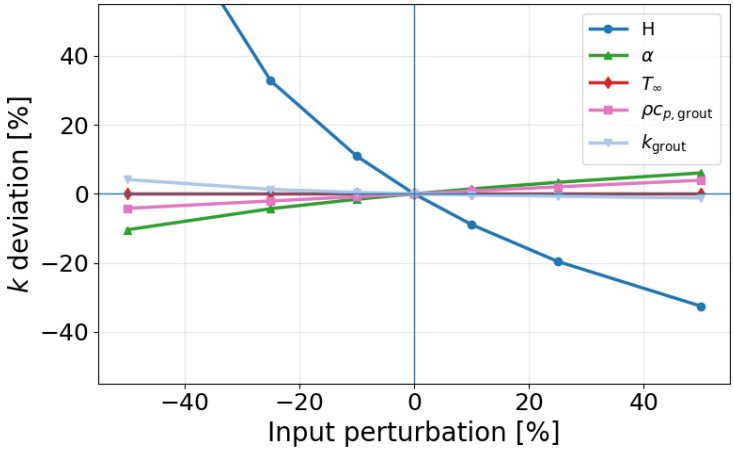


(b) Sensitivity analysis R_b^* ILS

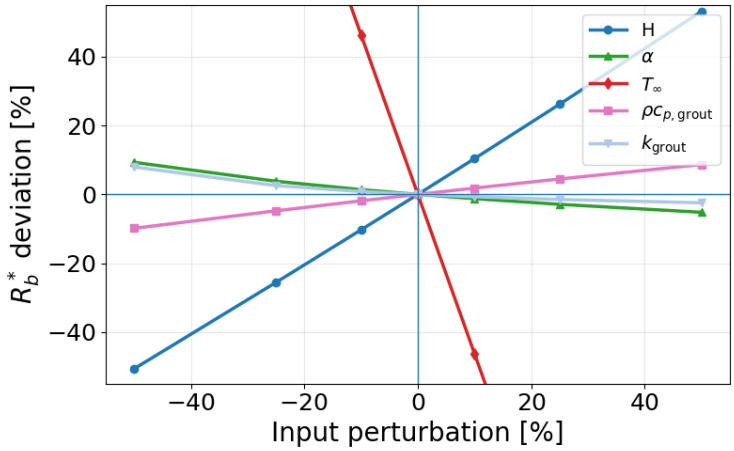
Figure 11.4: Sensitivity analysis of the estimated k (a) and R_b^* (b) to parameter perturbations, averaged over the 23 TRTs, for the ILS model. Each curve represents the relative change in the output parameter resulting from a ±50%, ±25%, and ±10% variation of a single input parameter, namely borehole length H, borehole radius r_b, thermal diffusivity α, or undisturbed ground temperature T_∞, around the baseline value.

The same sensitivity analysis was then performed for the STS model. The resulting sensitivities are shown in Figure 11.5(a) for k and Figure 11.5(b) for R_b^*. All parameters listed previously in Section 9.4 were evaluated. However, for visual clarity, only the parameters that produced a relative influence larger than 5% on either k

or R_b^* over the full perturbation range are included in the figures. These parameters are the borehole depth H, the thermal diffusivity α, the undisturbed ground temperature T_∞, the grout thermal conductivity k_g, and the grout volumetric heat capacity $(\rho c_p)_g$. It was not possible to test the influence of r_b due to geometrical constraints inside the STS model, but it likely has similar behavior as for the ILS model.



(a) Sensitivity analysis k STS



(b) Sensitivity analysis R_b^* STS

FIGURE 11.5: Sensitivity analysis of the estimated k (a) and R_b^* (b) to parameter perturbations, averaged over the 23 TRTs, for the STS model. Each curve represents the relative change in the output parameter resulting from a ±50%, ±25%, and ±10% variation of a single input parameter, namely borehole length H, grout volumetric heat capacity $(\rho c_p)_g$, thermal diffusivity α, undisturbed ground temperature T_∞, or grout thermal conductivity k_g, around the baseline value.

The influence of H and T_∞ is very similar to the behavior observed for the ILS model. The thermal diffusivity α also has a significant influence on both k and R_b^*, with a larger influence on the calculated k-values compared to ILS. This is important since α is generally not known precisely and must be estimated. The grout properties, more specifically the thermal conductivity k_g and volumetric heat capacity $(\rho c_p)_g$, also have a noticeable influence on the STS results. This indicates that accurate knowledge of the grout characteristics is important when applying transient TRT models. In practice, these values are typically available from technical datasheets provided by the grout supplier, making their uncertainty rather limited.

Interestingly, the variation in R_b^* caused by changes in α is much smaller for the STS model than for the ILS model. This is likely because the ILS model represents the borehole as an ideal line source that is directly and fully surrounded by the ground, making the result more sensitive to the assumed ground diffusivity. In the STS model, the borehole components are represented more explicitly, so the transient heat transfer first develops through the borehole materials before the ground response becomes dominant. This reduces the direct influence of α on the estimated R_b^*. Although this result was unexpected, it suggests that the STS model may provide a more reliable basis for estimating R_b^* than the ILS model, especially knowing that α is a parameter with significant uncertainty.

The STS methodology has a larger number of required input parameters compared to ILS, which can introduce more uncertainty. Nevertheless, the sensitivity analysis shows that most of these additional parameters have only a limited influence on the final TRT results. The main additional uncertainty source for k using STS compared to ILS is the ground thermal diffusivity α, which affects the STS results and is generally not precisely known. In contrast, the R_b^* values are more sensitive to the ground thermal diffusivity α for ILS compared to STS, which is an advantage for STS. In any case, the overall effect of α remains much smaller than the influence of T_∞ on the estimated R_b^*, which highlights the importance of the careful estimation of T_∞.

11.5 Conclusion

This chapter evaluated the STS model using the 23 Terra Energy TRTs. The comparison with the conventional ILS model showed that STS provides consistent parameter estimates, with an average deviation of 3.65% for k and 6.03% for R_b^*. The agreement is stronger for k than for R_b^*, which is expected because R_b^* is more sensitive to modeling assumptions and measurement uncertainty.

The main value of the STS model is not that it produces substantially different final parameter estimates, but that it can reach comparable estimates earlier. The convergence time was reduced on average by 17.7 h for the 10% accuracy band, 9.8 h for the 5% accuracy band, and 5.5 h for the strict 2.71% accuracy band. The 5%

accuracy band reduction is especially relevant because it is close to the 10 h early-time interval normally discarded in ILS analysis. This interpretation is supported by the cutoff-time analysis, which showed that the convergence advantage of STS decreases as the STS cutoff time is increased toward the 10 h cutoff used in the ILS analysis. This confirms that the reduction in required TRT duration is mainly caused by the ability of the STS model to use early-time data that are discarded in the conventional ILS approach. The larger reduction for the 10% band further suggests that including early-time data not only extends the usable dataset, but also stabilizes the early convergence behavior. Although this trend was clear on average, not every individual TRT showed a reduction in convergence time.

In addition, when evaluated using the same definition as Liu et al. [12], namely relative to the total TRT duration and with a 5% accuracy band, the STS approach achieved an average time reduction of 48.7% for the 23 Terra Energy TRTs, significantly exceeding their reported TRT duration reductions between 21 and 46%.

The sensitivity analysis showed that the STS model introduces additional input-parameter dependence, mainly through the thermal diffusivity α. As in the ILS model, the borehole depth H strongly affects k, while the undisturbed ground temperature T_∞ is the dominant parameter for R_b^*. However, most additional STS input parameters have only limited influence. An interesting result is that the influence of α on R_b^* is smaller for STS than for ILS, suggesting that the more explicit representation of the borehole components may reduce the dependence of R_b^* on uncertain ground diffusivity assumptions.

Overall, the STS model can be considered a consistent alternative to the conventional ILS model for reducing TRT duration. It provides similar final parameter estimates while making use of early-time data, with the practical reliability mainly depending on the accuracy of H, T_∞, and α.

Chapter 12

Field Test Results

This chapter discusses the results of the conducted field tests, following the methodology explained in Chapter 10. Section 12.1 discusses the results of the three CP-TRTs, while Section 12.2 discusses the results of the two CIT-TRTs. Finally, Section 12.3 compares both TRT methods in terms of operational stability, parameter estimation, and convergence behavior.

12.1 CP-TRTs

The three CP-TRTs were performed using the operating conditions listed previously in Table 10.2. The main difference between the tests is the thermal power setpoint of the electric heater, namely 2 kW, 4 kW, and 6 kW. CP-TRT1 and CP-TRT3 were both performed on borehole B2, while CP-TRT2 was performed on borehole B3. These boreholes are expected to be highly similar, apart from slight differences in grout properties.

Section 12.1.1 discusses the test output, more specifically the measured fluid temperatures and injected thermal power of the three CP-TRTs. Section 12.1.2 presents the parameter estimation of T_∞, k, and R_b^*. Section 12.1.3 then discusses the convergence behavior of the parameter estimation.

12.1.1 Test Output

Fluid Temperatures

Figure 12.1 shows the evolution of the three measured temperatures as a function of time for the three CP-TRTs. As expected, larger heater power setpoints result in higher fluid temperatures throughout the test.

The measurements show small temperature peaks approximately every 24 hours. These peaks are most pronounced for the heater supply temperature T_2. Since they consistently occur during the afternoon, they are most likely caused by ambient temperature effects on the water inside the different components of the TRT device.

Although these temperature fluctuations appear relatively small, they influence the parameter estimation results, as discussed further in Section 12.1.2. The effect is less pronounced in CP-TRT3 compared to the other two tests, especially during the first 48 hours. This is likely due to a combination of the additional insulation applied to the above-ground pipes between CP-TRT2 and CP-TRT3 and the milder weather conditions during the first two days of CP-TRT3.

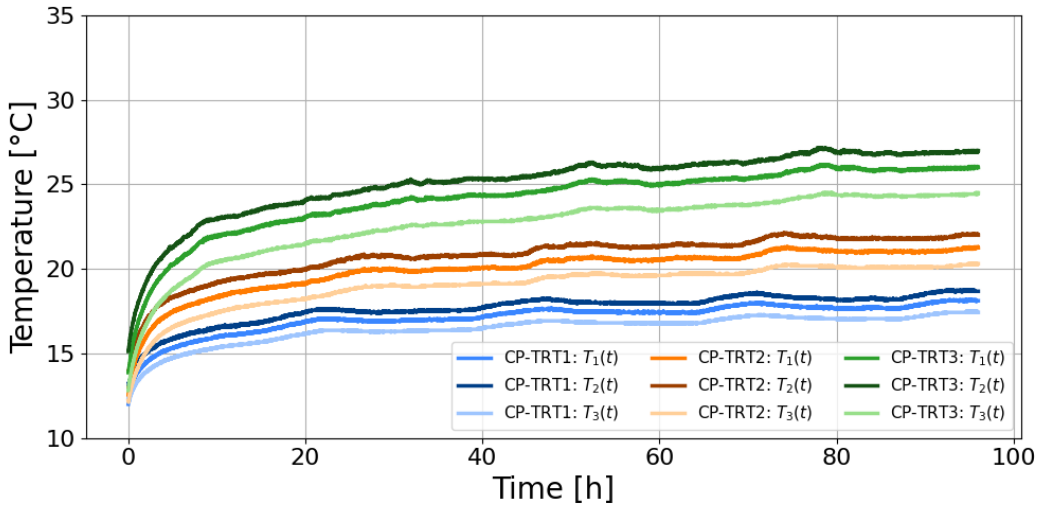


Figure 12.1: Measured fluid temperatures [°C] as a function of time [h] for CP-TRT1, CP-TRT2, and CP-TRT3, showing T_1, T_2, and T_3.

Thermal Power

The thermal power injected into the borehole is calculated as the product of the volumetric flow rate $\dot{V}$, the density ρ and heat capacity c_p of the fluid, and the temperature difference between T_1 and T_3, following Equation 10.1. Figure 12.2 shows the resulting thermal power for each CP-TRT.

In a CP-TRT, the injected thermal power should remain as constant as possible. This is achieved reasonably well for all three tests. The observed fluctuations are comparable to CP-TRT data published in literature, for example by Aydin et al. [26], shown previously in Figure 3.2. These variations are partly caused by the resolution of the flow and temperature sensors.

The periodic peaks are also visible in the thermal power profiles. Another observation is that the average injected thermal powers, namely 1.7 kW, 2.8 kW, and 4.1 kW, are significantly lower than the installed electric heater powers of 2 kW, 4 kW, and 6 kW. This corresponds to thermal losses of 15%, 30%, and 32%, respectively. In other words, a considerable part of the thermal power generated by the heater is lost to the environment instead of reaching the borehole.

Compared to values typically reported in literature, these thermal losses are relatively large, although still realistic for this type of setup. The large buffer tank likely contributes to these losses, since the heated water remains in the system longer before entering the borehole. Improved insulation of all components would most likely reduce these thermal losses further. An interesting observation is that the relative thermal losses for CP-TRT3 remain similar to those of CP-TRT2, despite the higher thermal power setpoint. This indicates that the additional insulation applied to the above-ground pipes, as discussed in Section 7.4.1, effectively reduced the heat losses to the environment.

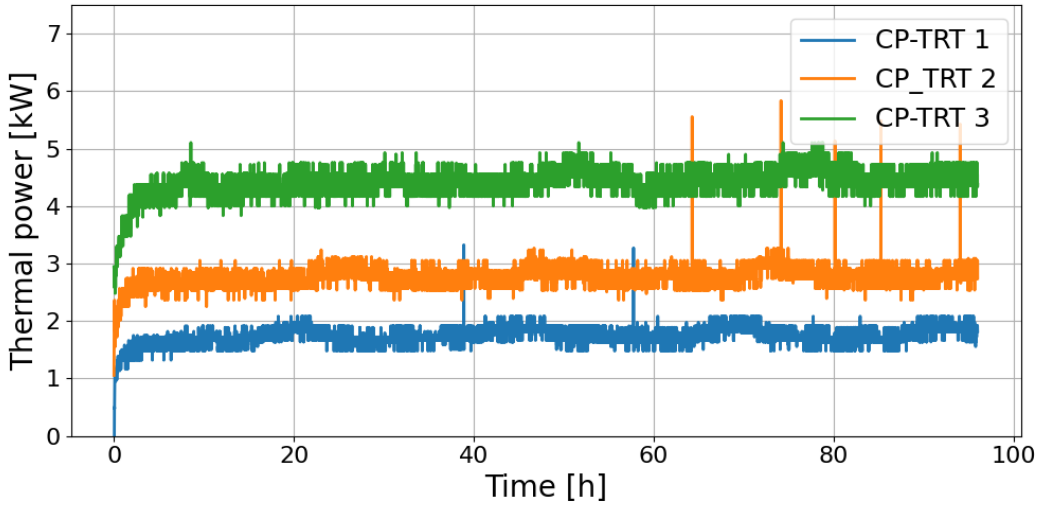


FIGURE 12.2: Thermal power [kW] calculated from measured $\dot{V}$, T_1, and T_3 as a function of time [h] for CP-TRT1, CP-TRT2, and CP-TRT3.

12.1.2 Parameter Estimation

Undisturbed Ground Temperature T_∞

As explained in Section 10.2.2, the undisturbed ground temperature T_∞ is determined by circulating the fluid through the borehole without activating the heater and analyzing the resulting temperature response over time. Figure 12.3 shows the response of the inlet and outlet temperatures T_1 and T_3 during one hour of circulation without activating the heater for CP-TRT1. The other two tests showed a similar result.

In this TRT setup, the measured temperatures are influenced by the water volume inside the buffer tank. Ideally, the circulation test would be performed without a buffer tank, so that only the fluid temperature inside the borehole affects the measurements. Alternatively, a temperature probe inside the borehole would provide a more direct measurement.

Because the objective is to capture the temperature of the water originally present in the borehole, rather than that of the water in the buffer tank, it is more appropriate to consider only the first ten minutes of circulation. During this initial period, the average temperature is $12.3°C$ for CP-TRT1. The measurements show that the fluid temperatures stabilize around 6 to 9 minutes, which is likely close to the average temperature of the water that was inside the borehole. Afterwards, the measured temperature gradually increases, most likely due to the influence of the warmer water inside the buffer tank, which had a temperature of approximately 15 $°C$ before the start of the test. This demonstrates that accurately estimating T_∞ becomes more difficult when the initial buffer tank temperature differs from the actual ground temperature.

Following the recommendations of Gehlin and Nordell [25], discussed previously in Section 10.2.2, T_∞ is typically determined after approximately 20 minutes of circulation. However, considering the higher flow rate used in this setup and the temperature response shown in Figure 12.3, T_∞ is determined after 10 minutes of circulation as the average of T_1 and T_3. The T_∞ values for all CP-TRTs were determined using the same methodology and are shown in Table 12.1.

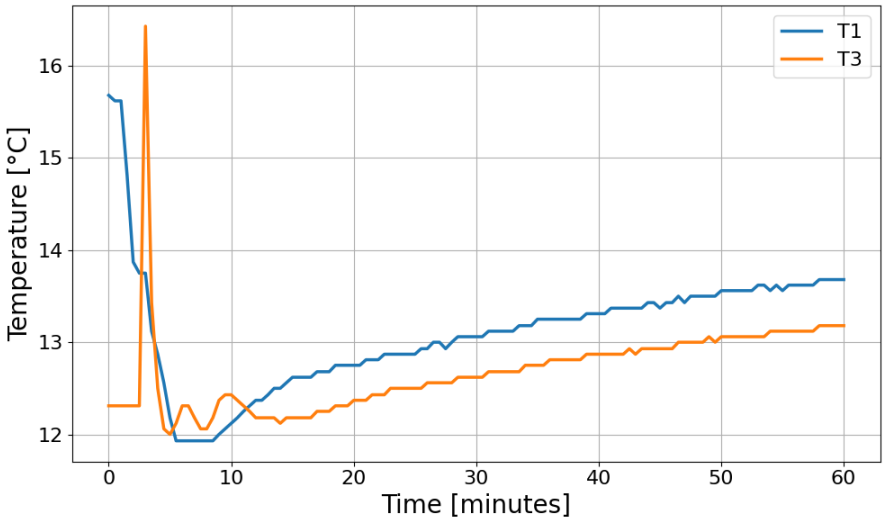


Figure 12.3: Borehole inlet temperature T_1 and borehole outlet temperature T_3 during one hour of circulation without heater activation for CP-TRT1.

Thermal conductivity k and borehole resistance R_b^*

Figure 12.4 shows the mean fluid temperature, calculated as the average of T_1 and T_3, together with the linear fit corresponding to the ILS solution. The obtained linear fits are reasonably good and comparable to CP-TRT results reported in literature, such as the example shown in Figure 5.2 based on the measurement data of Aydin et al. [26]. The resulting parameter values are shown in Table 12.1. The obtained k-

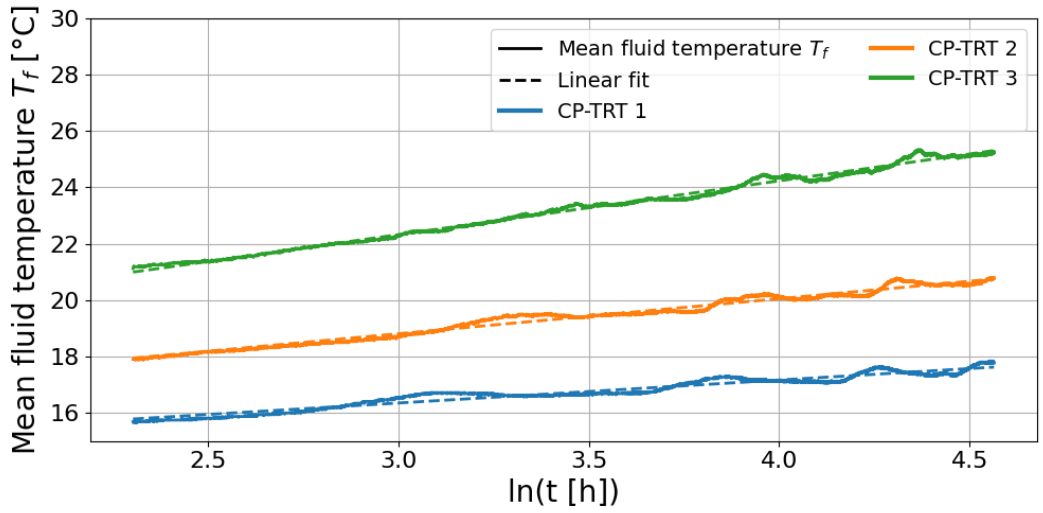


FIGURE 12.4: Mean fluid temperature $\overline{T}_f(t)$ [°C] and corresponding linear ILS fit as a function of $\ln(t)$, with t in hours, for CP-TRT1, CP-TRT2, and CP-TRT3.

values are 1.728, 1.793 and 1.865 $W/(mK)$ for CP-TRT1, CP-TRT2, and CP-TRT3, respectively. These values seem realistic, since they are relatively close to each other and reasonably consistent with geological estimates. For this location and borehole depth, Smart Geotherm predicts a k-value of 2.1 $W/(mK)$, which is slightly higher than the values obtained from the CP-TRTs but still within a plausible range. The corresponding MAPE values are 2.52 %, 1.40 %, and 0.87 %, and are shown as a percentage deviation behind the parameter estimations in Table 12.1. The downward trend suggests an increased measurement quality, and the value of CP-TRT3 is of a similar order of magnitude as the value of 0.50% for a CP-TRT reported by Aydin et al. [26].

TABLE 12.1: Overview of the CP-TRT results, including operating conditions, estimated parameters, and fit quality.

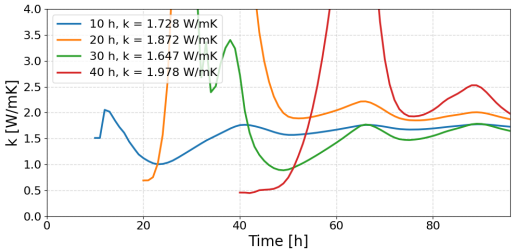
Test	**Power [kW]**	**Flow rate [m^3/h]**	T_∞ [°C]	k **[W/(mK)]**	R_b^* **[mK/W]**	**MAPE [%]**
CP-TRT1	2	2.4	12.3	1.728	0.133	2.52
CP-TRT2	4	2.4	12.4	1.793	0.135	1.40
CP-TRT3	6	2.4	13.2	1.865	0.112	0.87

The corresponding R_b^*-values are 0.133, 0.135, and 0.112 mK/W. These values also lie relatively close to each other, although R_b^* is more borehole-specific and generally more sensitive to measurement uncertainty than k. The multipole method, introduced in Chapter 5, is an a priori method used for estimating R_b^* and results in a

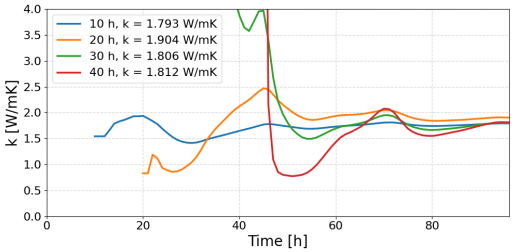
value of 0.118 mK/W for CP-TRT1 and CP-TRT3, and a value of 0.114 mK/W for CP-TRT2, with the only difference being the grout thermal conductivities of the boreholes. This matches reasonably well with the obtained CP-TRT estimates, especially with CP-TRT3. CP-TRT1 and CP-TRT3 were both performed on borehole B2, but still result in a noticeable difference in R_b^*. This difference may be related to the changed insulation conditions and the influence of ambient temperature fluctuations.

12.1.3 Convergence

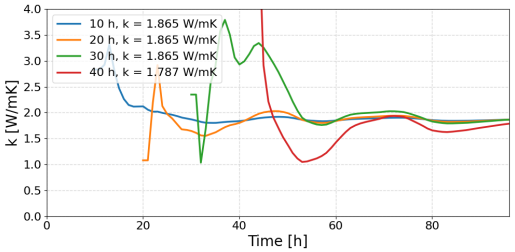
Figures 12.5(a), 12.5(b), and 12.5(c) show the convergence tests for the three CP-TRTs. Clear differences are observed between the tests. CP-TRT1 shows significant fluctuations and poor convergence, while CP-TRT2 shows improved convergence. CP-TRT3 shows strong convergence, with an identical k-value of 1.865 $W/(mK)$ for cutoff times of 10 h, 20 h, and 30 h. A cutoff time of 40 h is also shown to evaluate further convergence, but this is generally too close to the end of the test.



(a) Convergence test CP-TRT1



(b) Convergence test CP-TRT2



(c) Convergence test CP-TRT3

Figure 12.5: Convergence tests for CP-TRT1 (a), CP-TRT2 (b), and CP-TRT3 (c), showing the k-values calculated with the ILS model as a function of time for cutoff times of 10 h, 20 h, 30 h, and 40 h.

This improved convergence is directly linked to the reduced temperature fluctuations during the first 30 hours of CP-TRT3, indicating a lower influence of ambient conditions on the measurements. This was most likely caused by a combination of the additional insulation applied to the above-ground pipes and the milder weather conditions during the test period.

The convergence of CP-TRT3 shows that the developed TRT device can generate stable CP-TRT data under favorable operating conditions. If this behavior is reproduced in future CP-TRTs, it suggests that this TRT device is suitable for industry use.

12.2 CIT-TRTs

The two CIT-TRTs were performed on different boreholes using the operating conditions listed previously in Table 10.2. CIT-TRT1 was performed with a heater supply temperature setpoint of 20 $°C$, while CIT-TRT2 had a setpoint of 30 $°C$. A major operational difference between both tests was the additional insulation of the heater temperature sensor before CIT-TRT2, as explained in Section 7.4.2.

The CIT-TRT results are discussed using the same structure as for the CP-TRTs. Section 12.2.1 discusses the measured fluid temperatures and injected thermal power. Section 12.2.2 presents the parameter estimation results, focusing mainly on the thermal conductivity k. The T_∞-values are determined using the same methodology as for the CP-TRTs and are therefore only reported in the results table. Section 12.2.3 then discusses the convergence behavior of the CIT-TRTs.

12.2.1 Test Output

Fluid Temperatures

Figure 12.6 shows the evolution of the three measured temperatures as a function of time for the two CIT-TRTs. The $T_2(t)$ line represents the heater supply temperature, which is the actively controlled temperature in the CIT-TRT setup. For CIT-TRT1, the fluctuations around the setpoint are clearly larger than for CIT-TRT2. The more stable behavior of CIT-TRT2 has two plausible explanations. First, the heater supply temperature sensor was better insulated before CIT-TRT2, reducing the direct influence of ambient temperature on the control signal. Second, the higher temperature setpoint may make the relative influence of ambient temperature smaller. Since CIT-TRT2 was performed under high ambient temperatures at the end of May 2026, the improved insulation of the temperature sensor is likely the dominant explanation. This difference between CIT-TRT1 and CIT-TRT2 is important because fluctuations in the controlled temperature directly affect the thermal power profile and therefore the parameter estimation. As discussed in Section 12.2.2, the unstable temperature control of CIT-TRT1 strongly affects the reliability of the resulting analysis.

Thermal Power

Figure 12.7 shows the calculated thermal power injected into the borehole during the two CIT-TRTs. Both tests show a large initial peak, during which the electric heater delivers high thermal power to reach the temperature setpoint as quickly as

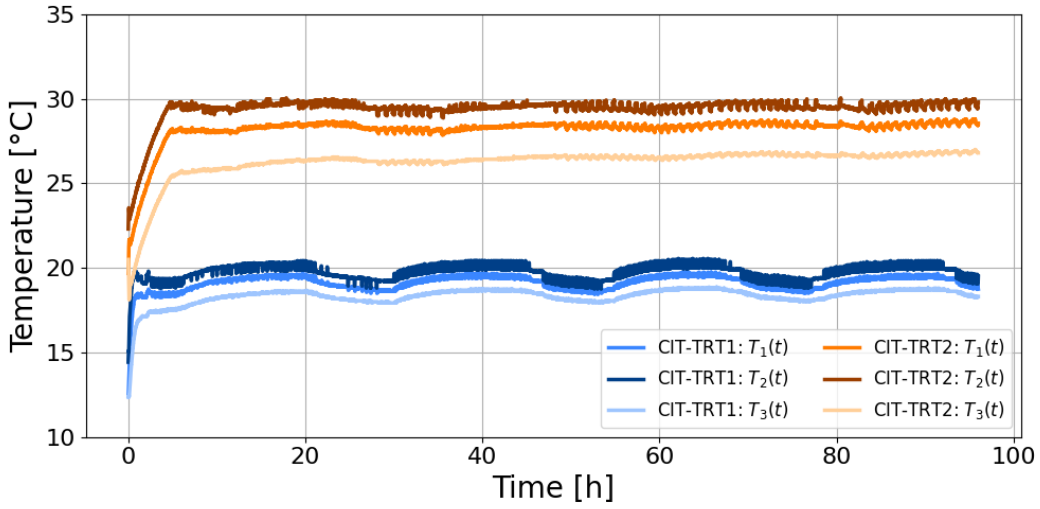


Figure 12.6: Measured fluid temperatures [°C] as a function of time [h] for CIT-TRT1 and CIT-TRT2, showing T_1, T_2, and T_3.

possible. After this initial phase, the thermal power gradually decreases toward a more stable value as the ground and borehole system heat up.

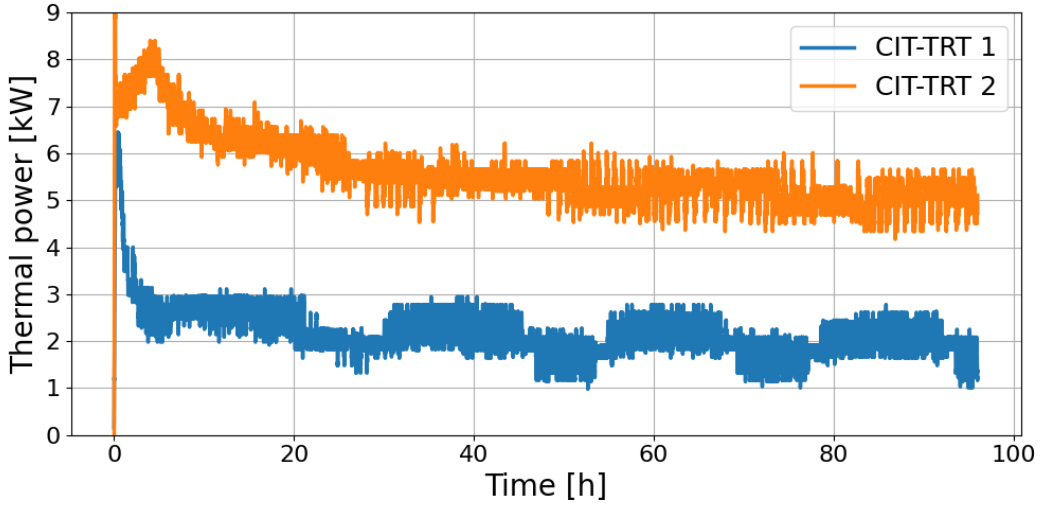


Figure 12.7: Thermal power [kW] calculated from measured $\dot{V}$, T_1, and T_3 as a function of time [h] for CIT-TRT1 and CIT-TRT2.

The initial peak is earlier and shorter for CIT-TRT1, because the 20 $°C$ setpoint is reached faster than the 30 $°C$ setpoint of CIT-TRT2. The overall shape corresponds to the CIT-TRT data published by Aydin et al. [26], shown previously in Figure 3.3. However, important differences remain. For CIT-TRT1, the tempera-

ture fluctuations are clearly reflected in the thermal power profile. CIT-TRT2 shows a more stable thermal power evolution, although the variations remain larger than in the literature example. These remaining variations are likely caused by residual temperature-control fluctuations and by the limited resolution of the flow meter.

12.2.2 Parameter Estimation

Undisturbed Ground Temperature T_∞

The undisturbed ground temperature T_∞ is determined using the same procedure as for the CP-TRTs. Therefore, the procedure is not repeated here. The resulting T_∞ values for the two CIT-TRTs are shown in Table 12.2.

Thermal conductivity k and borehole resistance R_b^*

Figure 12.8 shows the inverse of the thermal power per unit borehole length $1/q(t)$, together with the linear fit corresponding to the constant-temperature analytical solution. The linear fit of CIT-TRT2 is reasonably consistent with the example shown in Figure 5.3, based on the measurement data of Aydin et al. [26], although the scale is different. In contrast, CIT-TRT1 shows large fluctuations that stem from the temperature fluctuations that were shown earlier. The results of CIT-TRT1 are therefore likely unreliable, although the calculated k-value from this measurement seems realistic.

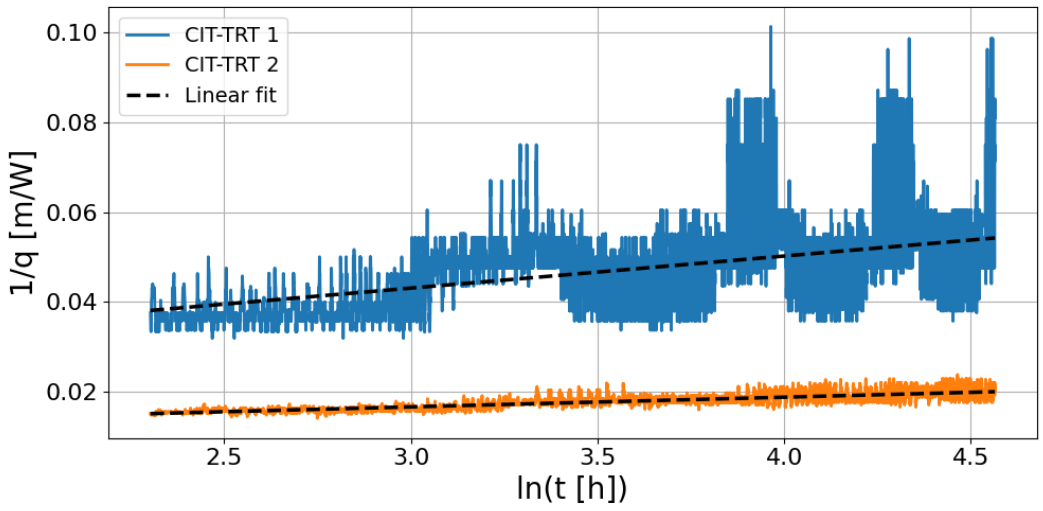


FIGURE 12.8: Inverse thermal power per unit borehole length $1/q(t)$ [m/W] and corresponding linear fit as a function of $\ln(t)$, with t in hours, for CIT-TRT1 and CIT-TRT2.

The resulting k-values are shown in Table 12.2. The obtained values are 2.02 $W/(mK)$ for CIT-TRT1 and 2.53 $W/(mK)$ for CIT-TRT2. The value obtained

for CIT-TRT1 is close to the Smart Geotherm estimate of 2.1 $W/(mK)$, but the reliability of this result is limited by the strong fluctuations in the thermal power profile. The value obtained for CIT-TRT2 is higher than both the CP-TRT results and the Smart Geotherm estimate. This may be related to differences between boreholes, the higher temperature setpoint, remaining measurement fluctuations, or an inherent difference in CIT-TRT and CP-TRT results. The corresponding MAPE values are 12.78% and 4.27%, and are shown as a percentage deviation behind the parameter estimations in Table 12.2. This shows the low measurement quality of CIT-TRT1 and the improvement for CIT-TRT2, although the MAPE remains significantly higher than for the CP-TRTs. This is the same conclusion as Aydin et al. [26] found, as their CIT-TRT showed a MAPE of 2.9%. It suggests that CIT-TRTs show larger measurement fluctuations and therefore have a larger uncertainty.

Compared to CIT-TRT1, CIT-TRT2 shows a more stable controlled temperature and a more reliable linear fit. This indicates that additional insulation of the heater supply temperature sensor significantly improves the quality of the CIT-TRT measurement data. Further reducing ambient temperature effects would likely improve the reliability of the CIT-TRT results. In any case, more CIT-TRTs should be performed to draw firm conclusions. To determine the reliability and the stability of the results, it is important to look at the convergence, which is discussed in Section 12.2.3.

Table 12.2: Overview of the CIT-TRT results, including operating conditions, estimated thermal conductivity, and fit quality.

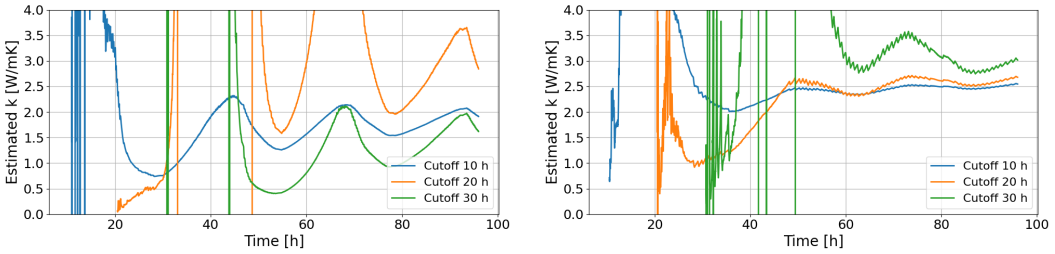
Test	**Temperature** [°C]	**Flow rate** [$\mathbf{m^3/h}$]	$\mathbf{T_\infty}$ [°C]	k $[W/(mK)]$	**MAPE** [%]
CIT-TRT1	20	2.4	13.0	2.02	12.78
CIT-TRT2	30	2.4	13.0	2.53	4.27

12.2.3 Convergence

Figures 12.9(a) and 12.9(b) show the convergence tests for CIT-TRT1 and CIT-TRT2. The convergence behavior differs strongly between the two tests. CIT-TRT1 shows poor convergence, which is consistent with the large temperature and thermal power fluctuations observed in Figures 12.6 and 12.7. The estimated k-value remains sensitive to the selected fitting window, indicating that the measurement data is not sufficiently stable for reliable convergence.

CIT-TRT2 shows improved convergence behavior compared to CIT-TRT1. This is consistent with the more stable heater supply temperature and smoother thermal power profile. However, the convergence is still worse than CP-TRT3. This indicates that the practical stability of the temperature-control system is a decisive factor for the performance of CIT-TRTs. A possible explanation for the poorer convergence

compared to the CP-TRTs is that the current TRT device is better suited for CP-TRT operation than for CIT-TRT operation. The CIT-TRT results may also have been affected by the warm ambient conditions during CIT-TRT2, or by an inherent sensitivity of CIT-TRTs to temperature-control fluctuations. Additional tests are required to evaluate these hypotheses.



(a) Convergence test CIT-TRT1 (b) Convergence test CIT-TRT2

FIGURE 12.9: Convergence tests for CIT-TRT1 (a) and CIT-TRT2 (b), showing the k-values calculated as a function of time for cutoff times of 10 h, 20 h, and 30 h.

12.3 Comparison of CP- and CIT-TRTs

The CP- and CIT-TRTs are compared based on operational stability, parameter estimation, and convergence time. In terms of operational stability, the CP-TRTs performed more reliably than the CIT-TRTs. The injected thermal power in the CP-TRTs remained reasonably stable, although thermal losses and daily ambient-temperature effects were still visible. For the CIT-TRTs, the controlled heater supply temperature was more sensitive to ambient temperature effects. This was especially clear for CIT-TRT1, where the fluctuations in T_2 strongly affected the calculated thermal power. CIT-TRT2 showed a substantial improvement after additional sensor insulation, confirming the importance of proper insulation for CIT-TRT operation.

In terms of parameter estimation, the CP-TRTs produced consistent k-values between 1.728 and 1.865 $W/(mK)$. These values are somewhat lower than the Smart Geotherm estimate of 2.1 $W/(mK)$, but remain within a realistic range. The CIT-TRTs produced k-values of 2.02 and 2.53 $W/(mK)$. CIT-TRT1 is close to the geological estimate, but its reliability is limited by strong measurement fluctuations. CIT-TRT2 shows better measurement stability, but gives a higher k-value than the CP-TRTs and the Smart Geotherm estimate.

Table 12.3 summarizes the convergence times for the estimated k-values of all field tests. For the strict 2.71% accuracy band, CIT-TRT1 and CIT-TRT2 reach convergence after 95.2 h and 90.3 h, respectively. For the 5% accuracy band, the corresponding convergence times are 94.5 h and 67.5 h. For the 10% accuracy band, they

are 84.0 h and 44.8 h. These values show that CIT-TRT2 clearly performs better than CIT-TRT1, but that the CIT-TRTs show significantly slower convergence than the CP-TRTs in the conducted field tests. Based on these results, the hypothesis that CIT-TRTs reach stable parameter estimates faster and can therefore reduce the required TRT duration is not confirmed. However, additional CIT-TRTs with improved thermal stability are needed before a definitive conclusion can be drawn.

Table 12.3: Convergence times t_c for the estimated thermal conductivity k of the CP- and CIT-TRTs for accuracy bands of 2.71%, 5%, and 10%.

Test	t_c **2.71% [h]**	t_c **5% [h]**	t_c **10% [h]**
CP-TRT1	90.4	58.1	35.1
CP-TRT2	82.0	57.3	38.6
CP-TRT3	49.4	26.1	21.1
CIT-TRT1	95.2	94.5	84.0
CIT-TRT2	90.3	67.5	44.8

12.4 Conclusion

This chapter presented the results of the field tests performed with the developed TRT device. The CP-TRTs produced realistic and relatively consistent k-values between 1.728 and 1.865 $W/(mK)$, which are somewhat lower than but still reasonably close to the Smart Geotherm estimate of 2.1 $W/(mK)$. The measurement quality improved over the three CP-TRTs, as shown by the decreasing MAPE values of 2.52%, 1.40%, and 0.87%. This improvement was also reflected in the convergence behavior, as CP-TRT3 showed the most stable result, with the same k-value obtained for cutoff times of 10 h, 20 h, and 30 h. These results show that the developed device is ready for industry use in CP-TRT operating mode, provided that sufficient insulation and stable operating conditions are maintained.

The CP-TRTs also revealed an important practical limitation of the setup. The average injected powers were 1.7, 2.8, and 4.1 kW for heater setpoints of 2, 4, and 6 kW, corresponding to thermal losses of 15%, 30%, and 32%. These losses are relatively large and show that further insulation of the above-ground components remains important. Nevertheless, the improved behavior of CP-TRT3 indicates that the applied insulation measures already reduced the influence of ambient conditions on the measurements.

The CIT-TRTs showed that constant inlet temperature testing is possible with the developed device, but also that the method is highly sensitive to temperature-control stability. CIT-TRT1 was strongly affected by temperature and power fluctuations, resulting in a high MAPE of 12.78%. CIT-TRT2 improved after additional insulation of the heater supply temperature sensor, reducing the MAPE to 4.27%, but its

convergence remained worse than that of the best CP-TRT. The CIT-TRTs therefore showed clear improvement after insulation, but still larger uncertainty than the CP-TRTs.

Overall, the field tests confirm that the developed device is currently better suited for CP-TRT operation than for CIT-TRT operation. In this setup, the hypothesis that CIT-TRTs reach stable parameter estimates faster than CP-TRTs was not confirmed. The main limitation of the CIT-TRTs was not the analytical method itself, but the practical stability of the temperature-control system and its sensitivity to ambient conditions. Additional CIT-TRTs with improved thermal control are required before drawing general conclusions about the performance of CIT-TRTs relative to CP-TRTs.

Part V

Conclusion and Suggestions for Further Research

Chapter 13

Conclusion

This thesis investigated whether the required duration of thermal response tests can be reduced by incorporating transient borehole effects into the analysis and compared CP-TRTs with CIT-TRTs. This chapter formulates a comprehensive answer to the research questions introduced in Chapter 1. The research focused on three elements: the implementation of the STS model on the Terra Energy dataset (RQ1), the development of a TRT device (RQ2), and the experimental comparison between CP- and CIT-TRTs (RQ3).

Implementation of the STS model (RQ1)

The clearest result of this thesis is that transient borehole modeling can reduce the required duration of CP-TRTs. The STS model, applied to the 23 Terra Energy TRTs, produced thermal conductivity k and borehole resistance R_b^* estimates that were in good agreement with the conventional ILS model. The average deviation between ILS and STS was 3.65% for the thermal conductivity k and 6.03% for the effective borehole thermal resistance R_b^*. This indicates that the STS model remains close to the conventional interpretation while allowing earlier parts of the TRT data to be used.

The main advantage of the STS model was observed in the convergence analysis. Compared to the conventional ILS approach, the average convergence time was reduced by 17.7 h for the 10% accuracy band, 9.8 h for the 5% band, and 5.5 h for the strict 2.71% band. Relative to the average Terra Energy test duration of approximately 73 h, these reductions correspond to 24.2%, 13.4%, and 7.5%, respectively. The most practically relevant result is the reduction of 9.8 h for the 5% accuracy band, since this band is close to typical TRT uncertainty and approximately corresponds to the 10 h early-time interval discarded in the ILS approach. This interpretation was confirmed by the cutoff-time analysis, which showed that the convergence advantage of STS decreases as the STS cutoff time is increased toward the 10 h cutoff used in the ILS analysis. The larger reduction of 17.7 h for the 10% band suggests that the early-time data does not only extend the usable dataset, but also stabilizes the early convergence behavior of the calculated k-values. When

evaluated using the same reduction definition as Liu et al. [12], namely relative to the total TRT duration and with a 5% accuracy band, the STS approach achieved an average reduction of 48.7%, significantly exceeding their reported TRT duration reductions between 21 and 46%.

This allows an answer to RQ1. Incorporating transient borehole effects through the STS model is an effective way to reduce the required duration of CP-TRTs while maintaining thermal conductivity estimates close to the conventional ILS model. The reduction is not obtained for every individual test, but the overall trend across the 23 TRTs is significant. The main practical advantage is that this reduction is achieved through improved data interpretation, without changing the physical TRT setup. The only disadvantages are the additional input parameters, higher sensitivity of k to some uncertain parameters, especially α, and slightly increased computational effort. However, the influence of α on R_b^* was smaller for STS than for ILS, which is an unexpected advantage of the STS model for estimating R_b^*.

Development of the TRT device (RQ2)

The developed TRT device successfully performed both CP- and CIT-TRTs. The CP-TRT results were realistic and relatively consistent, with thermal conductivities of 1.728, 1.793, and 1.865 $W/(mK)$. The measurement quality improved throughout the CP-TRTs, as shown by the decreasing MAPE values of 2.52%, 1.40%, and 0.87%. Convergence behavior also improved from CP-TRT1 to CP-TRT3, suggesting that the system became more stable during operation. CP-TRT3 even showed identical final k-values for cutoff times of 10 h, 20 h, and 30 h. These results show that the TRT device is ready for industry use in CP-TRT operating mode, provided that sufficient insulation and stable operating conditions are maintained.

At the same time, the field tests revealed several practical limitations, especially ambient temperature effects, heat losses, and the influence of the buffer tank on the determination of T_∞. These effects were reduced by additional insulation, but not fully eliminated. Further improvements are therefore still possible, including improved insulation, ambient temperature control, a bypass or redesign of the buffer tank, and optimization of the measurement interval and flow rate measurement.

This allows an answer to RQ2. A TRT device capable of performing both CP- and CIT-TRTs was successfully developed and generated useful experimental datasets, particularly for CP-TRTs. The device can produce stable CP-TRT data under sufficiently controlled field conditions. However, further improvements are required before CIT-TRTs can be considered equally reliable.

Experimental comparison between CP- and CIT-TRTs (RQ3)

The comparison between CP- and CIT-TRTs was less conclusive. This is mainly because larger datasets are needed to draw clear conclusions. The CIT-TRTs showed

the expected thermal behavior, with an initially high thermal power peak followed by a gradual decrease toward a more stable condition. However, CIT operation proved more sensitive to control instability because the imposed boundary condition depends directly on the heater supply temperature. Any fluctuation in this controlled temperature directly affects the thermal power profile and therefore the parameter estimation. This was also reflected in the MAPE values: CIT-TRT1 had a MAPE of 12.78%, while CIT-TRT2 improved to 4.27% after additional insulation of the heater supply temperature sensor. These values are higher than for the CP-TRTs, indicating larger measurement uncertainty for the CIT-TRTs in this setup.

This sensitivity affected the results. CIT-TRT1, performed at $20°C$, was strongly disturbed by temperature fluctuations. CIT-TRT2, performed at $30°C$ after additional insulation of the heater supply temperature sensor, improved substantially. Nevertheless, the derived thermal conductivity value of 2.53 $W/(mK)$ for CIT-TRT2 differs significantly from the CP-TRT-derived values and the Smart Geotherm estimate. The convergence times likewise did not show an advantage for CIT-TRTs in this setup. CP-TRT3 reached the 10%, 5%, and 2.71% bands after 21.1 h, 26.1 h, and 49.4 h, respectively, while CIT-TRT2 required 44.8 h, 67.5 h, and 90.3 h. The hypothesis that CIT-TRTs could inherently provide a shorter TRT duration is therefore not confirmed.

This allows an answer to RQ3. In the conducted field tests, CP-TRTs were more robust, produced more consistent parameter estimates, and converged faster than CIT-TRTs. The hypothesis that CIT-TRTs can reduce the required TRT duration was therefore not confirmed in this experimental setup. However, this conclusion is based on only two CIT-TRTs and should not be generalized without further testing. CIT-TRTs remain theoretically interesting, but their practical performance depends strongly on temperature-control stability and shielding from ambient influences.

Main Research Question

The main research question of this thesis was:

> **To what extent can the required duration of TRTs be reduced by incorporating transient borehole effects into the TRT analysis, and how do CP- and CIT-TRTs compare in terms of parameter estimation and test duration?**

The overall answer is that the required duration of CP-TRTs can be reduced effectively by including transient borehole effects in the interpretation model. For the Terra Energy dataset, the STS model shortened the average convergence time by 17.7 h, 9.8 h, and 5.5 h for the 10%, 5%, and 2.71% accuracy bands, while maintaining good agreement with the conventional ILS interpretation. This demonstrates that meaningful time savings can be achieved through improved modeling rather than changes to the physical test setup.

In contrast, the conducted CIT-TRTs did not reduce the required test duration. Although they showed the expected thermal response, they were more sensitive to temperature-control instability and ambient influences, resulting in less stable parameter estimation and slower convergence than the CP-TRTs in this experimental setup.

Therefore, the central conclusion of this thesis is that transient borehole modeling is a practically effective method to reduce TRT duration, while CIT-TRTs were not shown to reduce test duration in the developed experimental setup. Larger CIT-TRT datasets are needed to draw clear conclusions.

Chapter 14

Suggestions for Future Research

This chapter presents recommendations for future research and for the practical development of TRT devices. Section 14.1 discusses practical design lessons from the developed TRT device and identifies possible improvements to the specific setup used in this research. Section 14.2 discusses further work related to transient borehole modeling. Section 14.3 focuses on future research on CIT-TRTs and their comparison with conventional CP-TRTs.

14.1 TRT device

14.1.1 Guidelines for future TRT device builders

Several practical lessons were learned during the design and operation of the TRT device, as discussed in Chapter 7. These lessons can be useful for future TRT device development.

First, the required device complexity depends strongly on the intended test type. If the device is only intended for CP-TRTs, the design can be simplified considerably. For example, the buffer tank could be removed or reduced in size, and the electric heater could be replaced by electrical resistance heaters. This would reduce device size, investment cost, transport cost, and operational complexity. However, the buffer tank also proved useful for both test types, especially for CIT-TRTs. It reduced temperature fluctuations caused by heater instability and external disturbances. Removing the buffer tank would therefore probably reduce test quality. A smaller buffer tank could be a better compromise, since it would retain part of the stabilizing effect while reducing cost and size.

The buffer tank also affects the determination of the undisturbed ground temperature T_∞, which has a significant influence on borefield sizing. It is therefore recommended to consider a bypass that allows the buffer tank to be decoupled during the T_∞ measurement. However, pump heating could negatively affect the measurement. For this reason, reducing the buffer tank volume may be a more practical solution. In any case, the measurement of T_∞ should be considered explicitly during design.

Ambient temperature was the most important external disturbance observed during the measurements. It affected the stability of the TRT data, which can lead to less reliable parameter estimation and longer required test durations. Therefore, the influence of ambient temperature should be minimized as much as possible. This requires limiting the above-ground pipe length and carefully insulating all above-ground components. A smaller container is useful for transport, but the device still needs sufficient shielding from solar radiation and adequate insulation. Additional temperature control by ventilation or cooling could also be investigated.

In conclusion, a TRT device should be kept as compact as possible to reduce transport and investment costs. However, insulation and shielding should not be compromised, because they directly affect test quality. The design should also explicitly consider the measurement of T_∞, since the optimal configuration for this measurement may differ from normal TRT operation.

14.1.2 Further TRT device research

Several aspects of the developed TRT device should be investigated further to improve test quality. The determination of T_∞ should be considered carefully. As discussed above, this could be improved by design changes such as adding a bypass around the buffer tank or reducing the buffer tank volume.

The measurement interval could be optimized further. It was set to 30 seconds for all measured variables. A longer interval would improve the flow-rate resolution, because more pulses would be counted per measurement period. However, it would also reduce the temporal resolution of the temperature measurements, which may affect the calculated thermal power. This trade-off could be optimized in future research. A better solution would be to keep a short measurement interval for the temperature sensors while using a longer interval for the flow meter. This was not possible with the data acquisition system used in this research, but it is physically possible.

The flow rate could also be optimized further. Future research could examine the effect of both lower and higher flow rates on test quality. A higher flow rate improves heat transfer and allows the system to react faster to control changes. The disadvantages are higher operational costs and the need for a larger and more expensive pump.

Finally, the selected power and temperature setpoints could be studied further. This research does not draw clear conclusions on which setpoints lead to the best test quality. For CIT-TRTs, the temperature setpoint should at least be higher than the maximum expected ambient temperature, to reduce the influence of ambient temperature on the test. However, higher power and temperature setpoints also increase operational costs.

14.2 Transient modeling

The transient modeling results in this research showed a clear reduction in required TRT duration. The Terra Energy dataset showed positive results for different locations, boreholes, flow rates, ambient conditions, and operating conditions. A relevant next step is the development of active stopping criteria for practical TRT operation. In current practice, TRT operators often use a fixed test duration. Instead, the test could be stopped when the estimated k-value remains within a defined convergence band for a specified period of time. Such stopping criteria can also be used with conventional models, but they are especially relevant for evaluating the actual time reduction enabled by the STS model.

Another possible research direction is the implementation of the STS model for CIT-TRTs. This was not investigated in this research because no suitable datasets were available. However, it could become relevant if CIT-TRTs are used more widely in practice.

14.3 CIT-TRTs

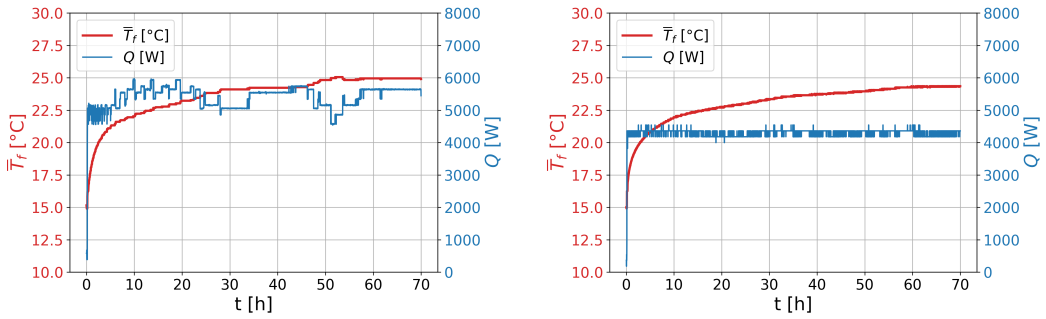
The CIT-TRTs performed in this research did not show a clear advantage over CP-TRTs. Nevertheless, further research is needed before drawing general conclusions about the method. A first step should be to improve the TRT device design so that CIT-TRTs can be performed under more stable operating conditions.

After improving the experimental setup, further research should investigate whether the observed difference between CP- and CIT-derived parameter estimates remains present. If such a discrepancy remains, it should be examined why it occurs and which test method gives results that are closer to the actual ground and borehole properties. A useful starting point would be to generate additional high-quality CP- and CIT-TRT datasets on the same borehole using the same TRT device. The device developed in this research could be used for this purpose. A larger dataset is needed to draw more reliable conclusions, since the current literature on CIT-TRTs remains limited.

Appendix A

Terra Energy TRTs

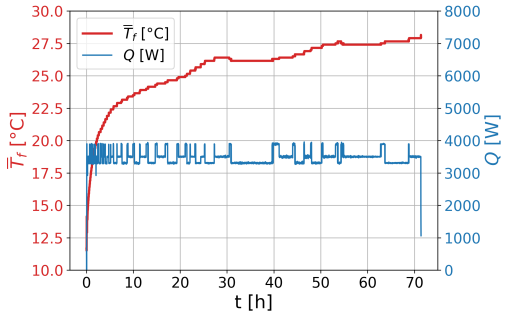
This appendix presents the measurement data of all 25 Terra Energy CP-TRTs. It shows the mean fluid temperatures $\overline{T}_f$ in $°C$ and the borehole injected thermal powers Q in W as a function of time for the entire TRT duration. Figure A.1 presents TRT1 and TRT2. Figure A.2 presents TRT3 to TRT8, Figure A.3 presents TRT9 to TRT14, Figure A.4 presents TRT15 to TRT20, and Figure A.5 presents TRT21 to TRT25.



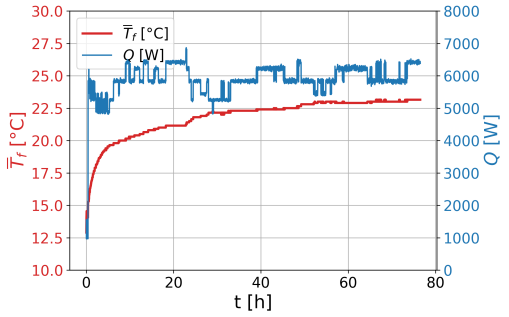
(a) Fluid temperature $\overline{T}_f$ and thermal power Q as a function of time for Terra Energy TRT1.

(b) Fluid temperature $\overline{T}_f$ and thermal power Q as a function of time for Terra Energy TRT2.

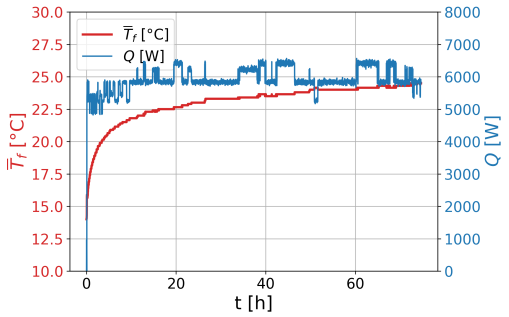
FIGURE A.1: Fluid temperature $\overline{T}_f$ and thermal power Q as a function of time for Terra Energy TRT1 and TRT2.



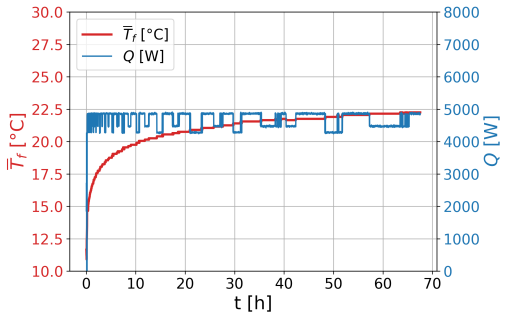
(a) Fluid temperature $\overline{T}_f$ and thermal power Q as a function of time for Terra Energy TRT3.



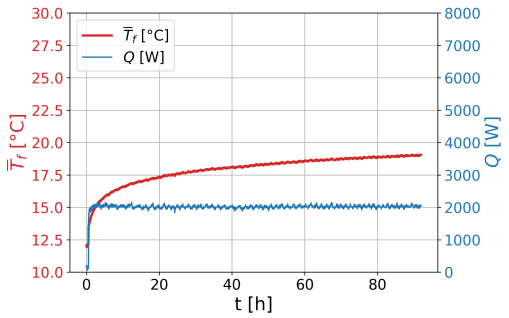
(b) Fluid temperature $\overline{T}_f$ and thermal power Q as a function of time for Terra Energy TRT4.



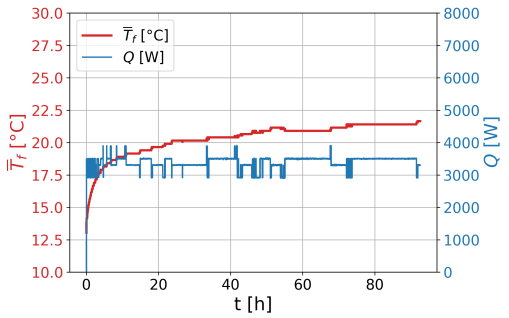
(c) Fluid temperature $\overline{T}_f$ and thermal power Q as a function of time for Terra Energy TRT5.



(d) Fluid temperature $\overline{T}_f$ and thermal power Q as a function of time for Terra Energy TRT6.

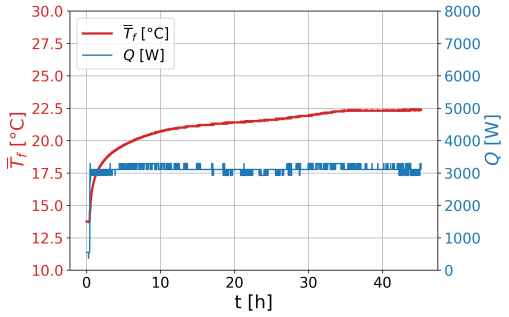


(e) Fluid temperature $\overline{T}_f$ and thermal power Q as a function of time for Terra Energy TRT7.

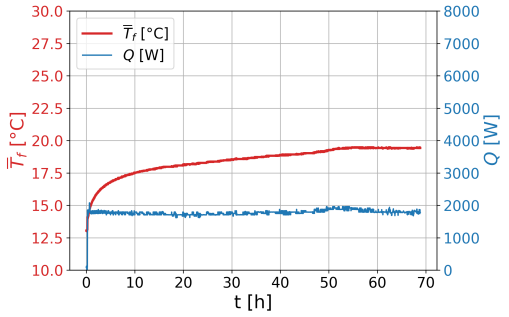


(f) Fluid temperature $\overline{T}_f$ and thermal power Q as a function of time for Terra Energy TRT8.

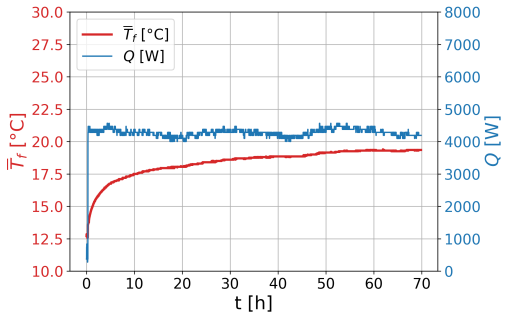
Figure A.2: Fluid temperature $\overline{T}_f$ and thermal power Q as a function of time for Terra Energy TRT3–TRT8.



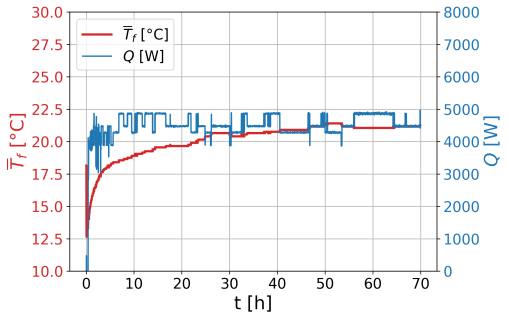
(a) Fluid temperature $\overline{T}_f$ and thermal power Q as a function of time for Terra Energy TRT9.



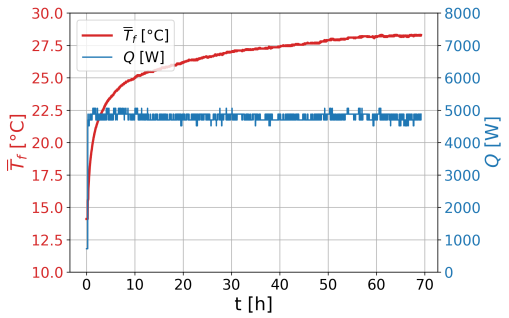
(b) Fluid temperature $\overline{T}_f$ and thermal power Q as a function of time for Terra Energy TRT10.



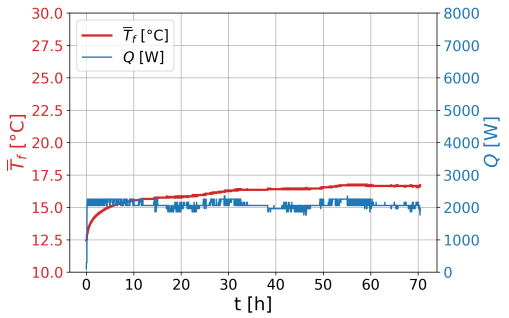
(c) Fluid temperature $\overline{T}_f$ and thermal power Q as a function of time for Terra Energy TRT11.



(d) Fluid temperature $\overline{T}_f$ and thermal power Q as a function of time for Terra Energy TRT12.

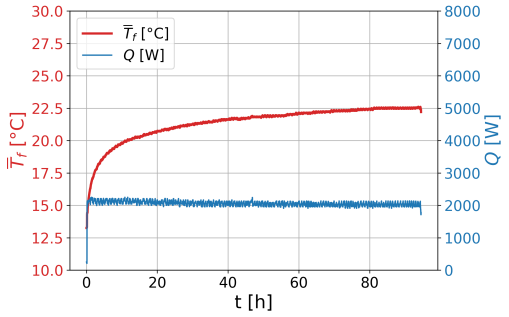


(e) Fluid temperature $\overline{T}_f$ and thermal power Q as a function of time for Terra Energy TRT13.

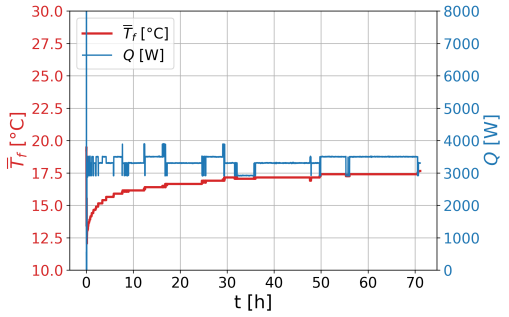


(f) Fluid temperature $\overline{T}_f$ and thermal power Q as a function of time for Terra Energy TRT14.

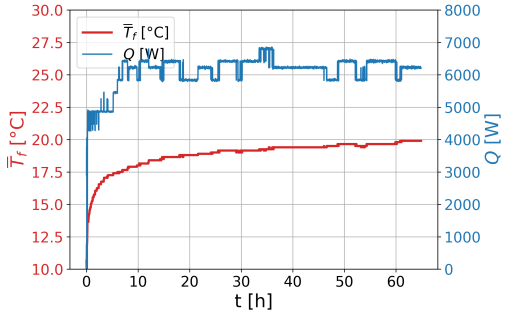
FIGURE A.3: Fluid temperature $\overline{T}_f$ and thermal power Q as a function of time for Terra Energy TRT9–TRT14.



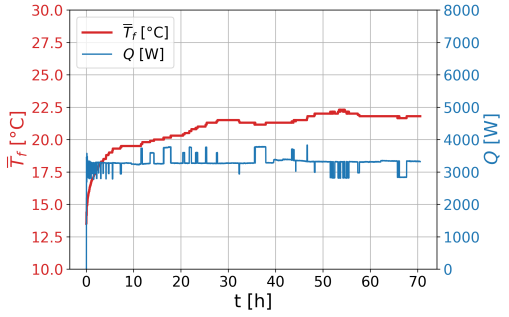
(a) Fluid temperature $\overline{T}_f$ and thermal power Q as a function of time for Terra Energy TRT15.



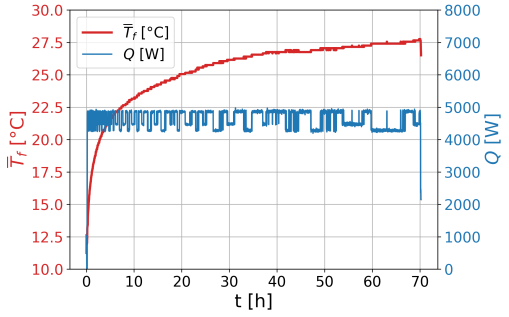
(b) Fluid temperature $\overline{T}_f$ and thermal power Q as a function of time for Terra Energy TRT16.



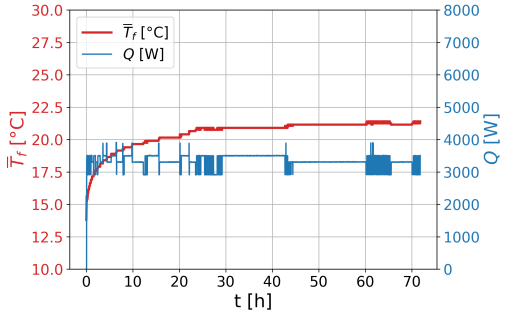
(c) Fluid temperature $\overline{T}_f$ and thermal power Q as a function of time for Terra Energy TRT17.



(d) Fluid temperature $\overline{T}_f$ and thermal power Q as a function of time for Terra Energy TRT18.

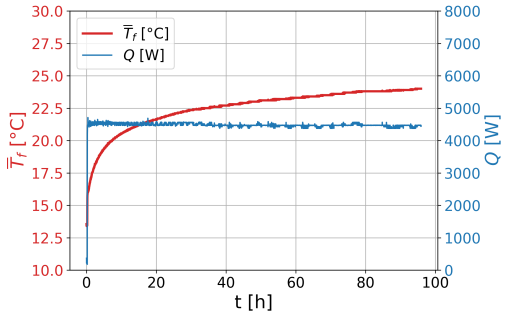


(e) Fluid temperature $\overline{T}_f$ and thermal power Q as a function of time for Terra Energy TRT19.

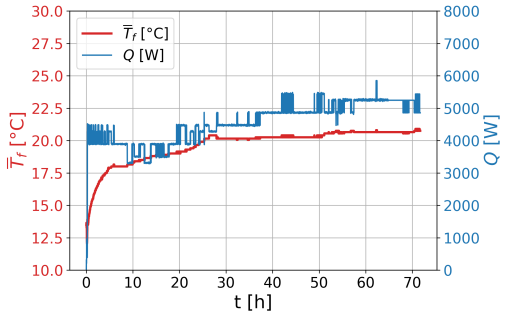


(f) Fluid temperature $\overline{T}_f$ and thermal power Q as a function of time for Terra Energy TRT20.

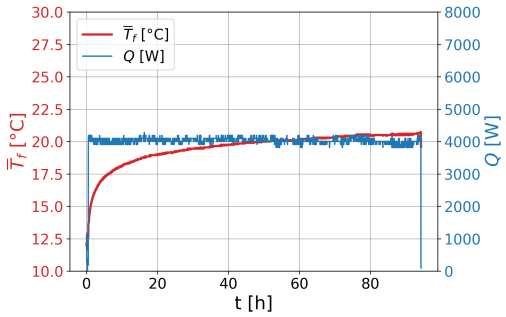
Figure A.4: Fluid temperature $\overline{T}_f$ and thermal power Q as a function of time for Terra Energy TRT15–TRT20.



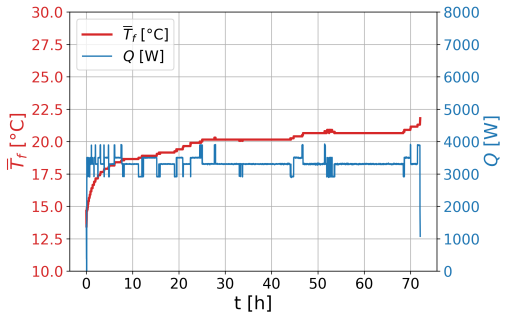
(a) Fluid temperature $\overline{T}_f$ and thermal power Q as a function of time for Terra Energy TRT21.



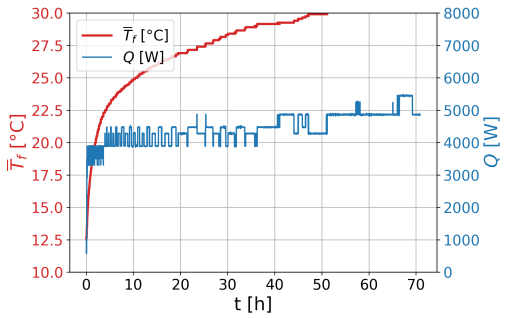
(b) Fluid temperature $\overline{T}_f$ and thermal power Q as a function of time for Terra Energy TRT22.



(c) Fluid temperature $\overline{T}_f$ and thermal power Q as a function of time for Terra Energy TRT23.



(d) Fluid temperature $\overline{T}_f$ and thermal power Q as a function of time for Terra Energy TRT24.



(e) Fluid temperature $\overline{T}_f$ and thermal power Q as a function of time for Terra Energy TRT25.

FIGURE A.5: Fluid temperature $\overline{T}_f$ and thermal power Q as a function of time for Terra Energy TRT21–TRT25.

Bibliography

[1] M. Crippa, D. Guizardi, F. Pagani, M. Banja, M. Muntean, E. Schaaf, *et al.*, *GHG emissions of all world countries-2025 report*. 2025.

[2] European Commission, "Heat pumps." https://energy.ec.europa.eu/topics/energy-efficiency/heat-pumps_en, 2025. Accessed: May 25, 2026.

[3] European Commission, "2050 long-term strategy." https://climate.ec.europa.eu/eu-action/climate-strategies-targets/2050-long-term-strategy_en, 2019. Accessed: May 31, 2026.

[4] A. M. Omer, "Ground-source heat pumps systems and applications," *Renewable and Sustainable Energy Reviews*, vol. 12, pp. 344–371, 2008.

[5] T. Aprianti, E. Tan, C. Diu, B. Sprivulis, G. Ryan, K. Srinivasan, and H. T. Chua, "Performance comparison of ground source heat pump (GSHP) against air source heat pump (ASHP) for domestic applications: A case study in perth, australia," *Teknomekanik*, vol. 4, pp. 55–63, 2021.

[6] J. D. Spitler and M. Bernier, "Vertical borehole ground heat exchanger design methods," in *Advances in Ground-Source Heat Pump Systems* (S. J. Rees, ed.), pp. 29–61, Woodhead Publishing, 2016.

[7] C. Han and X. Yu, "Sensitivity analysis of a vertical geothermal heat pump system," *Applied Energy*, vol. 170, pp. 148–160, 2016.

[8] S. Javed and J. D. Spitler, "Calculation of borehole thermal resistance," in *Advances in Ground-Source Heat Pump Systems* (S. J. Rees, ed.), pp. 63–95, Elsevier Inc., 2016.

[9] M. Ouzzane, P. Eslami-Nejad, M. Badache, and Z. Aidoun, "New correlations for the prediction of the undisturbed ground temperature," *Geothermics*, vol. 53, pp. 379–384, 2015.

[10] S. Gehlin, *Thermal Response Test: Method Development and Evaluation*. Doctoral dissertation, Luleå University of Technology, Luleå, Sweden, 2002.

[11] I. Sass and C. Lehr, "Improvements on the thermal response test evaluation applying the cylinder source theory," in *Proceedings of the Thirty-Sixth Workshop on Geothermal Reservoir Engineering*, (Stanford, California, USA), 2011.

[12] X. Liu, R. Clemenzi, and S. Liu, "Advanced testing method for ground thermal conductivity," 2017.

[13] H. Wang, C. Qi, H. Du, and J. Gu, "Improved method and case study of thermal response test for borehole heat exchangers of ground source heat pump system," *Renewable Energy*, vol. 35, pp. 727–733, 2010.

[14] A. Walch, X. Li, J. Chambers, N. Mohajeri, S. Yilmaz, M. Patel, and J.-L. Scartezzini, "Shallow geothermal energy potential for heating and cooling of buildings with regeneration under climate change scenarios," *Energy*, vol. 244, p. 123086, 2022.

[15] C. S. Blázquez, I. M. Nieto, J. C. García, P. C. García, A. F. Martín, and D. González-Aguilera, "Comparative analysis of ground source and air source heat pump systems under different conditions and scenarios," *Energies*, vol. 16, p. 1289, 2023.

[16] N. Bartolini, A. Casasso, C. Bianco, and R. Sethi, "Environmental and economic impact of the antifreeze agents in geothermal heat exchangers," *Energies*, vol. 13, p. 5653, 2020.

[17] J. W. Lund, B. Sanner, L. Rybach, R. H. Curtis, and G. Hellström, "Geothermal (ground-source) heat pumps: A world overview," *Geo-Heat Center Quarterly Bulletin*, vol. 25, pp. 1–10, 2004.

[18] British Geological Survey, "Thermal properties of rocks." https://shop.bgs.ac.uk/Shop/Product/GRC_C107, 2019. Accessed: May 4, 2026.

[19] X. Xu and J. Spitler, "Modeling of vertical ground loop heat exchangers with variable convective resistance and thermal mass of the fluid," 2006.

[20] L. Meertens, "Invloed van dynamische korte-termijneffecten op de dimensionering van geothermische boorvelden," master's thesis, KU Leuven, Leuven, Belgium, 2024.

[21] C. Zhang, Z. Guo, Y. Liu, X. Cong, and D. Peng, "A review on thermal response test of ground-coupled heat pump systems," *Renewable and Sustainable Energy Reviews*, vol. 40, pp. 851–867, 2014.

[22] E. Heim, M. Laska, R. Becker, and N. Klitzsch, "Estimating the subsurface thermal conductivity and its uncertainty for shallow geothermal energy use—a workflow and geoportal based on publicly available data," *Energies*, vol. 15, p. 3687, 2022.

[23] C. P. Remund, "Borehole thermal resistance: Laboratory and field studies," *ASHRAE Transactions*, vol. 105, pp. 439–445, 1999. Symposia, Paper No. CH-99-2-1.

[24] P. Eskilson, *Thermal Analysis of Heat Extraction Boreholes*. Doctoral dissertation, University of Lund, Department of Mathematical Physics, Lund, Sweden, 1987.

[25] S. Gehlin and B. Nordell, "Determining undisturbed ground temperature for thermal response test," *ASHRAE Transactions*, vol. 109, pp. 151–156, 2003.

[26] M. Aydin, A. Ozdogan Dolcek, M. Onur, and A. Sisman, "Flow-controlled thermal response test and its comparison with the conventional test methods," *Geothermics*, vol. 120, p. 103011, 2024.

[27] A. Franco and P. Conti, "Clearing a path for ground heat exchange systems: A review on thermal response test (TRT) methods and a geotechnical routine test for estimating soil thermal properties," *Energies*, vol. 13, p. 2965, 2020.

[28] M. Aydin, A. Gültekin, and A. Sisman, "The effects of test temperature and duration on the results of constant temperature thermal response test," (Rotterdam, The Netherlands), 2017.

[29] X. Yu, Y. Zhang, N. Deng, H. Ma, and S. Dong, "Thermal response test for ground source heat pump based on constant temperature and heat-flux methods," *Applied Thermal Engineering*, vol. 93, pp. 678–682, 2016.

[30] M. Aydin, M. Onur, and A. Sisman, "A new method for analysis of constant-temperature thermal response tests," *Geothermics*, vol. 78, pp. 1–8, 2019.

[31] M. Aydin, A. Sisman, and A. Gultekin, "Long term performance prediction of a borehole and determination of optimal thermal response test duration," in *Proceedings of the Thirty-Ninth Workshop on Geothermal Reservoir Engineering*, (Stanford University, Stanford, California, USA), 2014.

[32] A. A. Serageldin and K. Nagano, "A novel oscillatory thermal response test method for efficient characterization of ground thermal properties: Methodology and data analysis," *Renewable Energy*, vol. 230, p. 120674, 2024.

[33] H. S. Carslaw and J. C. Jaeger, *Conduction of Heat in Solids*. Oxford, United Kingdom: Clarendon Press, 2nd ed., 1959.

[34] M. Cimmino and M. Bernier, "A semi-analytical method to generate g-functions for geothermal bore fields," *International Journal of Heat and Mass Transfer*, vol. 70, pp. 641–650, 2014.

[35] M. Cimmino, M. Bernier, and F. Adams, "A contribution towards the determination of g-functions using the finite line source," *Applied Thermal Engineering*, vol. 51, pp. 401–412, 2013.

[36] J. Claesson and S. Javed, "An analytical method to calculate borehole fluid temperatures for time-scales from minutes to decades," *ASHRAE Transactions*, vol. 117, pp. 279–288, 2011.

[37] Y. Guo, J. Komar, W. V. Liu, M. Sepehri, and Y. Pourrahimian, "Considering groundwater advection on the design of borehole heat exchanger—a review of analytical solutions," in *GeoEdmonton 2018*, (Edmonton, Alberta, Canada), Canadian Geotechnical Society, 2018.

[38] S. Javed, *Thermal Modelling and Evaluation of Borehole Heat Transfer*. Doctoral dissertation, Chalmers University of Technology, Göteborg, Sweden, 2012.

[39] J. Claesson and P. Eskilson, "Conductive heat extraction to a deep borehole: Thermal analyses and dimensioning rules," *Energy*, vol. 13, pp. 509–527, 1988.

[40] L. Meertens, W. Peere, and L. Helsen, "Influence of short-term dynamic effects on geothermal borefield size," Oklahoma State University Library, 2024.

[41] W. Peere, "GHETool: issue26 – include short-term effects in sizing." https://github.com/wouterpeere/GHEtool/tree/issue26-include-short-term-effects-in-sizing, 2024. GitHub repository branch. Accessed: Feb. 24, 2026.

[42] M. Li, P. Li, V. Chan, and A. C. K. Lai, "Full-scale temperature response function (g-function) for heat transfer by borehole ground heat exchangers (GHEs) from sub-hour to decades," *Applied Energy*, vol. 136, pp. 197–205, 2014.

[43] LOBO Geothermische Boringen. https://www.lo-bo.be/, 2026. Accessed: May 27, 2026.

[44] Vaillant, "eloblock." https://www.vaillant.be/consumenten/producten/eloblock-94528.html, 2026. Accessed: May 31, 2026.

[45] Vaillant, "allstor plus." https://www.vaillant.be/consumenten/producten/allstor-plus-834.html, 2026. Accessed: May 31, 2026.

[46] Grundfos, "MAGNA3 25-100 (product no. 97924247)." https://product-selection.grundfos.com/be/products/magna/magna3/magna3-25-100-97924247, 2026. Accessed: May 27, 2026.

[47] Vaillant, "sensocomfort." https://www.vaillant.be/consumenten/producten/sensocomfort-94400.html, 2026. Accessed: May 31, 2026.

[48] Vaillant, "Stuurmodule vaillant vr71." https://www.va-shop.be/a-47840316/thermostaten/stuurmodule-vaillant-vr-71/, 2026. Accessed: May 31, 2026.

[49] Crodeon Technologies. https://www.crodeon.com/nl, 2026. Accessed: May 31, 2026.

[50] MPI, "Maddalena watermeter ds trp voorbereid puls 1:1 - r160 h." https://shop.mpi-pumps.com/pompaccessoires/waterpomp-toebehoren/watermeters/

maddalena-watermeter-ds-trp-voorbereid-puls-1-1-r160-h, 2026. Accessed: May 31, 2026.

[51] Euro Index, "Brv pompset groep v." https://euro-index.be/nl/product/pompset-groep-v/, 2026. Accessed: May 31, 2026.

[52] Terra Energy. https://terra-energy.be/nl/, 2026. Accessed: May 27, 2026.

[53] Buildwise, "Smart Geotherm ondergrondtool." https://tool.smartgeotherm.be/geo/alg, 2026. Accessed: May 27, 2026.

[54] RKV. https://www.rkv-germany.de/nederlands, 2026. Accessed: May 31, 2026.

[55] Euroquartz. https://www.euroquartz.be/, 2026. Accessed: May 31, 2026.

Code of conduct and transparency statement on the use of GenAI for KU Leuven-students (academic year 2025–2026)

Generative AI (GenAI) assistance tools can be used to generate various types of content, including text, images, code, video, music, or combinations thereof. Common examples of such tools include ChatGPT, Google Gemini, Microsoft Copilot, Midjourney, Claude.ai, Perplexity.ai, and DALL · E, among others.

This code of conduct is a tool that helps students to be transparent about the use of GenAI and fits within the university's principles on academic integrity.

Important guidelines and remarks

- **Sensitive or personal data:** Some GenAI tools protect your input and sensitive or personal data better than others. There is often no transparency on what the owners of the AI applications do with the data entered. Therefore, **do not enter sensitive or personal data in free GenAI tools.** More info about what sensitive and personal data are, is described in the three confidentiality levels of the KU Leuven data classification model (non-confidential, confidential, strictly confidential). For confidential data you should preferably use **M365 Copilot Chat with your KU Leuven account**. If you use another GenAI tool, you must be **absolutely certain** it does **not store or reuse the data you enter. Try to avoid entering these data. Do so only if strictly necessary, and only to the extent required. For personal data, work with anonymous or pseudonymized data.** Additionally, in case of strictly confidential data this should first be discussed with the teaching staff of the course or your thesis supervisor.
- **Copyrighted materials:** For **lawfully obtained copyrighted material** you should preferably use M**365 Copilot Chat with your KU Leuven**

account. If you use another GenAI tool, you must be **absolutely certain** it does n**ot store or reuse the data you enter.**

- GenAI assistance may not be used for data or topics covered by a Non-Disclosure Agreement (NDA). Even in the absence of an NDA, certain information may still need to be treated as confidential—for example, due to regulatory requirements or the risk of significant harm to the university if disclosed. In case of doubt, check with your teaching staff or supervisor.
- If your master's thesis is under embargo, you should first discuss with your supervisor whether the use of GenAI is permitted.
- Before using a GenAI tool, always consider whether its use is responsible, including from a sustainability perspective (e.g. when using GenAI as a search engine, language assistant,...).
- **Take a scientific and critical attitude** when interacting with GenAI assistance and interpreting its output, that may not always be correct.
- As a student you are responsible for complying with Article 84 of the Regulations on Education and Examinations: your report or thesis should reflect your own knowledge, understanding and skills. Be aware that plagiarism rules also apply to (work that is the result of) the use of GenAI assistance tools.
  Exam Regulations Article 84: *"Every conduct individual students display with which they (partially) inhibit or attempt to inhibit a correct judgement of their own knowledge, understanding and/or skills or those of other students, is considered an irregularity which may result in a suitable penalty. A special type of irregularity is plagiarism, i.e. copying the work (ideas, texts, structures, designs, images, plans, codes , ...) of others or prior personal work in an exact or slightly modified way without adequately acknowledging the sources. Every possession of prohibited resources during an examination (see article 65) is considered an irregularity."*
- In order to maintain academic integrity and avoid plagiarism, **more information about being transparent on the use of GenAI assistance and about correctly citing and referencing GenAI** can be found on this website for students (Dutch/English).
- **Additional reading: KU Leuven guidelines on responsible use of Generative AI tools, and other information** (Dutch/English)

A few final words

If you are uncertain whether or not you should declare your use of GenAI tools, we suggest that you discuss this with your instructor or supervisor. It is always safer to declare GenAI use, even when it is not strictly required. However, declaring GenAI use does not entail that its use is

allowed; the right column in the table below provides more detailed instructions in this regard (code of conduct).

Moreover, advanced AI tools are evolving rapidly, and their capabilities have expanded significantly in a short period of time. As a result, we do not yet have all the answers about their responsible use. Finally, it is important to follow-up on the most recent evolutions in AI technologies, to have an open mind but also to be a bit cautious, to communicate with instructors, teaching assistants, supervisors and peers, to be as transparent as we can, and to learn together as we move along.

Student name: Bart Vandenhout **Student number:** r0894352

Please indicate with "X" whether it relates to a course assignment or to the Bachelor's or Master's thesis:

O This form is related to a **course assignment.**
Course name: ..... **Course number:** .....

This form is related to my O **Bachelor's** or **X Master's thesis.**
Title Bachelor's or Master's thesis: Thermal Response Tests for Geothermal Borefields – Reducing Test Duration through Transient Borehole Modeling and Comparing Constant Power and Constant Temperature Methods **Supervisor:** Professor Lieve Helsen

Daily supervisor: Lone Meertens

Please indicate with "X":

O I **did not use** any GenAI assistance tool.

X I **did use** GenAI Assistance. In this case **specify which ones** (e.g. ChatGPT, M365 Copilot, ...): ChatGPT, Gemini

GenAI assistance used as/for:	**Name of the GenAI tool(s) used** If helpful, also describe in which way you were using GenAI related to what is specified as code of conduct.	**Code of conduct:** **For each of the categories below, always take into account the important guidelines and remarks mentioned above (e.g. copyrighted data, sensitive or personal data,. . .).**
As a language assistant for reviewing or improving texts I wrote myself	*ChatGPT*	This use is similar to using spelling and grammar check tools. In general, you do not have to refer to such kind of GenAI use in the text. **However, be careful:** • When using GenAI tools on texts you did not write yourself to improve the text, **you have to refer to the original source or author**, otherwise you are committing plagiarism and thus an irregularity.
As a paraphrasing tool	*ChatGPT*	This use is allowed except when it is prohibited by the teacher or the program of study. You may paraphrase your own text or texts by an author other than yourself and take inspiration from what a GenAI tool or another tool suggests (unless it is not allowed). In general, you do not have to refer to such kind of GenAI use or other paraphrasing tools in the text. **However, be careful**: • If it entails text by an author other than yourself, **you are not allowed to include that paraphrased text without reference to the original source or author**. Without such reference, you would be committing plagiarism and thus an irregularity.

For translation aid to improve texts I wrote myself or to better understand text from others	*ChatGPT*	This use is allowed except when it is prohibited by the teacher or the program of study. It is similar to using translation tools (Google translate, DeepL, ...). In general, you do not have to refer to such kind of GenAI use in the text. **However, be careful:** • **You are not allowed to include that translated text without reference to the original source or author.** Without such reference, you would be committing plagiarism and thus an irregularity. • Always check the translated text for correctness and meaning.
As a search engine to get information on a topic or to search for existing research on the topic	*ChatGPT, Gemini*	This use is similar to e.g. a Google search or checking Wikipedia. If you write your own text based on this information, you do not have to refer to the use of GenAI in the text. **You only have to refer to the existing research and references you have checked and used** (without such references you would be committing plagiarism and thus committing an irregularity). **However, be careful:** • Be aware that the output of the GenAI tool cannot be guaranteed as a 100% reliable source of information. The output may not be entirely correct and/or be limited due to the databases it uses. Moreover, knowledge evolves and may change over time; therefore, the database of the GenAI tool may not be up to date. Therefore, **verify the information and do not just copy-paste it** as you should understand and critically process everything you are writing.

For literature search	*ChatGPT*	This use is comparable to e.g. a Google Scholar search. You do not have to refer to such kind of GenAI use; **you only have to refer to the literature references you have checked and used** (without such references you would be committing plagiarism and thus committing an irregularity). **However, be careful:** • Be aware that the search output is restricted to the database the GenAI tool is built on. After this initial search, look for scientific sources and conduct your own analysis of the source documents. **Interpret, analyse and process the information you obtained; verify it and do not just copy-paste it** as you should understand and critically process everything you are writing. • Be aware that some GenAI tools may **output no or wrong references.** As a student you are responsible for further checking and verifying the absence or correctness of references; do not just copy-paste it.
For generating programming code	*ChatGPT*	Use of GenAI for coding is allowed except when it is prohibited by the teacher or the program of study. If used for coding, correctly mention the use of GenAI assistance in accordance with the instructions on the page on being transparant about the use of GenAI.

For generating new (research) ideas	/	This use of GenAI is allowed except when it is prohibited by the teacher or the program of study. Correctly mention the use of GenAI assistance in accordance with the instructions on the page on being transparent about the use of GenAI. **Be careful:** • Further verify in this case whether the idea is novel or not. It is likely that it is related to existing work. **If so, that existing work should be correctly referenced in the text** (without such reference you would be committing plagiarism and thus committing an irregularity).
For generating synthetic data	/	Use of GenAI for generating synthetic data is allowed, **provided that it is methodologically and ethically justifiable**, except when it is prohibited by the teacher or the program of study. Always correctly mention the use of GenAI assistance in accordance with the instructions on the page on being transparent about the use of GenAI. **Be careful:** • Always **carefully evaluate** the generated synthetic data for quality and possible bias since the output is highly dependent on the quality of the data on which the models are trained.

For generating blocks of text (other than the allowed use without referencing mentioned above)	/	According to Article 84 of the Regulations on Education and Examinations your text should allow to correctly and properly assess your own knowledge, understanding and skills. **Therefore, inserting blocks of text without quotes and a reference to GenAI assistance in your work is not allowed.** **Be careful:** • If it is really needed to insert a block of text from a GenAI tool, for instance because of the nature of your assignment, mention it as a citation by using quotes and correctly mention the use of GenAI assistance in accordance with the instructions page on being transparent about the use of GenAI. • However, in general, such GenAI use should be kept to an **absolute minimum**; you should always check the original sources.
For generating visuals, video or audio	/	Use of GenAI for generating visuals, audio or video is allowed except when it is prohibited by the teacher or the program of study. **Be careful:** • If used, refer to GenAI for visuals according to the usual referencing style, following the instructions on the page on referencing GenAI. • If you work with existing visuals, audio or video, **that existing work should be correctly referenced in the text** (without such reference you would be committing plagiarism and thus an irregularity). • Explain the usage in the methods section (if there is one) and optionally attach (or link to) the prompts with the full output (or history).

Other use (specify here; this may also include a combination of types of use mentioned above):	/	To make sure other use of GenAI is allowed within the course or thesis, and if so, the conditions that may apply, contact the teaching staff of the course or the supervisor of the thesis **beforehand** and explain the intended GenAI use. Also inform the programme director. Motivate how you would comply with Article 84 of the exam regulations. Explain the use and the added value of the AI tool you consider to use and how it is in accordance with the assignment or thesis and the KU Leuven guidelines on responsible use of Generative AI tools. Depending on the kind of GenAI use, it may be needed to properly reference it in the text, in accordance with the instructions page on being transparent about the use of GenAI.